NASA CR-170,417

NASA-CR-170419
19850005491

Flying Qualities and Control System Characteristics for Superaugmented Aircraft

Thomas T. Myers, Duane T. McRuer, and Donald E. Johnston

NF02571

NASA

National Aeronautics and
Space Administration

Flying Qualities and Control System Characteristics for Superaugmented Aircraft

Thomas T. Myers, Duane T. McRuer, and Donald E. Johnston
Systems Technology, Inc., 13766 South Hawthorne Boulevard, Hawthorne, California

NASA

National Aeronautics and
Space Administration
Ames Research Center
Dryden Flight Research Facility
Edwards, California 93523

N85-13800#

This Page Intentionally Left Blank

TABLE OF CONTENTS

LIST OF FIGURES

LIST OF FIGURES (Concluded)

LIST OF TABLES

a	Breakpoint in a limiter (Fig. 18)
a_y	Body axis normal acceleration
A	Amplitude of input signal to a nonlinearity (Fig. 18)
B	Amplitude of second input signal in dual sinusoidal describing function analysis (Fig. 18)
c	Aerodynamic chord
D	Time delay, drag
F_s	Force applied to manipulator
g	Gravitational acceleration
G_a	Forward loop equalization transfer function (Fig. 20)
G_c	Controller transfer function (Fig. 25)
G_f	Feedback transfer function (Fig. 20)
G_i	Command input transfer function (Fig. 20)
G_{wo}	Washout equalization (Table 4)
GM_{hi}	High frequency gain margin
GM_{lo}	Low frequency gain margin
G_δ^q	Pitch rate-to-pitch controller transfer function
G_δ^γ	Flight path angle-to-pitch controller transfer function
$G_{\delta\eta}^{q\gamma}$	Pitch-controller/disturbance coupling function
G_η^q	Pitch rate-to-disturbance transfer function
h	Altitude
$\dot{h}$	Rate of climb
h_c	Commanded altitude
h_e	Altitude error
I_y	Pitch moment of inertia

$\hat{K}$	Nondimensional loop gain, $-K_q M_\delta T_q$ (Fig. 6)
K_i	Pure gain G_i
K_q	Pitch rate feedback gain
m	Mass
n_{max}	Maximum allowable normal acceleration
N_δ^h	Altitude-to-pitch controller numerator
N_δ^q	Pitch rate-to-pitch controller numerator
N_δ^α	Angle-of-attack-to-pitch controller numerator
N_δ^γ	Flight path angle-to-pitch controller numerator
N_δ^θ	Pitch attitude-to-pitch controller numerator
$N_{\delta\eta}^{q\gamma}$	Pitch-controller/disturbance coupling numerator
P_c	Roll rate command
PR	Pilot rating
q	Pitch rate
q_c	Pitch rate command
q_e	Pitch rate error
q_{ss}	Steady-state pitch rate
Q_o	Equilibrium pitch rate
r	Correlation coefficient
R_o	Equilibrium yaw rate
s	Laplace operator
S	Wing planform area
SM	Static margin
t_m	Time of maximum pitch rate response for a step input (Fig. 6)
T	Generic time constant
T_{h_1}	Low frequency altitude lead time constant

T_q	Lead in superaugmentation equalization element (Fig. 2)
T_t	Rise Time (Fig. 6)
T_s	Torque applied to manipulator by pilot
T_{sp_1}	Time constant of stable first-order ("short period") pole of RSS airframe (Table 1)
T_{sp_2}	Time constant of unstable first-order ("short period") pole of RSS airframe (Table 1)
T_{wo}	Washout time constant
TAGR	Total Available Gain Range
T_{CL}	Time constant of pole in attitude closure (Eq. 27)
T_L	Pilot's first-order lead time constant
T_{θ_1}	Low frequency attitude lead time constant
T_{θ_2}	High frequency attitude lead time constant
u	x-axis velocity component (small perturbation)
u_g	x-axis gust velocity (small perturbation)
u_I	x-axis velocity component (small perturbation), inertially referenced
U_o	Trim speed
W	z-axis velocity component
X_s	Angular displacement of manipulator
Y_c	Controlled element describing function (Fig. 25)
Y_{c_θ}	Pitch attitude-to-controller controlled element describing function
Y_p	Pilot's describing function (Fig. 25)
Y_{p_h}	Pilot action on path deviation
Y_{p_θ}	Pilot action on attitude
α	Angle of attack
α_A	Aerodynamic angle-of-attack

α_I	Inertial angle-of-attack
γ	Flight path angle
δ	Generic pitch control surface deflection
δ_p	Pilot command
Δ	Characteristic polynomial
Δ_o	Characteristic polynomial at neutral stability
Δ_{sp}	Characteristic polynomial under short period approximation
ζ	Damping ratio
ζ_p	Damping ratio of phugoid mode
ζ_{p_o}	Damping ratio of the idealized phugoid mode (Eq. 3b)
η	Generic disturbance variable
θ	Pitch attitude
θ_c	Pitch attitude command
ρ	Density gain
σ	Standard deviation
τ	Generic effective time delay
τ_c	Time delay of conventional aircraft
τ_s	Time delay of superaugmented aircraft
τ_M	Delay margin
ϕ	Phase angle
ϕ_M	Phase margin
Φ	Bank angle
Φ_o	Equilibrium bank angle
ω	Generic frequency (rad/sec)
ω_a	Actuator break frequency (Fig. 3)
ω_{c_a}	Asymptotic crossover frequency (Fig. 5)

ω_n Undamped natural frequency

ω_p Undamped natural frequency of phugoid mode

ω_{p_0} Undamped natural frequency of the idealized phugoid mode (Eq. 3a)

ω_u Instability frequency ($\phi_M = 0$)

ω_{u_1} Phugoid restabilization frequency (Fig. 9)

ω_{u_2} High frequency instability frequency (Fig. 9)

LONGITUDINAL NONDIMENSIONAL STABILITY DERIVATIVES
(STABILITY AXIS SYSTEM)

DEFINITIONS   UNITS

$$C_D = \frac{drag}{qS}$$ 1/1

$$C_{D_a} = \frac{U}{2}\frac{\partial C_D}{\partial U}$$ 1/1

$$C_{D_\alpha} = \frac{\partial C_D}{\partial \alpha}$$ 1/rad

$$C_{D_\delta} = \frac{\partial C_D}{\partial \delta}$$ 1/rad

$$C_L = \frac{lift}{qS}$$ 1/1

$$C_{L_u} = \frac{U}{2}\frac{\partial C_L}{\partial U}$$ 1/1

$$C_{L_\alpha} = \frac{\partial C_L}{\partial \alpha}$$ 1/rad

$$C_{L_\alpha} = \frac{\partial C_L}{\partial(\dot{\alpha}c/2U)}$$ 1/rad

$$C_{L_q} = \frac{\partial C_L}{\partial(qc/2U)}$$ 1/rad

$$C_{L_\delta} = \frac{\partial C_L}{\partial \delta}$$ 1/rad

$$C_M = \frac{M}{qSc}$$ 1/1

$$C_{M_u} = \frac{U}{2}\frac{\partial C_M}{\partial U}$$ 1/1

$$C_{M_\alpha} = \frac{\partial C_M}{\partial \alpha}$$ 1/rad

$$C_{M_\alpha} = \frac{\partial C_M}{\partial(\dot{\alpha}c/2U)}$$ 1/rad

$$C_{M_q} = \frac{\partial C_M}{\partial(qc/2U)}$$ 1/rad

$$C_{M_\delta} = \frac{\partial C_M}{\partial \delta}$$ 1/rad

LONGITUDINAL DIMENSIONAL STABILITY DERIVATIVES
(STABILITY AXIS SYSTEM)

QUANTITY	DIMENSIONAL DEFINITIONS	DIMENSIONAL UNIT	NONDIMENSIONAL
X_u	$\dfrac{1}{m}\dfrac{\partial X}{\partial u}$	$\dfrac{1}{\text{sec}}$	$\dfrac{\rho S U}{m}\left(-C_D - C_{D_u}\right)$[a]
X_w	$\dfrac{1}{m}\dfrac{\partial X}{\partial w}$	$\dfrac{1}{\text{sec}}$	$\dfrac{\rho S U}{2m}\left(C_L - C_{D_\alpha}\right)$
X_δ	$\dfrac{1}{m}\dfrac{\partial X}{\partial \delta}$	$\dfrac{\text{ft}}{\text{rad-sec}^2}$	$\dfrac{\rho S U^2}{2m}\left(-C_{D_\delta}\right)$
Z_u	$\dfrac{1}{m}\dfrac{\partial Z}{\partial u}$	$\dfrac{1}{\text{sec}}$	$\dfrac{\rho S U}{m}\left(-C_L - C_{L_u}\right)$[b]
Z_w	$\dfrac{1}{m}\dfrac{\partial Z}{\partial w}$	$\dfrac{1}{\text{sec}}$	$\dfrac{\rho S U}{2m}\left(-C_{L_\alpha} - C_D\right)$
$Z_{\dot w}$	$\dfrac{1}{m}\dfrac{\partial Z}{\partial \dot w}$	$\dfrac{1}{1}$	$\dfrac{\rho S c}{4m}\left(-C_{L_{\dot\alpha}}\right)$
Z_q	$\dfrac{1}{m}\dfrac{\partial Z}{\partial q}$	$\dfrac{\text{ft}}{\text{rad-sec}}$	$\dfrac{\rho S U c}{4m}\left(-C_{L_q}\right)$
Z_δ	$\dfrac{1}{m}\dfrac{\partial Z}{\partial \delta}$	$\dfrac{\text{ft}}{\text{rad-sec}^2}$	$\dfrac{\rho S U^2}{2m}\left(-C_{L_\delta}\right)$
M_u	$\dfrac{1}{I_y}\dfrac{\partial M}{\partial u}$	$\dfrac{1}{\text{ft-sec}}$	$\dfrac{\rho S U c}{I_y}\left(C_M + C_{M_u}\right)$
M_w	$\dfrac{1}{I_y}\dfrac{\partial M}{\partial w}$	$\dfrac{1}{\text{ft-sec}}$	$\dfrac{\rho S U c}{2 I_y}C_{M_\alpha}$
$M_{\dot w}$	$\dfrac{1}{I_y}\dfrac{\partial M}{\partial \dot w}$	$\dfrac{1}{\text{ft}}$	$\dfrac{\rho S c^2}{4 I_y}C_{M_{\dot\alpha}}$
M_q	$\dfrac{1}{I_y}\dfrac{\partial M}{\partial q}$	$\dfrac{1}{\text{sec}}$	$\dfrac{\rho S U c^2}{4 I_y}C_{M_q}$
M_δ	$\dfrac{1}{I_y}\dfrac{\partial M}{\partial \delta}$	$\dfrac{1}{\text{rad-sec}^2}$	$\dfrac{\rho S U^2 c}{2 I_y}C_{M_\delta}$

---

[a]The thrust gradient terms are neglected here in the interests of symmetry and consistency.

[b]For $C_{L_u} = 0$, as in subsonic flight, and $C_L = W/(\rho U^2 S/2)$, as in trimmed flight for $\gamma_o = 0$, $Z_u = -2g/U_o$.

This Page Intentionally Left Blank

SECTION I

INTRODUCTION AND OVERVIEW

Major advances in flight control system technology have brought multiple-redundant, full-authority, fail-operational, fly-by-wire flight control systems to a highly mature state. Such systems now are operational in the F-16, F-18, and Shuttle. This practical acceptance of fail-operational FCS in operational aircraft, itself an enormous step forward, now makes it possible to optimize aircraft configurations without any need for compromise with stability and control considerations other than the provision of adequate control power.

"Superaugmented" aircraft are an important subclass of actively controlled, highly-augmented aircraft. In this report the term superaugmented is applied to aircraft which:

- are statically unstable without augmentation.

- have a degree of pitch attitude stability with respect to inertial space (as opposed to weathercock stability) which is provided by the flight control system.

- have pitch attitude command response characteristics which are largely independent of the aerodynamic stability derivatives except for pitch control effectiveness.

In this usage an unstable aircraft stabilized with a high gain $\alpha \rightarrow \delta_e$ feedback would be considered "conventional" and not be termed superaugmented. Superaugmented aircraft are of special interest here because of some important advantages and unconventional dynamic characteristics.

There are powerful motives for flying aircraft balanced to be statically unstable in open-loop conditions, using the automatic flight control system to compensate for and counter the major deficiencies. These reasons include:

- reduced trim drag.

- reduced tail and/or fin size.

- lower observables.

- improved structural mode stability (e.g., via active structural mode control which may, incidentally, result in reduced static margin).

- larger aspect ratio made possible by maneuver and gust load control (which can, again, lead to reduced effective static margins).

- inherent reduction in control system sensitivity to many aircraft characteristics (e.g., for some FCS types the only "important" rigid body aircraft stability derivatives are the surface effectivenesses).

High gain, large bandwidth controllers are required to stabilize the airplane-alone divergence. In solving the control problem an "equivalent vehicle" is created in which the key (closed-loop) dynamic properties presented to the pilot depend primarily on the controller dynamics. As noted above, the equivalent vehicle dynamics may no longer correspond to those of conventional aircraft. Instead, they may differ in kind as well as degree. These differences provide both new challenges and new opportunities at the pilot-vehicle interface.

The primary quantitative measure of longitudinal static instability is the stability derivative M_α. The sign of this derivative becomes positive when the aircraft-alone is made statically unstable to achieve the desirable ends listed above. From a flying qualities standpoint the nominal longitudinal linearized dynamics of superaugmented aircraft for small perturbations about trim will exhibit the following properties:

- The effective pitch-attitude/pilot-command characteristics may be different from those of a conventional aircraft (e.g., in a rate command/ attitude hold type of control system the effective aircraft possesses "inertial" rather than weathercock or speed stability, there is an absence of speed cue in stick force, etc.).

- The flight-path/pitch-attitude characteristics will be substantially unchanged from those of the same aircraft flown with stable c.g. locations.

- There may be some time lag and delay effects introduced by the control system, stick filters, etc.

- Atmospheric disturbances (gusts and shears) will excite the aircraft differently (because of the sign changes in M_α) and hence the responses to disturbances may be "unusual."

The flying qualities near the limits of controller effectiveness will, of course, be markedly different. When the control surface is saturated the aircraft will be unstable and will tend to diverge until control can be restored. Typically this would be in a short time. If pilot command is the cause of the limiting he would modify his input; if an atmospheric disturbance were the cause presumably it would ultimately change sign. In either case the control system feedback signals may also help back off the surface from its limiting condition. However, control power and surface limiting are critical issues for superaugmented designs.

Other key properties of superaugmented aircraft relate primarily to the control system. These include:

- Extensive potential for tailoring of effective pilot-command/aircraft-response characteristics, including task-dependent tailoring.

- Relative insensitivity of the nominal closed-loop aircraft/flight control system to variations and uncertainties in aircraft rigid body stability derivatives.

- The large controller bandwidth places more emphasis on those design factors which limit gain directly (e.g., higher frequency aircraft and controller modes) or indirectly (e.g., aircraft control power).

This new technology is not an unmixed blessing. Greater FCS complexity and cost are obvious disadvantages, but other unfavorable effects are more subtle, being of the nature of side effects which accompany the favorable major effects. These are discussed and illustrated with examples in this report.

Current problems with superaugmented aircraft dynamics are primarily related to the high bandwidth controller requirements, which make the system vulnerable to airframe/controller/pilot/environment high-frequency dynamic modes and noise. For example, sensitivity of the

controls design is increased to flexible vehicle and actuator dynamics; to sensor, computation, and equalization dynamics and noise introduction, to pilot remnant and vibration feedthrough, and to external environmental disturbances which must be regulated against. Aircraft control power and rate requirements to accomplish regulation and command functions may also be larger than normal. And last, but not least, the new flight control technology can provide mission task oriented flying quality characteristics which border on an absolute optimum -- if only someone could define what that is!

The following sections of this report address the various aspects noted above. Section II investigates aircraft-alone dynamics and super-augmented control system fundamental regulatory properties including stability and regulatory responses of the basic closed-loop system; fundamental high and low frequency margins and governing factors; and sensitivity to aircraft and controller parameters. Alternative FCS mechanizations, and mechanizational side effects are also discussed.

Section III follows with an overview of flying qualities considerations. This encompasses general pilot operations as a controller in unattended, intermittent and trim, and full-attention manual regulatory or command control; effective vehicle primary and secondary response properties to pilot inputs and disturbances; pilot control architectural possibilities; and comparison of superaugmented and conventional aircraft path responses for different forms of pilot control.

Results of a simple experimental investigation into pilot dynamic behavior in attitude control of superaugmented aircraft configurations with high frequency time lags and time delays are presented in Section IV. This starts with the theoretical distinction between time lags and pure time delays which leads to crossover regression. The experimental setup is described and results are presented which substantiate the regression theory and indicate sensitivity of pilot behavior and opinion to time delay magnitude.

Section V follows with basic conclusions of the study and recommendations on solidifying those conclusions which can only be tentative at this time.

SECTION II

FUNDAMENTAL PROPERTIES OF SUPERAUGMENTED CONTROL SYSTEMS

A. AIRCRAFT CHARACTERISTICS AND BASIC CONTROLLER

1. Aircraft Dynamics

An understanding of the dynamics of relaxed static stability (RSS) aircraft logically begins with the airframe poles and zeros. For the important class of aircraft with flight control system (FCS) response feedbacks to a single control point (e.g., elevator), or common feedbacks to a composite control point (e.g., coupled elevator, flap, canard, etc.) the aircraft transfer function <u>numerators</u> related to control response are not modified by the feedbacks. In the composite case, of course, the control effectiveness derivatives (e.g., Z_δ, M_δ) in the numerators refer to the composite rather than elevator alone. Further, static margin variations primarily influence the poles and have less effect on the control numerators. Consequently our primary interest is on the characteristic roots (airframe poles).

The most important distinguishing feature of a relaxed static stability aircraft is an unstable (positive) static margin (SM = dC_M/dC_L), which implies a positive (unstable) M_α derivative:

$$M_\alpha = U_0 M_w = \frac{\rho S U_0^2 c}{2 I_y} C_{M_\alpha}$$

$$= \frac{\rho S U_0^2 c}{2 I_y} \frac{dC_M}{dC_L} C_{L_\alpha}$$

(1)

The effect of static margin on the aircraft poles, can be seen by expanding the characteristic polynomial, Δ, in terms of M_α and the characteristic polynomial at neutral stability, Δ_0 (1 g, level flight, Ref. 1). For many flight conditions M_u can be neglected and

$$\Delta = \Delta_0 - M_\alpha \left[s^2 - X_u s - \frac{g}{U_0} Z_u \right]$$

(2)

where

$$\Delta_0 = s(s - M_q) \left\{ (s - X_u)(s - Z_w) - X_w Z_u \right\}$$

$$- M_{\dot\alpha} s \left\{ s^2 - X_u s - \frac{g}{U_0} Z_u \right\}$$

The quadratic polynomial multiplied by M_α may be recognized as the idealized "Lanchester" phugoid mode with undamped natural frequency and damping ratio given by

$$\omega_{p_0} = \sqrt{-Z_u g/U_0} \doteq \sqrt{2}\, g/U_0 \tag{3a}$$

$$\zeta_{p_0} = -X_u/2\omega_{p_0} \tag{3b}$$

Configuration design considerations which change M_α (tail down-sizing being a common example) will also affect other derivatives, but the M_α effect is typically dominant. Equation 2 can be reduced to a useful idealization by neglecting $M_{\dot\alpha}$, and X_w. With these approximations the neutral characteristic polynomial is simply

$$\Delta_0 \doteq s(s - X_u)(s - M_q)(s - Z_w) \tag{4}$$

where

$$X_u = -\frac{\rho S U_0}{m}(C_D + C_{D_u}) \doteq -\frac{\rho S U_0}{m} C_D$$

$$M_q = \frac{\rho S U_0 c^2}{4 I_y} C_{M_q}$$

$$Z_w = -\frac{\rho S U_0}{2m}(C_{L_\alpha} + C_D) \doteq -\frac{\rho S U_0}{2m} C_{L_\alpha}$$

This idealization reveals three uncoupled first-order modes. These are speed, pitch attitude, and heave modes with inverse time constants X_u, M_q, Z_w respectively. Fundamental aerodynamics imply that these three modes will invariably be stable and, since each derivative is proportional to ρU, the roots will tend to move together as flight conditions change and thereby maintain their relative positions throughout the flight envelope. Furthermore, the relative order of the roots will be the same for most aircraft. The speed mode time constant will be

longest followed by the pitch mode with the heave mode generally some-what faster, i.e.,

$$|X_u| < |M_q| < |Z_w| \tag{5}$$

The variation of the airframe characteristic determinant, Δ, with static margin can be studied by treating Eq. 2 as a feedback system in which M_α is the gain, the Lanchester phugoid is the "numerator," and the characteristic polynomial Δ_0 (for $M_\alpha = 0$) is the "denominator." Using this technique, the characteristic poles as a function of M_α are summarized in the conventional and Bode root loci of Fig. 1 for stable and unstable M_α values.

Relaxed static stability aircraft will have low stable or unstable static margins with the latter case ($M_\alpha > 0$) of primary interest here. As M_α is increased from zero (Fig. 1b), the pitch (M_q) and speed (X_u) modes rapidly couple to form the phugoid mode. The heave root (Z_w) and the free s form real "short period" roots, one stable $\left(1/T_{sp_1}\right)$ and the other $\left(1/T_{sp_2}\right)$ unstable. A convenient $|M_\alpha|$ reference point is the horizontal Bode asymptote between ω_{p_0} and $-M_q$. This is the maneuver point (where $|M_\alpha| = |Z_w M_q|$) which typically corresponds to a static margin several percent unstable. For greater instabilities (lower on the Bode loci) the phugoid is essentially fixed, and the real roots approach the high frequency Bode asymptote. The approximate values of $1/T_{sp_1}$ and $1/T_{sp_2}$, and relationships between them, from the "short-period" (2 DOF heave-pitch) approximations are given in Table 1 for the three regions of $|M_\alpha|$. The corresponding control numerators are summarized in Table 2. Note that, to a first approximation, none of the numerator characteristics are strong functions of M_α.

2. Basic Control System for Stabilization

a. Cross Section of Possibilities

As developed above, the price of the performance benefits which relaxed static stability aircraft enjoy is short-period divergence.

$$G(s) = \frac{-M_\alpha\left[s^2 - X_u s - \frac{g}{U_0} Z_u\right]}{s(s - X_u)(s - M_q)(s - Z_w)}$$

$M_\alpha < 0$

Short Period

Z_w M_q

ω_{p_0}

X_u

Phugoid

$M_\alpha > 0$

Phugoid

ω_{p_0}

Z_w M_q

X_u

ω (rad/sec)

Manuever Point

$|M_\alpha| = |Z_w M_q|$

Short Period
(coupled
heave-pitch)

$\omega_{sp}^2 \doteq M_\alpha$

Phugoid

$\omega_{p_0} \doteq \sqrt{2}\ g/U_0$

— Real axis
(σ) locus

- - - Bode asympote

+++ Complex locus

$\frac{1}{T_{sp_1}}$ (stable real pole)

$\frac{1}{T_{sp_1}} \cdot \frac{1}{T_{sp_2}} \doteq -M_\alpha$

$\frac{1}{T_{sp_2}}$
(unstable real pole)

Phugoid

$\omega_{p_0} \doteq \sqrt{2}\ g/U_0$

a) Stable Static Margin

b) Unstable Static Margin
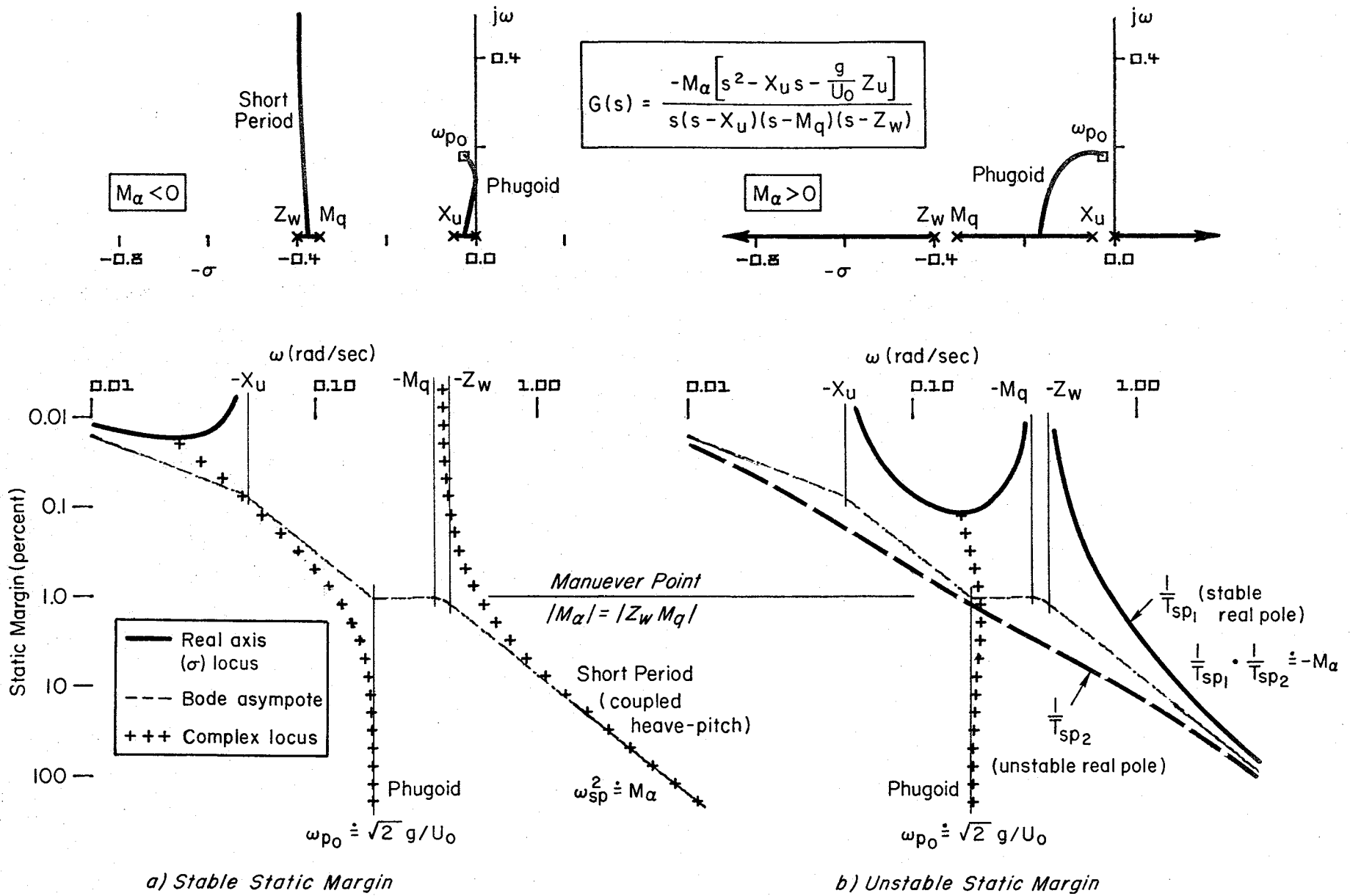
Figure 1. Variation of Aircraft Longitudinal Roots with M_α

TABLE 1. SHORT PERIOD ROOT RELATIONS, RELAXED
STATIC STABILITY CASE ($M_\alpha > 0$)

1. The short-period roots are always real and are limited by

$$1/T_{sp_1} > -Z_w$$

$$-M_q > 1/T_{sp_2}$$

2. These roots are related by

$$1/T_{sp_2} = -(Z_w + M_q) - 1/T_{sp_1}$$

$$\left(1/T_{sp_1}\right)\left(1/T_{sp_2}\right) = Z_w M_q - M_\alpha$$

3. Approximations include

a. When $\left|-M_\alpha\right| \ll Z_w M_q$, then

$$1/T_{sp_1} \doteq -Z_w > 0; \qquad\qquad 1/T_{sp_2} \doteq -M_q > 0$$

b. When $M_\alpha = Z_w M_q$ (zero maneuver margin), then

$$1/T_{sp_1} = -(Z_w + M_q); \qquad 1/T_{sp_2} = 0$$

c. When $\left|-M_\alpha\right| \gg Z_w M_q$

$$1/T_{sp_1} \doteq \left|1/T_{sp_2}\right| \doteq \sqrt{M_\alpha}$$

$$1/T_{sp_1} > \left|1/T_{sp_2}\right|$$

TABLE 2.   NUMERATOR POLYNOMIALS,
SHORT PERIOD APPROXIMATION

<u>CONTROL NUMERATORS</u> (for $\Delta = s\Delta_{sp}$)

$$N_\delta^\theta \;=\; \left(M_\delta + Z_\delta M_{\dot{w}}\right)s + \left(Z_\delta M_w - M_\delta Z_w\right)$$

$$\doteq\; M_\delta\left[s - \left(Z_w - \frac{Z_\delta}{M_\delta}M_w\right)\right]$$

$$\doteq\; M_\delta\left(s - Z_w\right)$$

$$U_o N_\delta^\alpha \;=\; Z_\delta s + \left(U_o M_\delta - Z_\delta M_q\right)$$

$$\doteq\; Z_\delta\left[s - \left(M_q - \frac{M_\delta}{Z_\delta}U_o\right)\right]$$

$$\doteq\; U_o M_q$$

$$s N_\delta^h \;=\; -Z_\delta\left[s^2 - \left(M_q + M_{\dot{\alpha}}\right)s - \left(M_\alpha - \frac{M_\delta}{Z_\delta}Z_\alpha\right)\right]$$

$$\doteq\; Z_\delta M_\alpha - M_\delta Z_\alpha \;\doteq\; M_\delta Z_\alpha$$

Also, low levels of short period damping may accompany tail size reductions. A variety of full-authority augmentation systems can be constructed to correct these deficiencies and, at the same time, significantly improve aircraft flying qualities and reduce pilot workload. The most obvious stability derivatives to augment are those that cause the trouble in the first place, i.e., M_q and M_α, to improve damping and stability, respectively. There are other alternatives which satisfy the same purposes. Some candidates are noted in Table 3.

To improve static stability, M_α can be augmented with an $\alpha \to \delta$ pitch feedback loop. From stability and pilot control standpoints either aerodynamic or inertial angle of attack will give the same result in principle, although responses to aerodynamic disturbances will depend on which is used. Alternatives include creation of a pitching moment due to pitch angle, M_θ, or its near equivalent, $M_{\int q}$, using integral of the pitching velocity, $\int q\, dt$. When one recalls that normal acceleration is $a_z = \dot{w} - U_0 q$, a similar attitude-like corrective moment can be developed from the integral of normal acceleration. Finally, creation of a pitching moment due to speed changes by creating an M_u can also eliminate divergence and provide static stability.

Although all these possibilities are theoretically suitable for improving modal damping and stability characteristics of the airplane's rigid body high frequency modes, all suffer from some deficiency as the basis for a control system design. Considerations of instrumentation and sensing, including biases and sensor excitation by disturbances, control system compensation needed for flight condition changes, redundancy and redundancy management, etc., must enter into comparative consideration of practical systems. Transition from one flight phase to another, effective dynamics as presented to the pilot, and response of the augmented aircraft to external disturbances are also affected by the particular feedbacks chosen and must be considered in fundamental comparisons of candidate systems.

b. Distinctions Between Sensor Possibilities

A second level, but nonetheless important, distinction between possible systems depends on the feedback architecture, especially as it is

TABLE 3. SOME ELEMENTARY FEEDBACK CONTROL POSSIBILITIES TO CORRECT
RSS AIRCRAFT STABILITY DEFICIENCIES

GENERAL EFFECT	PRIMARY EFFECTIVE STABILITY DERIVATIVE(S) AUGMENTED OR CREATED	FEEDBACK CONTROL POSSIBILITY
Improves Short Period Damping	$M_{\dot{\theta}}$	Pitch Attitude Rate $\theta \rightarrow \delta$
	M_q	Pitching Velocity $q \rightarrow \delta$
	$M_{\dot{\alpha}}$	Angle of Attack Rate $\dot{\alpha} \rightarrow \delta$
Increase Static Stability	M_{θ}	Pitch Attitude $\theta \rightarrow \delta$
	$M_{\int q}$ (Same as M_{θ} when $\Phi = 0$)	Integral of Pitching Velocity $\int q\ dt \rightarrow \delta$
	$U_o M_{\int a_z}$	Integral of Normal Acceleration $\int a_z\ dt \rightarrow \delta$
	M_{α}	Angle of Attack $\alpha \rightarrow \delta$
	M_u	Speed $u \rightarrow \delta$

determined by the sensors used. The sensors provide both desired and undesired signal components; the latter are considered side effects and can be corrected to some extent by increasing the degree of complexity in the system design. They amount to those incidental features of a particular system mechanization which are over and above its primary purpose of improving static stability and short period damping. For example, in a system based on $\delta_e = f(q, \int q \, dt)$, a primary side effect will be the need to provide an up-elevator compensation proportional to $R_o \tan \Phi_o$ in turns to offset the steady state pitching velocity, Q_o. In Table 4 this system is the second one listed, $\int q \, dt$, $q \rightarrow \delta_e$. A similar up-elevator correction would be needed for the first system listed, $q \rightarrow \delta_e$. This system, which involves pitching velocity only as a feedback, will go a long way toward improving the aircraft characteristics, including reduction of the divergence (but not complete elimination). It is probably the simplest system available for highly unstable aircraft control and has great merit as a backup.

When other sensors, such as normal accelerometers, pitch gyros, etc. are used, the side effects may become more involved. They derive, in general, from three sources.

- Biases associated with the particular instrumentation used in the system, e.g., normal accelerometers pick up the total acceleration whereas the augmentation system ideally needs only acceleration perturbed from steady state conditions.

- The degree of airspeed compensation for adjustment of the augmentor system total open-loop gain. This differs with the nature of the sensor (e.g., a_z has a component $U_o q$ so normal accelerometer based systems will typically require a greater range of airspeed compensation than will θ or q based systems).

- The potential for correction of the aperiodic divergence is different for different feedback quantities (e.g., the a_z/δ airplane transfer function has a low frequency zero, $1/T_{h_1}$,* which can, itself, be negative. When this is the case, the divergence due to the negative static margin cannot be stabilized but simply approaches the value of $1/T_{h_1}$).

---

*$1/T_{h_1} \doteq (1/3)(d\gamma/dV)$ when expressed in degrees/knot.

TABLE 4. SYSTEM ARCHITECTURAL POSSIBILITIES AND MECHANIZATIONAL
SIDE EFFECTS FOR SUPERAUGMENTED AIRCRAFT
A. Systems Based on Attitude, Pitch Rate, or Normal Acceleration

$q \rightarrow \delta$

  Reduces divergences, but does not get all the way to stability.
  Requires some up-elevator relief in turns; e.g., $q_e = q - R_0 \tan \Phi_0$

$\int q \ dt, \ q \rightarrow \delta$

  Generally suitable for complete correction of instability.
  Requires up-elevator relief in turns; e.g., $q_e = q - R_0 \tan \Phi_0$

$\int a_z \ dt, \ G_{wo}q \rightarrow \delta \ (G_{wo} = \text{Washout equalization})$

  Corrects for instability when operating on the frontside of the
    speed/power curves. Can have backside instability and
    equivalent backside in climbs.
  Has bias ($a_{z_0} \neq 1 \ g$) when accelerometer is not oriented along
    stability axis for level flight; further bias in climbs and
    dives; yet another bias with a roll limit cycle.
  Requires up-elevator relief in turns; e.g., $a_{z_e} = a_z - \cos \Theta_0 \sec \Phi_0$
    plus increment for q feedback in turn entry/exit.
  Requires more airspeed compensation than attitude-based systems.

$1/\left(T_{\theta_2}s + 1\right)\int Uq \ dt, \ G_{wo}q \rightarrow \delta \ [\text{Pseudo } a_z]$

  Generally suitable for complete correction of instability (replaces
    dγ/dV-based limitations with $1/T_{\theta_1}$; removes accelerometer bias
    issues).
  Requires up-elevator relief in turns.
  Requires more airspeed compensation than attitude-based systems.

$\theta, \ \dot{\theta} \rightarrow \delta$

  Generally suitable for complete correction of instability.
  Gain changes in turns, with associated F_s/g lightening, etc.
  Requires elevator signal relief (trim) for $\theta \neq 0$.

$\theta, \ q$ or $\theta, \ G_{wo}q \rightarrow \delta$

  Generally suitable for complete correction of instability.
  Gain changes in climbing/diving turns.
  Climb/dive steady-state signal relief.
  Requires up-elevator relief in turn entries/exits, depending on
    specifics of G_{wo}.

TABLE 4. (Concluded)

B. Systems Based on Angle of Attack or Speed

α_A, q or α_A, $G_{wo}q \rightarrow \delta$ (α_A = aerodynamic α)

    Generally suitable for correction of instability.

    Phugoid not much modified if G_{wo} focuses only on high frequencies.

    Gust sensitivity associated with α_A.

    α_{bias} position and scale factor errors (α sensor installation).

    Requires trim set point.

    Requires up-elevator relief in turn entries/exits, depending on
        specifics of G_{wo}.

α_I, q or α_I, $G_{wo}q \rightarrow \delta$ (α_I = inertial α)

    Generally suitable for correction of instability.

    Phugoid not much modified if G_{wo} focuses only on high frequencies.

    Requires trim set point.

    Requires up-elevator relief in turns, depending on specifics of G_{wo}.

Variants of α Systems

$$\hat{\alpha} \doteq \frac{U_0}{[Z_w - M_w(Z_\delta/M_\delta)]} \frac{a_z}{U^2}$$

and other means of computing α.

u_I, $G_{wo}q \rightarrow \delta$ (u_I = inertial u)

    Generally suitable for correction of the instability.

    May be subject to excessive pitching with a u_g input.

    Must establish a set point or trim, $U = U_0$.

    Phugoid damping ratio is reduced if G_{wo} focuses only on high
        frequencies.

    Requires up-elevator relief in turns, depending on specifics of G_{wo}.

u_A, $G_{wo}q \rightarrow \delta$

    As in item above.

    Gust Sensitivity associated with u_A.

    Scale and bias errors associated with u sensor installation.

Table 4A summarizes these side effects for the attitude type neutral stability systems. The effects on flying qualities depend inherently on the degree to which these characteristics are corrected. Clearly, in a multiple redundant system, the complexity of correction is a major issue since any single channel should be made as simple and troublefree as possible. The issue for a given system then becomes how far one must go to correct the side effect created by the architectures selected. These are matters which have to be considered on an ad hoc basis for each heavily augmented RSS design. In this sense the table simply presents a checklist for particular design possibilities.

Relaxed static stability aircraft which are heavily augmented with feedback of angle of attack or speed to correct static divergence have effective dynamic characteristics which are essentially conventional in form. These are summarized in Table 4B. As far as piloted control is concerned, the derivatives M_α or M_u are simply augmented to levels appropriate for static stability correction and good conventional aircraft flying qualities. For aircraft responses to disturbances however, a distinction between conventional and heavily augmented aircraft may be pertinent depending upon the nature of the sensors used in the augmentation system. The disturbance sensitivities will specifically depend on whether an angle of attack system is based upon inertial or aerodynamic angle of attack; similarly, for a speed system on whether inertial or air speed is used. The primary difference, however, between these types of systems and those based upon some form of attitude is in the nature of the stabilizing characteristics. An angle of attack system tends to stabilize the aircraft relative to the instantaneous (in the case of aerodynamic α_A) or steady state (for inertial $\alpha_I \doteq W/U_o$) velocity vector orientation. This is, in essence, a weathercock stability and may involve significant pitch attitude changes. A speed-based system creates pitching moment proportional to change from a trim or reference speed U_o. There can be significant sensitivity to wind shear and forward gusts with this type of system since the aircraft must pitch to accomplish a balance of fore and aft forces.

Neither angle of attack nor incremental speed feedbacks are simple to instrument, particularly on a multiple redundant basis. Systems of this type could make use of sophisticated complementary filter or state reconstruction/observer filters to generate the appropriate feedback signals. Unlike the attitude variety feedbacks, which do an excellent job in stabilizing the phugoid characteristics, angle of attack and speed are by themselves not appropriate for improving the phugoid dynamics. Indeed, in a normal airplane, angle of attack changes are very small in the phugoid oscillation. The stability derivative M_u tends to affect the phugoid frequency; to improve phugoid damping would require the creation of a new derivative, $M_{\dot{u}}$. Unfortunately this type of damping augmentation can create dramatic pitching motions when the aircraft is disturbed by forward gusts or shears. Consequently in both types of systems a certain amount of pitching velocity feedback, or its equivalent, is desirable to improve phugoid damping. These are indicated by the $G_{wo}q$ terms in Table 4B, which signify a washed-out pitching velocity feedback or its equivalent. This pitch rate feedback is, of course, also very effective for short period damping augmentation. When used for this purpose, with gains that are suitable for relatively heavily augmented aircraft, the effective short period characteristics are dominated by the pitching velocity feedback and can be very similar to those of the attitude based systems (as far as the short term time response characteristics are concerned).

The side effects and other properties for angle of attack or speed based systems do not compare favorably with those for the attitude systems. Based on these comparisons, heavily augmented aircraft using α or U as basic feedback quantities are probably not as likely as an attitude-based system. This statement applies especially when the required augmentation system is essential to flight safety and hence multiple-redundant. When special requirements exist, or where dual or single thread non-flight critical conditions are present, the advantages of attitude systems are not as prominent.

c. The Superaugmented FCS

As the basis for a generalized treatment of flight control systems for relaxed-static stability aircraft we will use the system shown in Fig. 2 from Ref. 2. This choice will suffice to illustrate most of the critical issues associated with superaugmented FCS. It will also be a major contender as far as arguments advanced in the last section are concerned. And, further, it serves as an excellent example of current and future practice. That is, the basic superaugmented structure shown in Fig. 2 corresponds to the basic pitch control channel of the Space Shuttle, the X-29A pitch system, and some advanced versions of the F-16 FCS (for certain flight conditions).

As a flight-critical system, all elements except possibly those involved in turn compensation would be multiple-redundant. This is one reason for basing the system on pitch rate sensors which are simple and hardy, introduce only minor scaling and bias errors, and are easily made part of a minimum complexity multiple-redundant system. With skewed sensors, for instance, five or six rate gyros can provide dual fail-operate capability for rates in all three axes.

The basic low-frequency control law which drives the pitch axis actuator(s) with a signal proportional to pitch rate error, q_e, and the integral of pitch rate error, q_e/s, is simply:

$$\delta = \underbrace{K_q q_e}_{\substack{\text{Propor-}\\\text{tional}\\\text{Term}}} + \underbrace{\frac{K_q/T_q}{s} q_e}_{\substack{\text{Inte-}\\\text{gral}\\\text{Term}}}$$

Note that the equation is just the block labeled "equalization" in Fig. 2. Consequently, the augmentor as a stabilizer creates a pitching moment proportional to q and one proportional to $\int q\, dt$. When the aircraft-alone dynamics include a divergence, the aircraft/augmentor combination will be conditionally stable and a minimum value for the gain,

$$Q_o = R_o \tan \phi_o$$

Turn Compensation

ϕ

R

Pilot Command δ_p

Command Filter

q_c

Pitching Velocity Error q_e

Equalization $\dfrac{K_q(s+1/T_q)}{s}$

Actuator and Bending Mode Filters

Pitch Control δ

Aircraft Dynamics

Yawing Velocity, R

Bank Angle, ϕ

Pitching Velocity, q

$$\frac{q}{q_{ss}} \rightarrow \frac{(T_q s + 1)}{s\left[\left(\dfrac{s}{\omega_n}\right)^2 + \dfrac{2\zeta}{\omega_n} s + 1\right]}$$

Pitch Rate Sensors
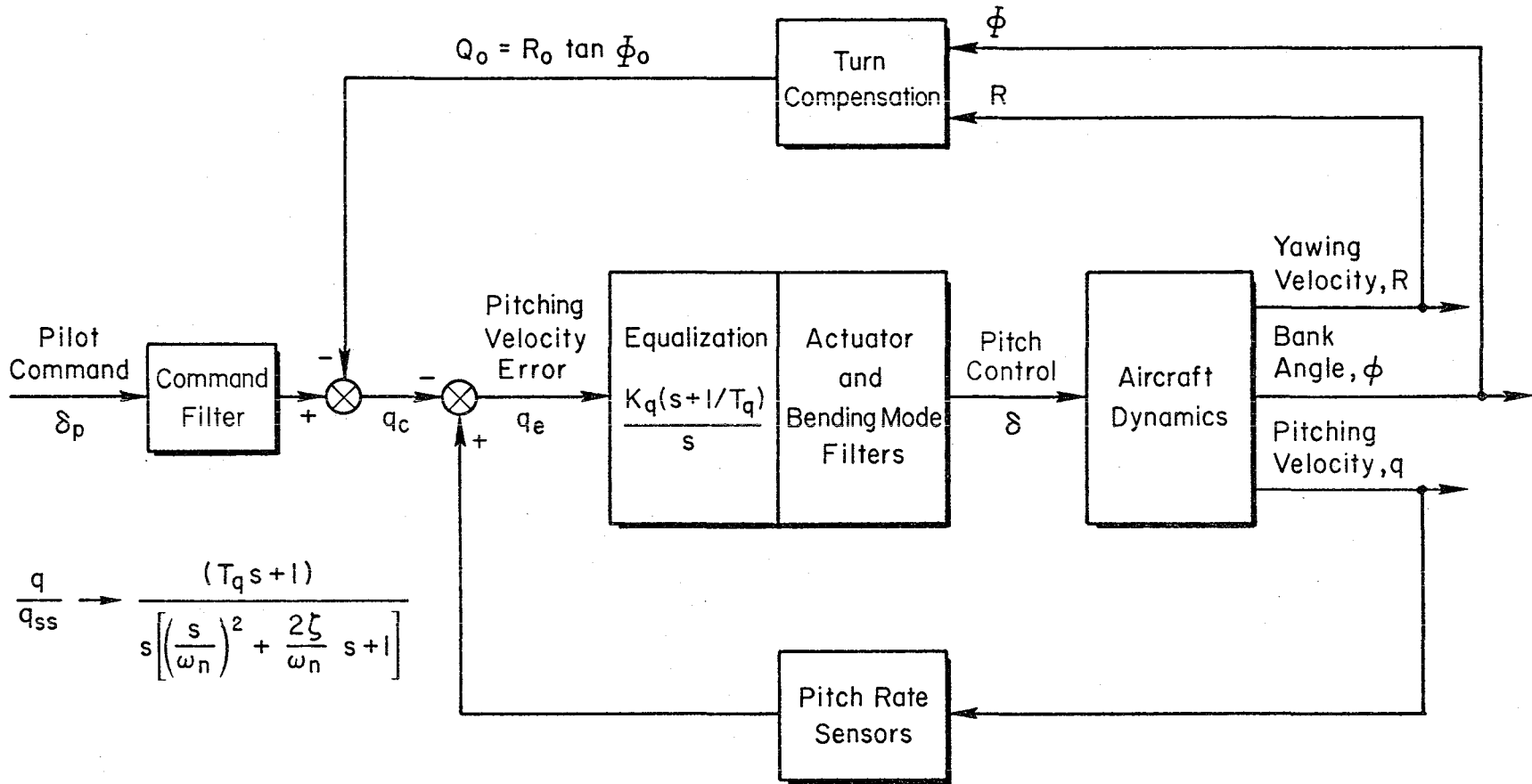
Figure 2. Typical Pitch SAS for Heavily Augmented Aircraft

K_q/T_q, is needed for stability. At the other extreme, the maximum gain possible is set by the closed-loop system high frequency stability limits. The latter will depend primarily on high-frequency lags (and leads) due to actuator(s), rate sensor, and other computational or filter dynamics within the flight control system, and on the aircraft flexible mode and other high frequency properties.

When the saturation characteristics of the aircraft control surface (and surface rates) are taken into account, the maximum gain may be further restricted. The higher the open-loop gain, K_q, of the augmentor, the smaller the pitching velocity error needed to saturate the control. If the aircraft alone has even some slight inherent stability, this may be of little consequence. However, when the aircraft-alone is divergent, a saturated control will not correct for this divergence. The pilot command input may be deliberately limited to avoid saturating the controls, but external disturbances generally are not. In fact, robustness to control saturation due to shears and other atmospheric disturbances is one reason for the selection of the Fig. 2 system. Some of the other stabilization possibilities listed in Table 3 result in systems which are not as tolerant external disturbances and can cause significantly higher probabilities of limiting elevator positions.

B. SUPERAUGMENTED CONTROL SYSTEM PRIMARY DYNAMIC CHARACTERISTICS AND REGULATORY PROPERTIES

1. Stability Characteristics of the Closed-Loop Aircraft/Controller System

The general class of superaugmented aircraft has characteristics markedly different from conventional aircraft. Figure 3 shows a system survey for a SM = 5 percent $\bar{c}$ unstable transport aircraft in cruise (Ref. 3). Actuator and other high frequency lags are lumped into a 12 rad/sec "effective actuator."

$$-\frac{q}{q_e} = \frac{1.935\ (0.0065)(0.459)(2.0)}{(-0.238)(0.941)[0.152\ ,\ 0.0781]}\ \frac{12.^2}{[.707,12]}$$

$$\underbrace{(1/T_{\theta_1})}\ \underbrace{(1/T_{\theta_2})}\ \underbrace{(1/T_q)}$$

$$\underbrace{(1/T_{sp_2})}\ \underbrace{(1/T_{sp_1})}\quad \underbrace{[\zeta_p\ ,\ \omega_p]}\quad \underbrace{[\zeta_a\ ,\ \omega_a]}$$

where

$$(a) \equiv (s+a)$$
$$[\zeta,\omega] \equiv [s^2 + 2\zeta\omega s + \omega^2]$$
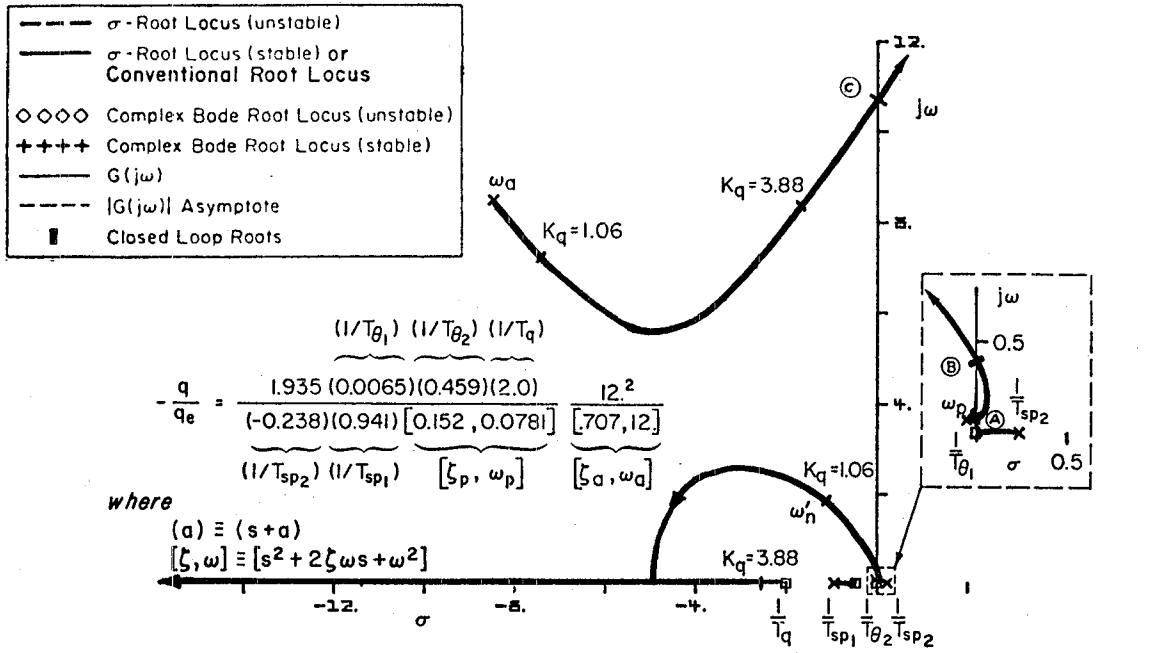
a) s-plane Root Locus
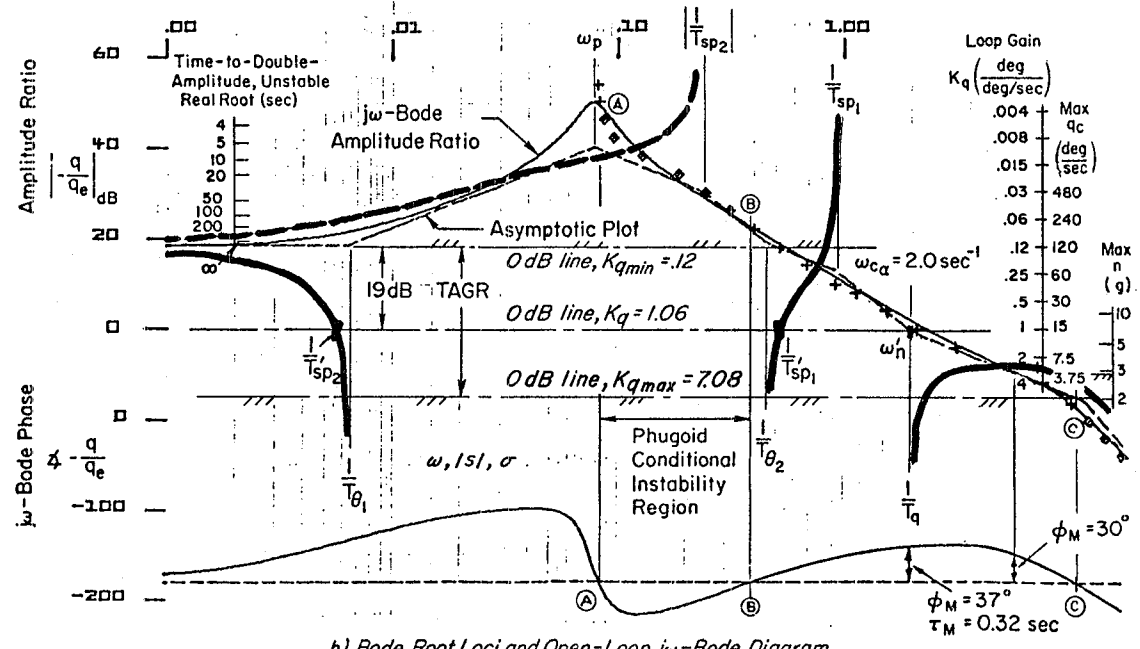
b) Bode Root Loci and Open-Loop jω-Bode Diagram

Figure 3. System Survey of Superaugmented Pitch Rate Loop
(SM = 5 Percent Unstable)

Following the loci in Fig. 3, as gain is increased the three aircraft-alone modes are modified as follows[*]:

- The airplane short-period divergence, $1/T_{sp_2}$, is decreased as gain, K_q, is increased; becomes stabilized as it passes through the $j\omega$-axis; and finally approaches the airplane attitude numerator zero at $-1/T_{\theta_1}$ to form the closed-loop speed mode.

- The short-period subsidence, $1/T_{sp_1}$, proceeds along the real axis to the right toward $-1/T_{\theta_2}$ to form the heave mode. Part of the damping given up by this subsidence is transferred as an increase in damping to the divergence.

- The phugoid, which for the airplane-alone is stable but lightly damped ($\zeta_p = 0.152$), initially becomes unstable (point (A)) as the augmentor gain is increased. For controller gains 0.004 ≤ K_q ≤ 0.06 deg/deg/sec the closed-loop phugoid is unstable (denoted by ◇◇◇ on the Bode root locus). This is the region between points (A) and (B). For larger gains the phugoid is driven back into the left half plane [at (B)] to form the second-order pitch mode [ζ', ω_n'].

The system with nominal gain $K_q = 1.06$ rad/rad/sec reflects several different "good" control system design, response, and stability considerations. These include (Ref. 3):

- Responses which are similar to those of low-order, well-damped, rapidly responding systems. The low-frequency open-loop poles ($1/T_{sp_1}$ and $1/T_{sp_2}$) are driven nearly into open-loop zeros (at $1/T_{\theta_1}$ and $1/T_{\theta_2}$), such that they essentially cancel, leaving a quadratic dominant mode.

- Insensitivity of the low frequency response components to gain changes. This is illustrated by the nearly vertical slopes of the Bode root loci in Fig. 3b as they drive into $1/T_{\theta_1}$ and $1/T_{\theta_2}$ around the reference crossover region.

---

[*]One or more primes on a variable or transfer function symbol indicate one or more loops have been closed.

- A well damped, stiff, and rapidly responding closed-loop system dominant pitch mode [$\zeta' = 0.51$, $\omega_n' = 2.22$ rad/sec].

- Closed-loop system bandwidth which is sufficiently large to be responsive to pilot command so little pilot lead is required to achieve precision control.

- System stability with large stability margins. A margin of 19 dB exists on the low-gain end relative to the reference $K_q = 1.06$. Thus, a gain reduction of nearly a factor of 10 would be needed to get back to the divergence. At the high-frequency end, the crossover frequency of $\omega_{c_a} = 2$ rad/sec (which sets the desired controller gain at $K_q = 1.06$) provides a gain margin of 16.8 dB, a phase margin, ϕ_M, of 37 deg and a delay margin, τ_M, of 0.32 sec. Thus, high frequency lags or parameter uncertainties currently ignored in the design would have to contribute 37 deg of phase lag, or the equivalent of a pure time delay of 0.32 sec, before the closed-loop system would be neutrally stable at the gain selected.

This system survey reflects only the rigid body airplane characteristics. It presumes that the high frequency amplitude ratios of the flexible modes are less than the nominal zero dB line, or alternatively, that these modes are phase stable. Otherwise the nominal gain would have to be reduced.

The discussion above has focused on superaugmentation characteristics in the nominal linear case. An additional important question is how these characteristics are affected by nonlinearities -- in particular control effector saturation. Returning to Fig. 3, the control system gain should be low enough so that the augmentor is very seldom saturated. Saturation may be viewed as reducing the effective gain K_q and thus shifting the (Fig. 3b) nominal 0 dB line upward. The closed-loop roots are then shifted back toward those of the open-loop aircraft. When completely saturated, the effective controller gain approaches zero and the effective aircraft dynamics are those of the airplane alone. Unfortunately, in this event the pilot also has no control available in one direction, since the surfaces are saturated. This will be considered further below.

For pilot command limiting these kinds of considerations are easy to show on the plot of Fig. 3b. They appear as commanded pitching velocities, $q_{c_{max}}$, which would just saturate the system when gains are set at particular levels. These can also be converted to load-factor commands via $\dot{q}_{c_{max}} = (n_{max} - 1)g/U_o$. Scales showing the maximum load factor and pitching velocity commandable without position limiting are shown on the right side of the Bode root locus plot next to that for the controller gain, K_q, in linear units. These values must be compatible with the $q_{c_{max}}$ required for a given task/flight phase, which typically will be determined by the maximum load factor requirement taken from the airplane "V-g" diagram.

2. Dominant Mode Characteristics

The pitch-attitude/pilot-input transfer functions for a conventional stable aircraft and for a superaugmented aircraft are shown in Fig. 4. For the simplest case when the relationship between the pilot's controller deflection and the pitch rate command $G_i(s)$ is a constant, the dominant mode of the superaugmented aircraft is identified with the short period characteristics of the flying qualities and flight control specifications (MIL-F-8785C and MIL-F-9490D). (Later we shall consider other possibilities.) The closed-loop pitching-velocity/pitch-rate-command transfer function has a form quite like that of the conventional aircraft except that the lead time constants are different. For the conventional aircraft it is T_{θ_2} (which is inversely proportional to the lift curve slope of the airplane), whereas for the superaugmented aircraft it is T_q (a control system quantity). The difference can be minimal (e.g., in the X-29 the control system parameters are adjusted so that the effective attitude lead is T_{θ_2}), or profound (e.g., in the Space Shuttle the two leads are different by a factor of three, $T_{\theta_2} = 3 T_q$).

The dominant mode properties for the closed-loop portion [$G_i(s)$ not included] of the superaugmented system are illustrated in Fig. 5. This is a blow-up of a limited frequency region around crossover. Figure 5 shows that the closed-loop characteristics [ζ' and ω_n'] are functions

δ_p → [G_i(s)] → q_c → (⊗) → q_ε → [-K_q ((s + 1/T_q)/s)] → δ → [q/δ] → q

Pilots Controller Deflection | Pitch Rate Command | Pitch Rate
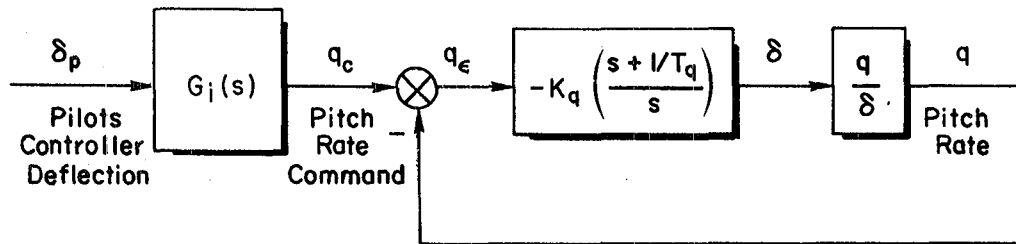
- **Effective Aircraft Response**

$$\frac{\theta}{\delta_p} = G_i(s)\frac{\theta}{q_c}$$

—— Superaugmented:

$$\frac{\theta}{q_c} \doteq \frac{K_i K_q M_\delta (s + 1/T_q) e^{-\tau_s s}}{s\left[s^2 + 2\zeta'\omega_n' s + \omega_n'^2\right]}$$

—— Conventional:

$$\frac{\theta}{q_c} = \frac{K_i M_\delta (s + 1/T_{\theta 2}) e^{-\tau_c s}}{s\left[s^2 + 2\zeta'\omega_n' s + \omega_n'^2\right]}$$

Figure 4. Pitch Attitude Characteristic for
Superaugmented and Conventional Aircraft
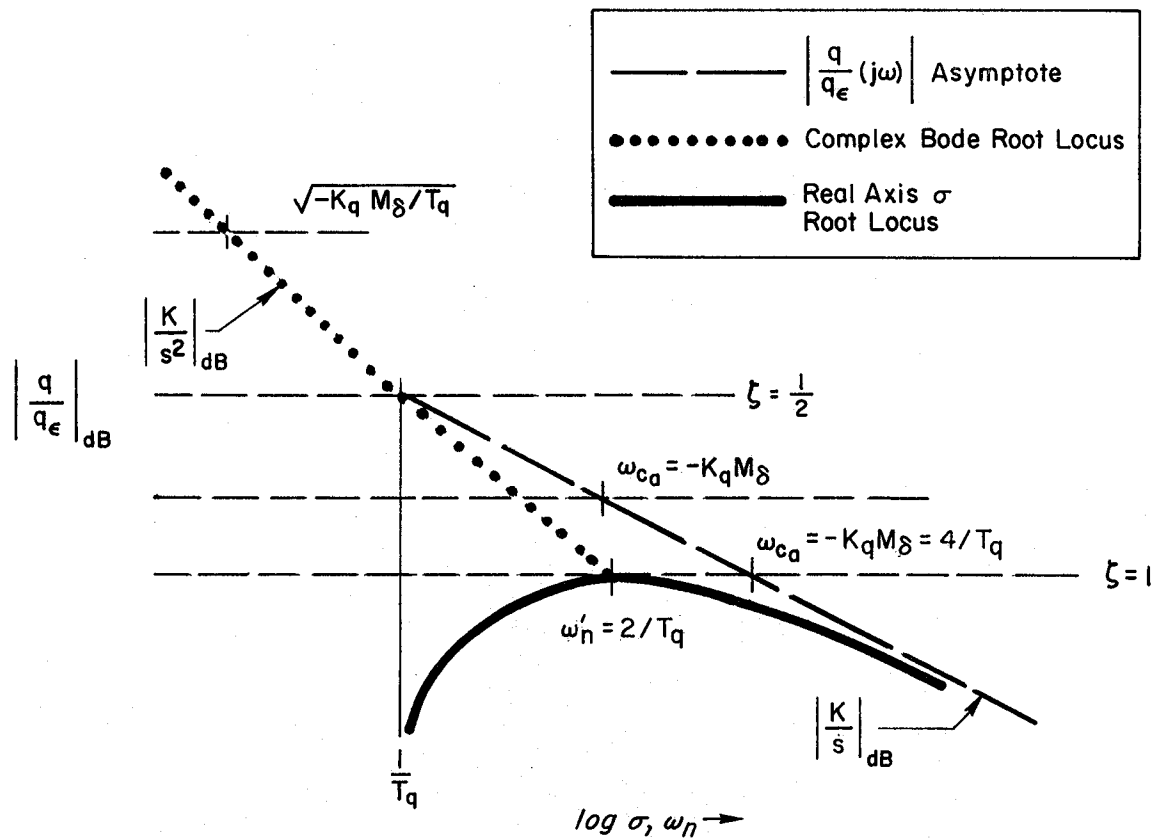
$$\left.\frac{q}{q_\epsilon}\right|_{\substack{\text{open}\\\text{loop}}} = \frac{-K_q M_\delta (s + 1/T_q)}{s^2}$$

$$\left.\frac{q}{q_c}\right|_{\substack{\text{closed}\\\text{loop}}} = \frac{(T_q s + 1)}{\left[\left(\dfrac{s}{\omega_n'}\right)^2 + \dfrac{2\zeta'}{\omega_n'} s + 1\right]}$$

$$\zeta' = \frac{1}{2}\sqrt{-K_q M_\delta T_q} = \frac{1}{2}\sqrt{\omega_{c_a} T_q}$$

$$\omega_n^{2\prime} = -K_q M_\delta / T_q = \omega_{c_a}/T_q$$

Figure 5. Superaugmented Dominant Mode Approximation

only of two parameters, the control system lead time constant, T_q, and the frequency, $\omega_{c_a} = -K_q M_\delta$, at the intersection of the selected (dB) gain line and the amplitude asymptote. The closed-loop damping ratio can also be simply related to open-loop phase margin which is

$$\phi_M = \tan^{-1} T_q \omega_{c_a}$$

$$\doteq \frac{\pi}{2} - \frac{1}{T_q \omega_{c_a}}$$

when high frequency lags and delays are neglected. Then, since $\zeta' = \sqrt{\omega_{c_a} T_q / 2}$,

$$\zeta' \doteq \frac{1}{4\left(\frac{\pi}{2} - \phi_M\right)}$$

Notice that the only airframe parameter of importance in the dominant mode characteristic is the control effectiveness M_δ. As shown in the more detailed Bode root-loci presented earlier, all the other rigid body aerodynamic characteristics are represented by nearly cancelling poles and zeros. This insensitivity to most airframe parameters is a key property of superaugmented systems.

The transient response characteristics of the dominant mode are illustrated in Figs. 6 and 7. (An initial dead time, τ, is included in Fig. 6 to account for the summation of high frequency leads and lags.) When contrasted with a conventional aircraft the pitch rate overshoot, q_{max}/q_c, of the superaugmented aircraft is highly constrained, as shown in Fig. 7. It depends, in fact, only on the damping ratio, ζ. A summary of the pitch response parameter differences between conventional and superaugmented aircraft is given in Table 5.
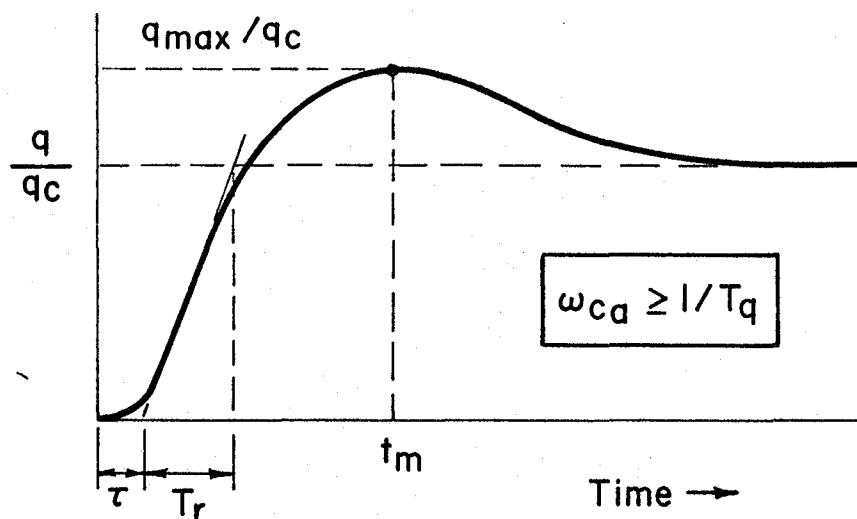
$$\bullet \quad \omega_{c_a} \equiv -K_q M_\delta \quad \text{for} \quad \frac{4}{T_q} > \omega_{c_a} \geqslant \frac{1}{T_q}$$

$$\bullet \quad T_r = 1/\omega_{c_a}$$

$$\bullet \quad \frac{t_m}{T_q} = \begin{cases} \pi/2 & \text{for } \omega_{c_a} T_q = 2 \\[2em] \dfrac{2 \tan^{-1}\left(\dfrac{\sqrt{\omega_{c_a} T_q}\ \sqrt{4 - \omega_{c_a} T_q}}{\left(\omega_{c_a} T_q - 2\right)}\right)}{\sqrt{\omega_{c_a} T_q}\ \sqrt{4 - \omega_{c_a} T_q}} & \text{for } 4 > \omega_{c_a} T_q \neq 2 \geqslant 1 \end{cases}$$

$$\bullet \quad \frac{q_{max}}{q_c} = 1 + e^{\omega_{c_a} t_m/2}$$

$$\leqslant \frac{q_{max}}{q_c}\bigg|_{\omega_{c_a} T_q = 1} = 1 + e^{-2\pi/3\sqrt{3}} \doteq 1.30$$

Figure 6. Superaugmented q/q_c Transient Response ($\omega_{c_a} \geqslant 1/T_q$, $G_1 = $ Constant)
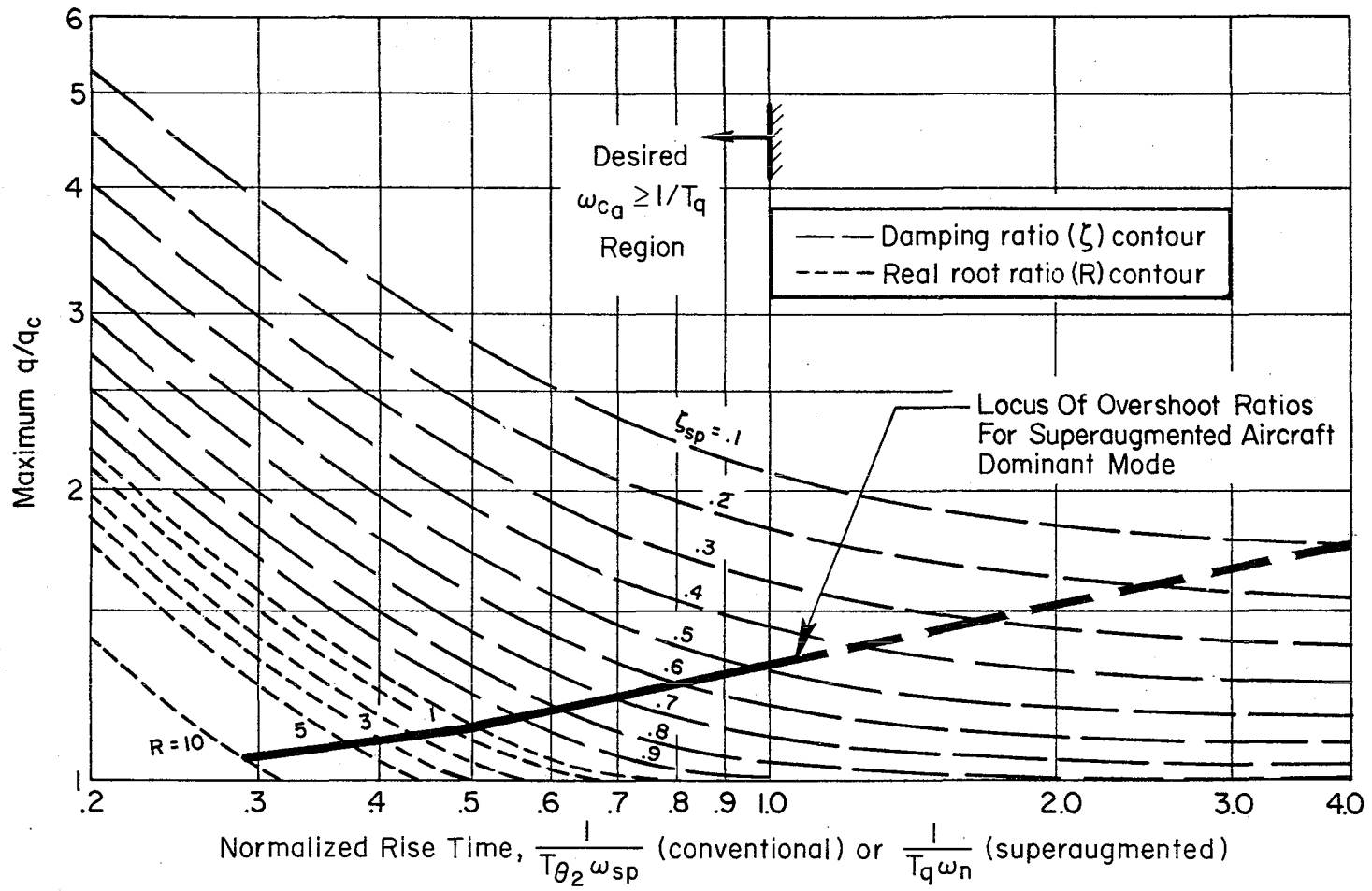
Figure 7. Maximum Pitch Rate Overshoot Variation for Superaugmented Aircraft

TABLE 5. COMPARISON OF PITCH ATTITUDE RESPONSE GOVERNING PARAMETERS
FOR CONVENTIONAL AND SUPERAUGMENTED AIRCRAFT

DYNAMIC PROPERTY	CONVENTIONAL		SUPERAUGMENTED	
	PARAMETERS	PRIMARY DESIGN FACTORS	PARAMETERS	PRIMARY DESIGN FACTORS
Lead Time Constant T	$\dfrac{1}{T_{\theta_2}} \doteq -Z_w + \dfrac{Z_\delta}{M_\delta} M_w$	C_{L_α}; wing	T_q	Governed predominantly by closed-loop control system Stability, Response, and Margins
Undamped Natural Frequency ω_n	$\omega_{sp}^2 = Z_w M_q - M_\alpha$	Maneuver Margin; $C_{M_{CL}}$; Tail	$\omega_n^2 = \dfrac{\omega_{ca}}{T_q}$ $= \dfrac{K_q}{T_q}[M_\delta]$	**Control System Parameters** T_q - Lead time constant K_q - Gain
Normalized Rise Time $\omega_n T_r$	$\dfrac{1}{T_{\theta_2} \omega_{sp}}$		$\dfrac{1}{T_q \omega_n} = \dfrac{1}{\sqrt{T_q \omega_{ca}}}$ $T_r = \dfrac{1}{\omega_{ca}}$	**Airframe Parameter** M_δ - Surface effectiveness (C_{m_δ})
Damping Ratio ζ	$(\zeta\omega)_{sp} = -(Z_w + M_q + M_{\dot\alpha})$	C_{L_α}; Wing C_{m_q}; Tail Pitch Damper	$\zeta = \dfrac{\sqrt{T_q \omega_{ca}}}{2}$ $= \dfrac{1}{2}\sqrt{K_q T_q [M_\delta]}$	
Delay Time τ_d		Actuator and Manual Control lags		Actuator lag + Stick filters + Bending Mode filters + Computational delays

Note: In the CONVENTIONAL PRIMARY DESIGN FACTORS column, a brace spans the Lead Time Constant, Undamped Natural Frequency, and Normalized Rise Time rows, labeled "Set Predominantly by Airframe".

3. Fundamental Stability Margins

a. Gain, Phase, and Delay Margins for the Linear Airframe

1) Low Frequency Gain Margin

(a) Divergence Critical

As noted previously there are two conditions which may set the low frequency gain margin for the basic superaugmented design: stabilization of the divergence, $1/T_{sp_2}$, and restabilization of the phugoid mode. For the example seen in Fig. 3 the most stringent requirement is that on the stabilization of the divergence, and we consider this case first.

Figure 8 shows that the gain of the low frequency Bode asymptote provides the criterion for stabilization of the divergence. This may be converted to a low frequency gain margin, GM_{lo}, given by Eq. 6.

$$GM_{lo} = \frac{\omega_{c_a}(1/T_q)}{|\omega_{sp}^2|}\left(\frac{1}{T_{\theta_1}T_{\theta_2}\omega_p^2}\right) \doteq \frac{\omega_{c_a}(1/T_q)}{|Z_w M_q - M_\alpha|(T_{\theta_1}T_{\theta_2}\omega_p^2)} \qquad (6)$$

where here $\omega_{sp}^2 = 1/T_{sp_1}T_{sp_2} < 0$. This gain margin is referenced to gain reflected by typical 0 dB line and the asymptotic crossover frequency ω_{c_a}.

(b) Phugoid Critical

As noted previously, there is a second conditional instability on the phugoid mode which might in some cases set the minimum gain required. Such a situation is shown hypothetically in Fig. 9. We wish to find an expression for point Ⓑ which sets $K_{q_{min}}$. This is more complicated than the previous case, but a straightforward approach would be application of the Routh-Hurwitz criterion. Unfortunately, this gives a
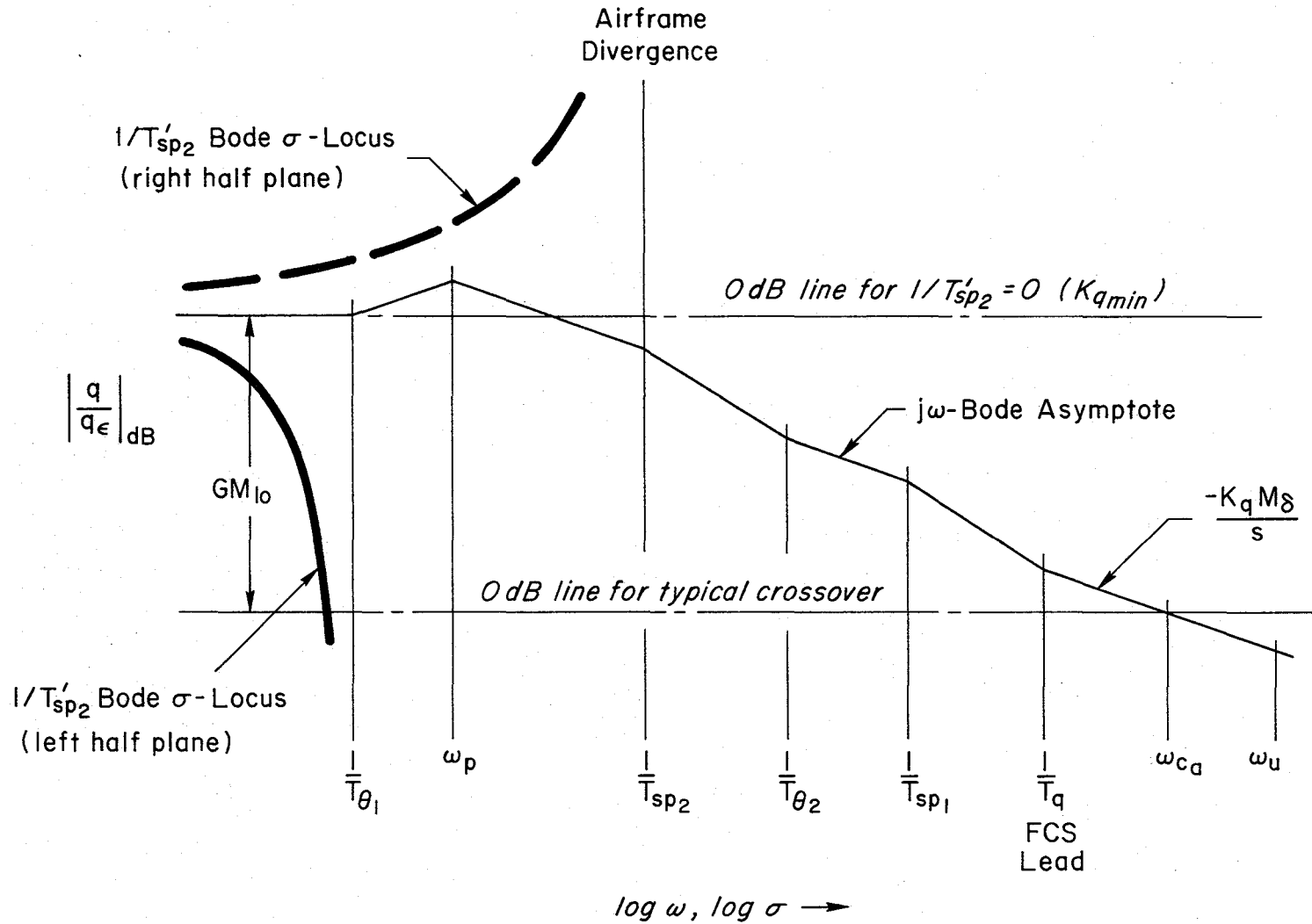
Figure 8. Partial Bode Sketch Showing $K_{q_{min}}$ Set by Requirement for Stabilization of the Divergent Real Pole, $1/T_{sp2}$
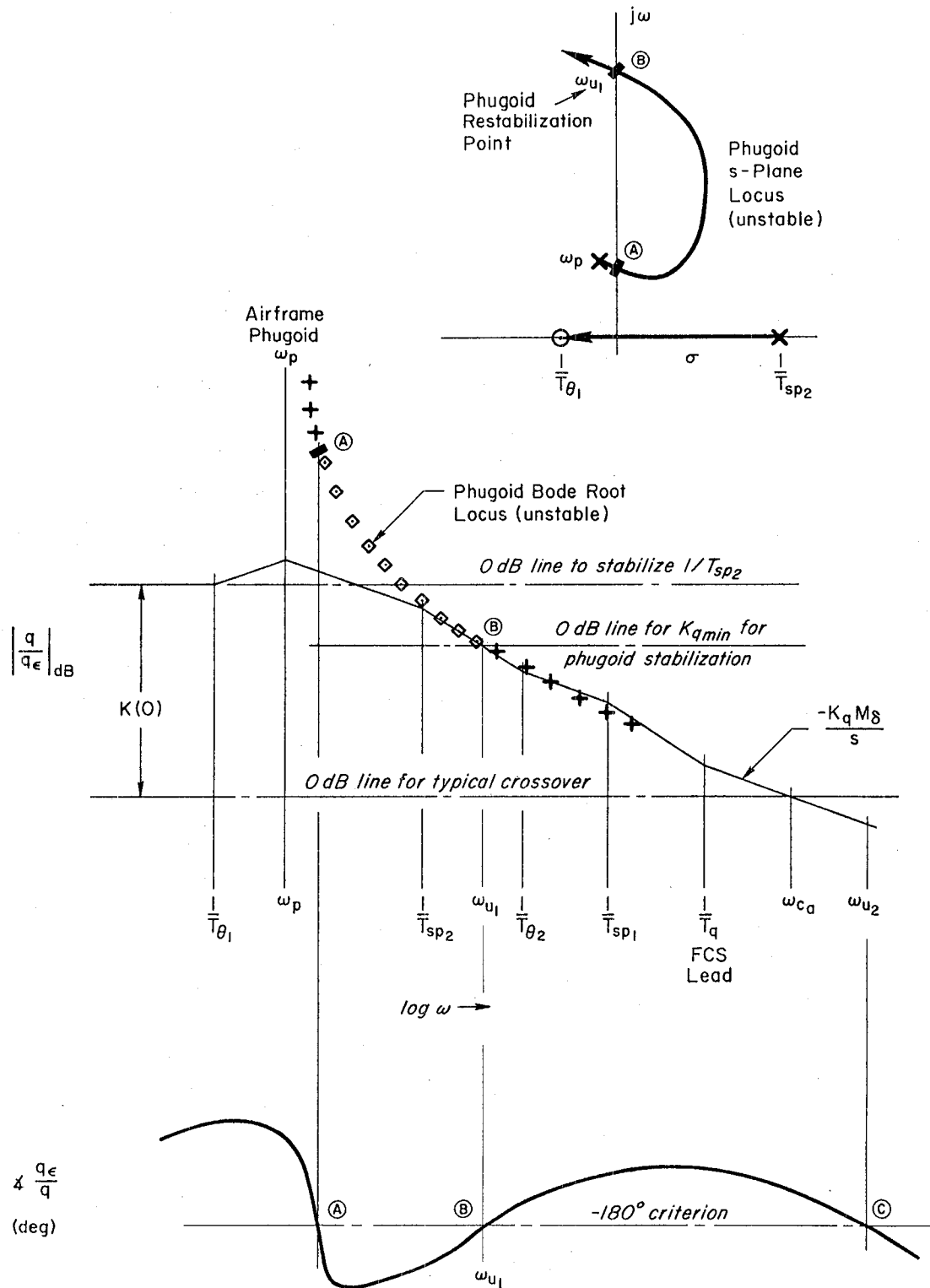
Figure 9. Partial System Survey Sketch

rather complex quadratic expression for $K_{q_{min}}$. While this could easily be solved numerically for a specific case, the approach does not achieve our basic goal of explicitly relating the stability boundary to generic literal airframe configuration parameters. An alternate approach, which does accomplish this goal, is to search for the points at which the phase angle curve crosses the −180 deg stability criterion line. This process (but not the Routh procedure) can be simplified by use of a short period approximation. [That a short period approximation can be used to determine "phugoid" stability is a somewhat surprising consequence of the unconventional nature of the superaugmented aircraft. Recall that this root begins at the airframe phugoid, but ultimately becomes the superaugmented pitch mode. The basis of the validity of the approximation is that the phase crossover point Ⓑ coincides with a section of the Bode amplitude asymptote (just below $1/T_{\theta_2}$) which is the same for the short period approximation and the complete 3-DOF form.] The implications of this approximation in the s-plane are illustrated in Fig. 10, where $Ⓑ_{sp} \doteq Ⓑ$.

a) 3 Degree-of-Freedom   b) Short Period Approximation
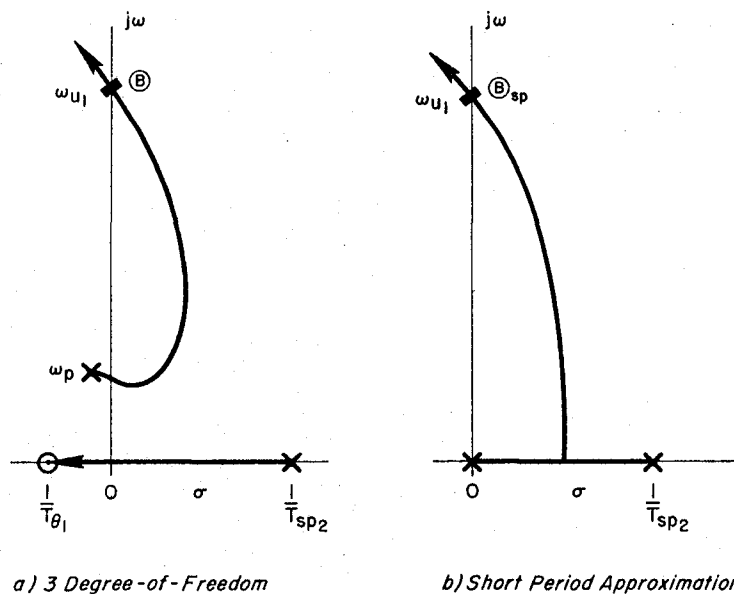
Figure 10. Low Frequency Differences in the Superaugmented Loop Closure Between 2 and 3 Degree-of-Freedom Models

When an expression for the open-loop phase angle is written, an approximate expression for the restabilization frequency ω_{u_1} can be developed as follows. The phase angle for the short period airplane plus controller (neglecting actuator and other high frequency effects) is given by,

$$\phi = -\frac{\pi}{2} + (-\pi + \tan^{-1} T_{sp_2}\omega) + \tan^{-1} T_{\theta_2}\omega$$

$$- \tan^{-1} T_{sp_1}\omega + \tan^{-1} T_q\omega$$

Using approximations appropriate for the phase around $\omega = \omega_{u_1}$,

$$\phi \doteq -\frac{3\pi}{2} + \left(\frac{\pi}{2} - \frac{1}{|T_{sp_2}|\omega}\right) + \left(T_{\theta_2} + T_q - T_{sp_1}\right)\omega$$

$$= -\pi - \frac{1}{|T_{sp_2}|\omega} + \left(T_{\theta_2} + T_q - T_{sp_1}\right)\omega$$

The phase will be just −180 deg when

$$-\frac{1}{|T_{sp_2}|\omega_{u_1}} + \left(T_{\theta_2} + T_q - T_{sp_1}\right)\omega_{u_1} = 0$$

Thus

$$\omega_{u_1} \doteq \sqrt{\frac{1}{|T_{sp_2}|\left(T_{\theta_2} + T_q - T_{sp_1}\right)}} \qquad (7)$$

Strictly speaking this approximation assumes

$$1/T_{sp_2} < 1/T_{\theta_2} \qquad (8)$$

which is valid only for low levels of unstable static margin, but from numerical checks Eq. 7 also appears to be reasonably accurate at fairly

high unstable static margins. Under these same assumptions a low frequency gain margin can be estimated at ω_{u_1} as

$$GM_{1o} \doteq \frac{\omega_{c_a}(1/T_q)}{\omega_{sp}^2} \frac{\sqrt{\left|T_{sp_2}\right|\left(T_{\theta_2} + T_q - T_{sp_1}\right)}}{T_{\theta_2}} \qquad (9)$$

The important question at this point is whether Eqs. 6 or 9 sets the minimum gain requirement. It may be seen from Eq. 6 that an answer to this question requires setting a strategy for scheduling the FCS time constant T_q. Several different possibilities can and have been used. For a highly unstable static margin the divergence is usually critical and Eq. 6 governs.

2) High Frequency Gain Margin

To establish the high frequency gain margin we will assume that crossover, ω_{c_a}, is set on or near a K/s-like region above $1/T_q$. The phase in the neighborhood of the high frequency crossover can then be approximated by (with lags and leads above crossover represented by a net effective τ)

$$\phi_{hi} \doteq -\pi + \tan^{-1} T_q\omega - \tau\omega$$

$$\doteq -\pi + \left(\frac{\pi}{2} - \frac{1}{T_q\omega}\right) - \tau\omega$$

$$= -\frac{\pi}{2} - \frac{1}{T_q\omega} - \tau\omega$$

Thus the high frequency phase in the crossover region, expressed in phase margin units, is

$$\phi_M(\omega) \doteq \tan^{-1} T_q\omega - \tau\omega \qquad (10a)$$

$$\doteq \frac{\pi}{2} - \frac{1}{T_q\omega} - \tau\omega \qquad (10b)$$

(Note, if the K/s-like region is established by $1/T_{\theta_2}$ instead of $1/T_q$, as it is in some systems, simply replace T_q by T_{θ_2} in the above equations.)

The effective time delay τ is a composite quantity which takes into account all the higher frequency (above ω_{c_a}) lags, leads, and pure delays. These may include actuator and sensor dynamics, various filters, and the high frequency flexible mode characteristics of the airplane (see, e.g., Ref. 3).

An approximation to the high frequency instability frequency ω_{u_2} may be found by setting phase margin in Eq. 10b to zero. Then

$$\omega_{u_2}^2 - \frac{\pi}{2\tau}\,\omega_{u_2} + \frac{1}{T_q\tau} = 0$$

$$\omega_{u_2} = \frac{1}{2}\left(\frac{\pi}{2\tau} \pm \sqrt{\left(\frac{\pi}{2\tau}\right)^2 - \frac{4}{T_q\tau}}\right)$$

The positive sign is appropriate,

$$\omega_{u_2} = \frac{1}{2}\left(\frac{\pi}{2\tau} + \frac{\pi}{2\tau}\sqrt{1 - \left(\frac{4}{\pi}\right)^2\frac{\tau}{T_q}}\right)$$

$$= \frac{\pi}{4\tau}\left[1 + \sqrt{1 - \left(\frac{4}{\pi}\right)^2\frac{\tau}{T_q}}\right]$$

$$\doteq \frac{\pi}{4\tau}\left[2 - \frac{1}{2}\left(\frac{4}{\pi}\right)^2\frac{\tau}{T_q} + \dots\right]$$

Finally,

$$\omega_{u_2} \doteq \frac{\pi}{2\tau} - \frac{2}{\pi}\frac{1}{T_q} \tag{11}$$

This point will generally lie on the −20 dB per decade asymptote above $1/T_q$. Under this assumption the high frequency gain margin will be

$$GM_{hi} = \frac{\omega_{u2}}{\omega_{c_a}} \doteq \frac{1}{\omega_{c_a}} \left(\frac{\pi}{2\tau} - \frac{2}{\pi T_q}\right) \qquad (12)$$

3) Phase and Delay Margins and Their Flying Qualities Implications

Phase margin and crossover frequency can be converted to a delay margin, τ_M, where

$$\tau_M = \phi_M/\omega_c \qquad (13)$$

Delay margin indicates how much additional pure time delay can be tolerated before producing neutral stability. When the phase in the immediate region of crossover is primarily dependent on the dominant mode characteristics, phase and delay margins can be further approximately related to the closed-loop damping ratio of the dominant mode. Figure 7 indicates that nominal superaugmented designs will exceed the MIL-F-8785C short period requirements of $\zeta = 0.35$ (Level 1) and $\zeta = 0.25$ (Level 2).

The actual system gain, as indicated by the asymptotic crossover frequency, will normally be restricted by the need for high frequency gain and phase margins. The phase margin will depend primarily on the control system lead, T_q, and the τ representing high frequency controller plus airframe lags. The available phase margin as a function of controller lead is given in Fig. 11. The phase margin will be a maximum when

$$\omega = \frac{1}{\sqrt{\tau \, T_q}} \sqrt{1 - \frac{\tau}{T_q}}$$

$$\doteq \frac{1}{\sqrt{\tau \, T_q}} \qquad (14)$$
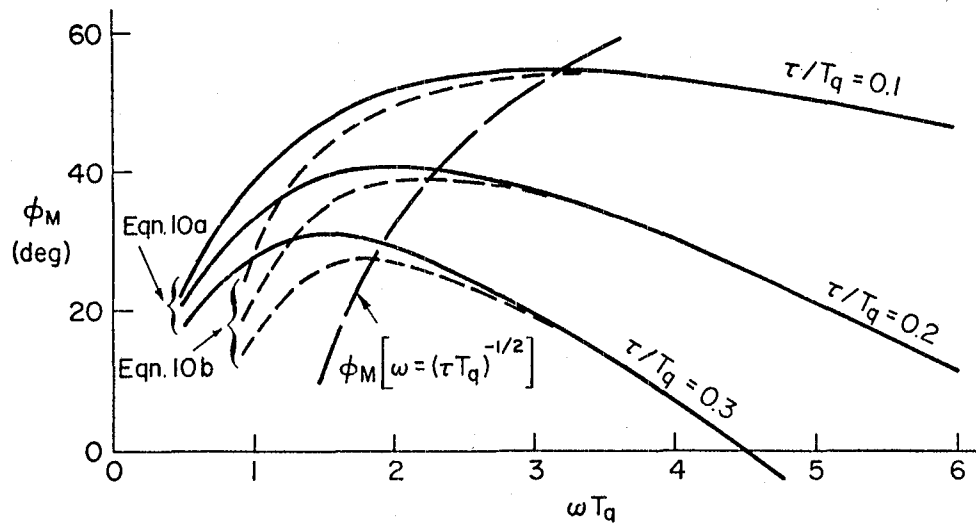
Figure 11. Phase Margin

Its value will be approximately,

$$\phi_{M_{max}} \doteq \frac{\pi}{2} - 2 \sqrt{\frac{\tau}{T_q}} \tag{15}$$

Values of $\phi_{M_{max}}$ using the approximate formula of Eq. 15 are spotted on the actual phase margins based on Eq. 10a in Fig. 11. Many designers will choose to establish the crossover frequency equal to or very near the frequency for maximum phase margin. In any event, the high frequency controller (actuators, filters, etc.) and airframe lags have their direct impact on the crossover frequency, and hence the dominant mode, via the phase margin selection.

b. Total Available Gain Range

The Total Available Gain Range (TAGR) parameter can now be defined as

$$\text{TAGR} = (GM_{lo})(GM_{hi})$$

$$= \frac{\frac{1}{T_q} \left(\frac{\pi}{2\tau} - \frac{2}{\pi T_q} \right)}{\left| \omega_{sp}^2 \right| \left(T_{\theta_1} T_{\theta_2} \omega_p^2 \right)} \tag{16}$$

$$\doteq \frac{1/T_q}{M_\alpha} \left(\frac{\pi}{2\tau} - \frac{2}{\pi T_q} \right) \left(\frac{1}{T_{\theta_1} T_{\theta_2} \omega_p^2} \right)$$

Notice that the asymptotic crossover frequency has canceled out. The TAGR parameter depends primarily on the degree of instability (M_α), the low frequency effect of high frequency control system and airframe flexible mode lags (τ) and the basic adjustment of the aircraft plus control system crossover region ($1/T_q$). To a first approximation the TAGR can be held constant as static instability is increased by adjusting the control system lead $1/T_q$ to compensate although diminishing returns soon set in because of the ($\pi/2\tau - 2/\pi T_q$) factor. TAGR is also affected by an airframe performance parameter, $1/T_{\theta_1}T_{\theta_2}\omega_p^2$, which is a measure of how close the airplane is trimmed to give maximum L/D. ($1/T_{\theta_1}T_{\theta_2}\omega_p^2 \doteq 1$ when the aircraft is operating at the bottom of the thrust required versus speed curve). This will be discussed further below.

Superaugmented flight control system design to minimize sensitivity to control-limiting-induced loss in effective gain can be achieved by adjusting $1/T_q$ to maximize TAGR. This could be done by setting T_q to its minimum value, i.e., $T_q \to \tau$ consistent with a positive phase margin. Then as $T_q \to \tau$ (while $\phi_M \to 0$).

The corresponding maximum value of TAGR is

$$\text{TAGR}_{max} = \frac{1}{\tau^2 M_\alpha}\left(\frac{\pi^2-4}{2\pi}\right)\left(\frac{1}{T_{\theta_1}T_{\theta_2}\omega_p^2}\right) \qquad (17)$$

This limiting case is not practical although it gives a very high upper bound and shows the general variation of TAGR with high frequency control system plus aircraft net lag, τ, static margin (as reflected in M_α), and aircraft performance (as associated with $1/T_{\theta_1}T_{\theta_2}\omega_p^2$). This last topic will be discussed more extensively below.

To gain a better appreciation of the control system/aircraft trade-offs involved in the Total Available Gain Range it is appropriate to connect the effective controller lead, T_q, with the net maximum attainable phase margin. Using the approximate expressions for $\phi_{M_{max}}$ this becomes,

$$\frac{\tau}{T_q} \doteq \frac{1}{4} \left(\frac{\pi}{2} - \phi_{M_{max}} \right)^2$$

$$= \frac{\lambda^2}{4}$$

where $\lambda = \pi/2 - \phi_{M_{max}}$. Combining this with the Eq. 16 approximation for TAGR, i.e.,

$$TAGR \doteq \frac{1/T_q}{M_\alpha} \frac{\pi}{2\tau} \left(1 - \frac{4\tau}{\pi^2 T_q} \right) \frac{1}{T_{\theta_1} T_{\theta_2} \omega_p^2}$$

results in a TAGR which is constrained by the condition that a maximum phase margin, $\phi_{M_{max}}$, <u>could</u> be obtained by an appropriate selection of system gain. (The TAGR parameter, as a total range, does not depend on whether the phase margin is actually set to any particular value.)

The result is

$$TAGR]_{\phi_{M_{max}}} \doteq \frac{\pi^3}{8\left(M_\alpha \tau^2\right)} \left(\frac{\lambda}{\pi} \right)^2 \left[1 - \left(\frac{\lambda}{\pi} \right)^2 \right] \left(\frac{1}{T_{\theta_1} T_{\theta_2} \omega_p^2} \right)$$

$$= \left\{ \frac{\pi^3}{8} \left(\frac{\pi/2 - \phi_{M_{max}}}{\pi} \right)^2 \left[1 - \left(\frac{\pi/2 - \phi_{M_{max}}}{\pi} \right)^2 \right] \right\} \left(\frac{1}{T_{\theta_1} T_{\theta_2} \omega_p^2} \right) \frac{1}{\left(M_\alpha \tau^2 \right)}$$

$$(18)$$

The phase margin-dependent factor in the brackets is illustrated in Fig. 12. A more complete practice of the possible TAGR attainable with a given spread between $\sqrt{M_\alpha}$, representing the static margin, and the net high frequency lag, τ, is provided in Fig. 13. This plot shows the overwhelming effect of the $\sqrt{M_\alpha} \tau$ product in that, for a given phase margin, TAGR is reduced in proportion to both the unstable static margin and the square of τ. The extreme sensitivity of superaugmented aircraft

The y-axis is labeled:

$$\frac{\pi^3}{8} \left(\frac{\pi/2 - \phi_{M_{max}}}{\pi}\right)^2 \left[1 - \left(\frac{\pi/2 - \phi_{M_{max}}}{\pi}\right)^2\right]$$

The x-axis (rad) is labeled: $\pi/8$, $\pi/4$, $3\pi/8$, $\pi/2$ (rad)

Phase Margin (deg): 22.5, 45, 67.5, 90

30° 60° Nominal Range of $\phi_{M_{max}}$
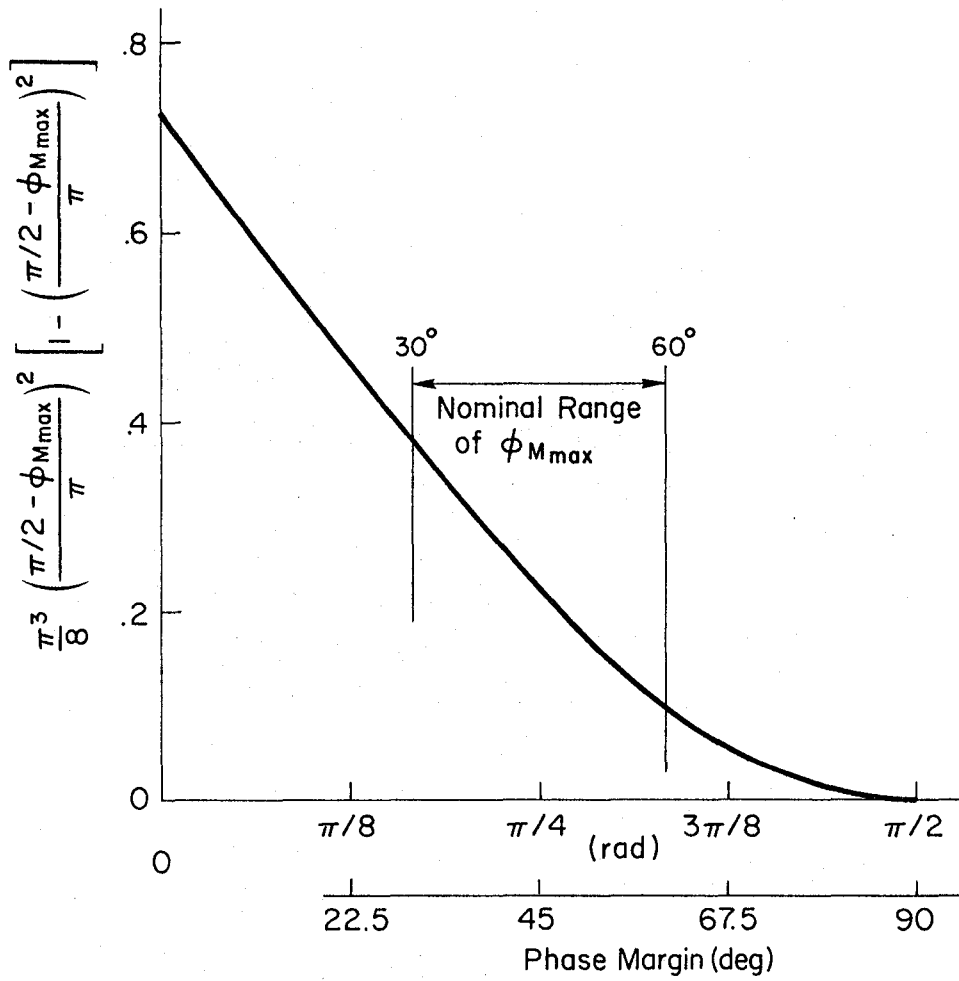
Figure 12.   TAGR Phase Margin Dependence

$\phi_{M_{max}}=$

TAGR (dB)

50 — 0

40 — 20
30

45

60 —

30 —

20 —

10 —

0 —

$\phi_{M_{max}}$ (deg)	τ / T_q	$\tau \omega$ at $\phi_{M_{max}}$
0	0.617	0.785
20	0.373	0.611
30	0.274	0.524
45	0.154	0.393
60	0.0686	0.262

Level 1

Level 3

Level 2

$\zeta' = 0.25$

$\zeta' = 0.35$

$\dfrac{1}{T_q} > \sqrt{M_\alpha}$

$\dfrac{1}{T_q} = \sqrt{M_\alpha}$

*Levels shown are for
MIL-F-8785C damping
ratio requirement*

0   .05   .10   .15   .20   .25   .30

$\sqrt{M_\alpha}\ \tau$, Increasingly Unstable Static Margin →
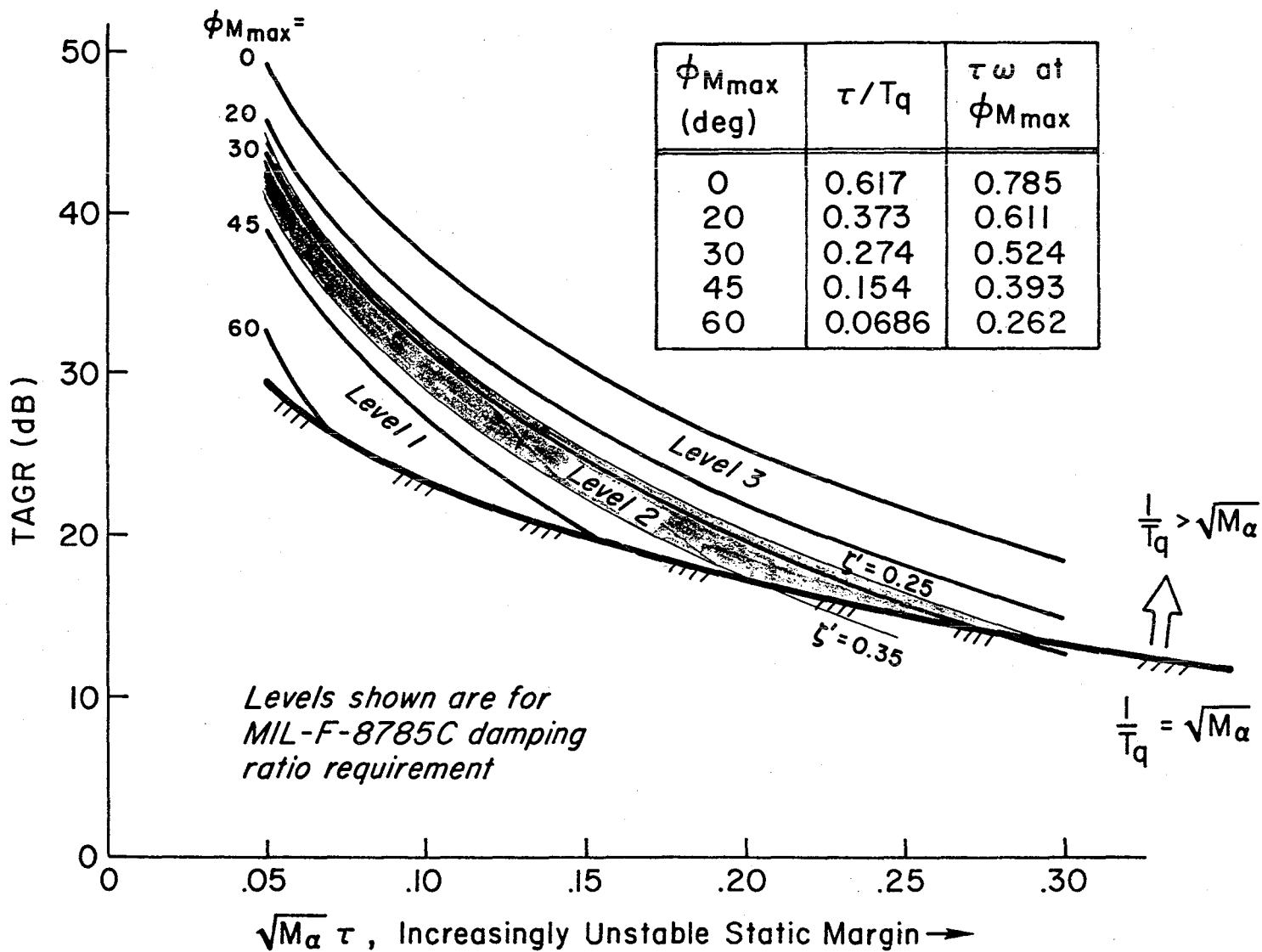
Figure 13. TAGR for Maximum Attainable Phase Margin as a Function of Static
Margin (M_α) and High Frequency System Properties (τ)

$$\left(1/T_{\theta_1} T_{\theta_2} \omega_p^2 = 1\right)$$

to these features is typified by noting that, with an $\sqrt{M_\alpha}$ to $1/\tau$ spread of a factor of ten a TAGR of 27 dB is possible if the phase margin s set to a nominal 45 degrees.

For superaugmented designs with $1/T_q$ placed above the aircraft dynamics region there is a lower bound provided by the $1/T_q \geqslant \sqrt{M_\alpha}$ curve in Fig. 13. Upper bounds are imposed by the phase margin requirements of various specifications. For instance, MIL-F-9490 requires $\phi_M \geqslant$ 45 degrees below the first elastic mode. The Space Shuttle specification required $\phi_M \geqslant 30$ degrees for Level 1 and $\phi_M \geqslant 20$ degrees for Level 2 ($\omega < 6$ Hz). Pitch mode damping ratio can be related to ϕ_M and Fig. 13 shows the MIL-spec short period ζ levels. Thus Fig. 13 indicates how increasing airframe instability constrains the basic superaugmented design options.

c. Relation to Configuration and Flight Condition

In addition to static margin effects, the low frequency gain margin will also be affected by configuration and flight condition. For example modern aircraft can show considerable difference in the low frequency gain margin expression in Eq. 6. We are interested in how the low frequency factor in Eq. 6, $1/[\omega_p^2 T_{\theta_1} T_{\theta_2}]$ (see Fig. 14) varies with configuration, throttle control, and flight condition. The relevant literal approximate factors (Refs. 1 and 4) are

$$\omega_p^2 \doteq \omega_{p_0}^2 \doteq 2(g/U_0)^2 \tag{19}$$

$$1/T_{\theta_2} \doteq -Z_w \tag{20}$$

$$1/T_{\theta_1} \doteq 1/T_{h_1} + \frac{g}{U_0} \frac{Z_u}{Z_w} \tag{21}$$

These expressions may be manipulated to form an approximation for the factor of interest,

$$\frac{1}{\omega_p^2 T_{\theta_1} T_{\theta_2}} = \frac{1}{1 - \left(T_{\theta_1}/T_{h_1}\right)} \tag{22}$$
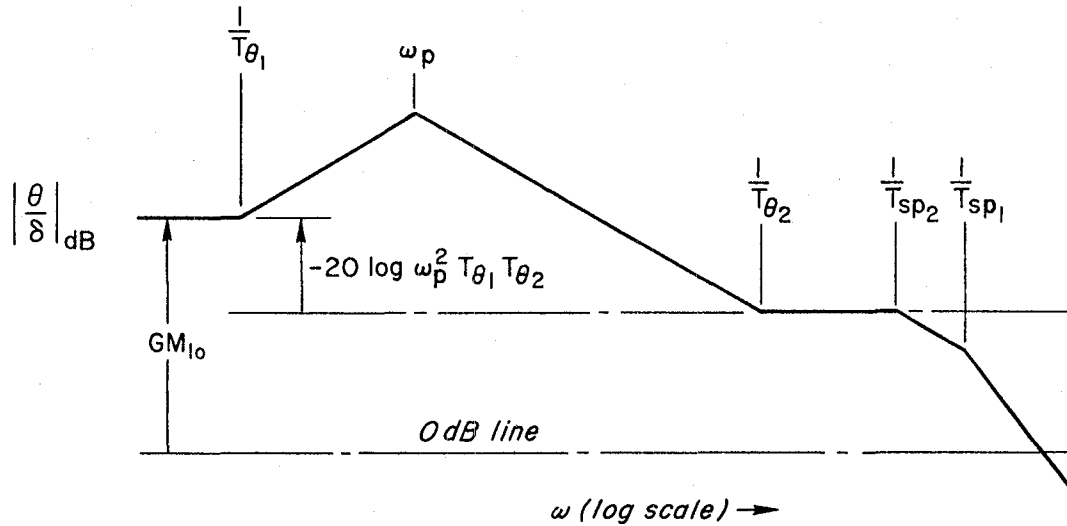
Figure 14. Aircraft Performance Parameter

The low frequency altitude lead, $1/T_{h_1}$, is approximately

$$\frac{1}{T_{h_1}} \; \doteq \; \frac{1}{m}\left(\frac{dD}{du} - \frac{\partial T}{\partial u}\right) \qquad (23)$$

This zero is in the left half plane when the aircraft is operating on the "front" side of the trim drag curve and migrates into the right half plane near the minimum drag speed. Consideration of Eq. 21 shows that $1/T_{\theta_1}$ will be more positive than $1/T_{h_1}$ and will almost invariably be in the left half plane. With this insight Eqs. 22 and 23 show that the low frequency gain margin factor is reduced as trim speed is reduced on the front side of the drag curve, becomes unity (zero dB) near the minimum drag speed and then less than one for operation on the back side of the drag curve. This analysis provides a fundamental connection between airframe drag and trim characteristics and the basic FCS stability margin.

4. Some Flying Qualities Implications

The two-parameter nature of the dominant mode, and all the corre-lates (e.g., rise time, T_r, undamped natural frequency, ω_n, damping

ratio, ζ, and peak overshoot, q_{max}/q_c, is graphically illustrated in Fig. 15a. This figure is repeated, in 15b, with an extensive set of boundaries representing various flying quality criteria constraints. These include:

- Damping Ratio (from MIL-F-8785C)

- Rise Time (from NLR, see Ref. 5)

- Conventional Fighter n/α (from MIL-F-8785C)

- Overshoot Limit (Shuttle Time Response Boundary)

To the extent that these criteria are valid they would be excellent starting points for the control system design to adjust dominant mode properties. At present the criterion which is most questionable is that from the Shuttle (labeled STS Overshoot Limit). As is now well known (e.g., Ref. 3), the shuttle time response boundaries are not good criteria for conventional aircraft. One the other hand, it is still not determined whether the shuttle-based overshoot limit is a good criterion for rate command/attitude hold (RCAH) aircraft.

Two features of RCAH that have received extensive comments from the flying quality community are

- Absence of stick force/speed cue;

- Tendency to float in flare, and need to push the stick forward to get the nose down

The first characteristic is allowed in MIL-F-8785C. The second property appears to be a pilot familiarization problem rather than anything fundamental. Research on both characteristics is still in process.

Both of the features above, and other flying quality problems as well, can be alleviated using the pilot command input shaping element, G_i. There are at least three special values of $G_i(s)$ which have some merit for superaugmented aircraft. These are listed below.

- Rate Command/Attitude Hold

$$G_i = K_i = \text{constant}$$
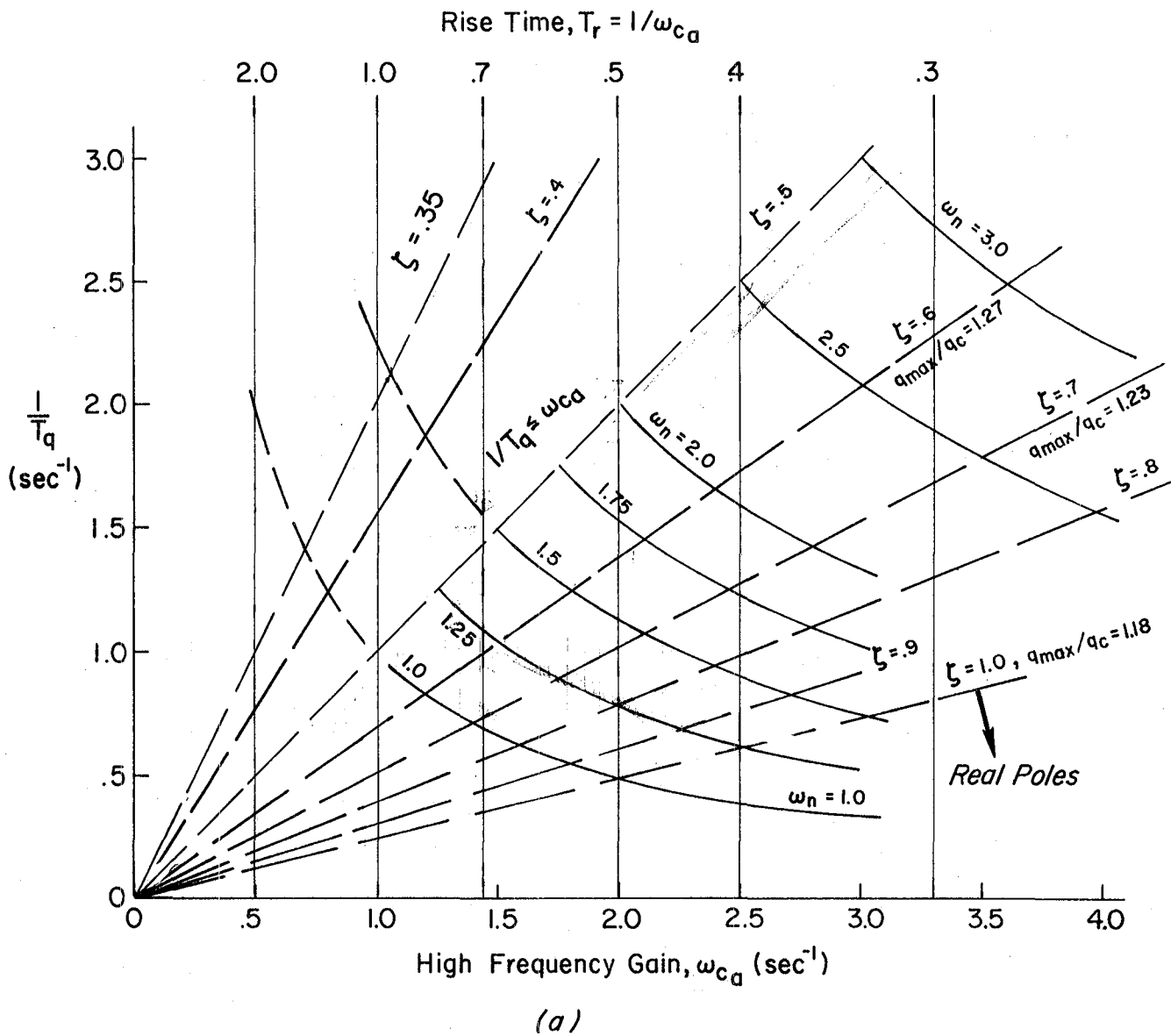
Figure 15. Superaugmented Dominant Mode Characteristics in the $1/T_q - \omega_{c_a}$ Parameter Plane

(b)
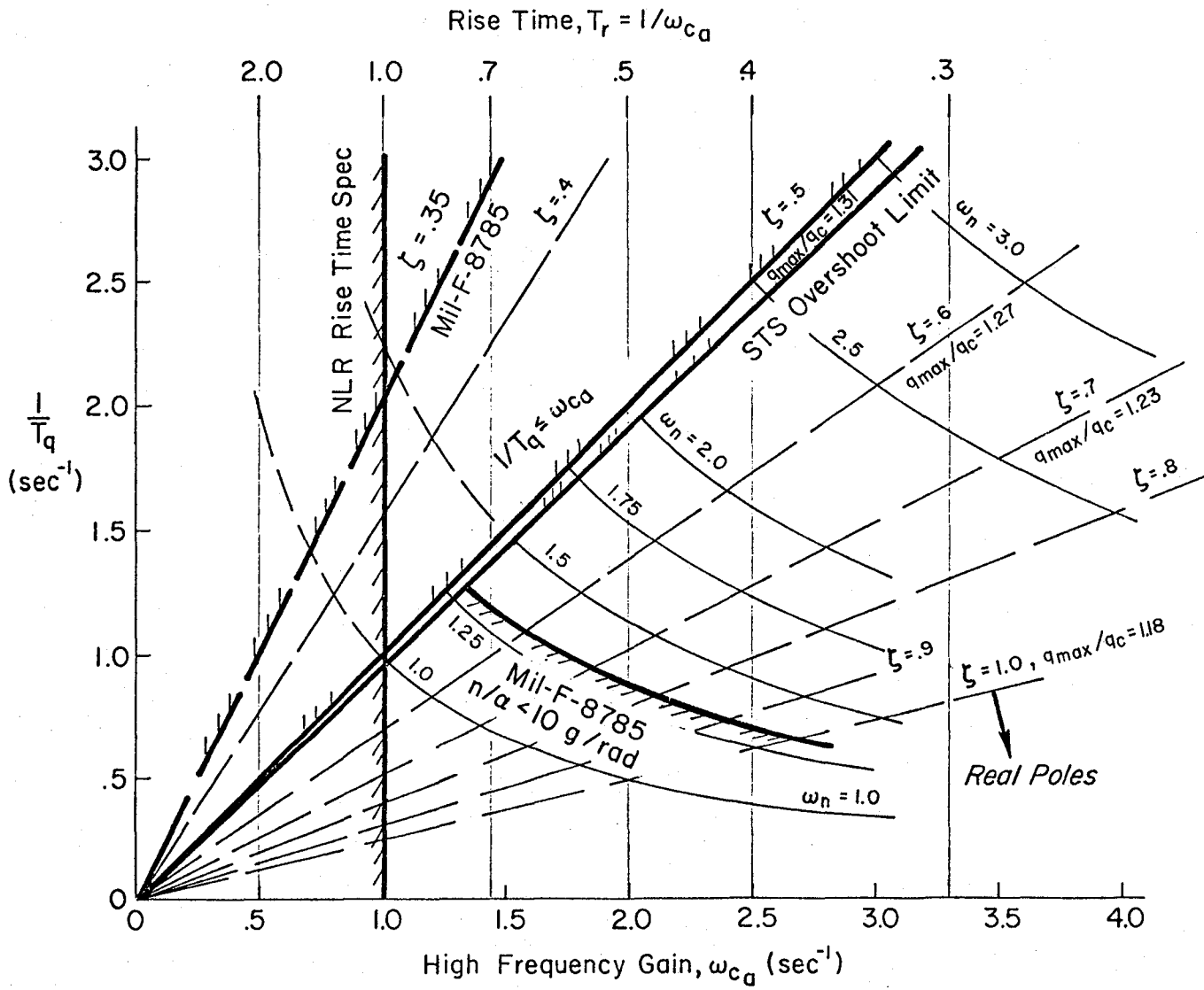
Figure 15. (Concluded)

- Extended Bandwidth

$$G_i = K_i \frac{(s + 1/T_1)}{(s + 1/T_q)}$$

  -- $1/T_1$ near but $< 1/T_q$

  -- $1/T_1 \rightarrow 1/T_{\theta_2}$ (Pseudo-Conventional)

- Attitude Command

$$G_i = \left[\frac{K_i\, s}{s + 1/T_{wo}} \right] \frac{(s + 1/T_1)}{(s + 1/T_q)}$$

  -- $1/T_{wo} \rightarrow 1/T_1$

Rate command/attitude hold is the most commonly encountered system and is presently that used on the Shuttle and X-29A. The extended bandwidth systems are of two kinds. In the first, the lead-lag is adjusted to provide some additional high frequency phase lead above crossover to partially offset high frequency lags incorporated in the $e^{-\tau s}$ effective delay. In the second the lead is adjusted to approximate the natural $1/T_{\theta_2}$ of the aircraft alone. When this is done the effective attitude to pilot input transfer characteristic corresponds to the short-period attitude characteristics of a conventional aircraft with a damping ratio and undamped natural frequency given by ζ' and ω_n'. The effective aircraft dynamics are not completely conventional in that the conventional phugoid is gone and the attitude hold feature is still present. A possible problem with the extended bandwidth G_i feature is an amplification of any high frequency noise inserted by the pilot. This could have implications for control power or other system saturation and/or limiting characteristics. The third type of G_i is a washout of the pilot's command. This modifies the effective aircraft dynamics to an attitude command/attitude hold system.

Both the $G_i = K_i$ and the extended bandwidth superaugmentation systems have rate command/attitude hold features. Such systems inherently

provide a neutral stick force gradient with speed. Although this is allowed by the current military flying quality specification it is still legislated against in the Federal Air Regulations. There are many simulations and flight experiments wherein the neutral stick force gradient with speed has not been an important issue when contrasted with the favorable features provided by rate command/attitude hold augmentation (e.g., Refs. 6-8). The flight tests of Refs. 7 and 8 concluded that there is no clear advantage to positive over neutral speed stability, at least when the aircraft was operated at the bottom or frontside of the thrust required vs. speed curve. On the other hand, pilot technique appears to require some initial familiarization especially in landing. The initial tendency, which is rapidly corrected by a few practice landings, is to land long.

Strictly speaking, neutral stick force speed gradient in a superaugmented aircraft does not imply neutral speed stability because (unlike a conventional aircraft with zero static margin) all the superaugmented poles are stable. The neutral stick force gradient is a consequence of the integrator in the effective command path (G_i = constant).

An associated feature of rate command/attitude hold systems has received some pilot comment. Consider that at the outset of flare the aircraft is trimmed and the pilot begins to pull back on the control stick to reduce sink rate. As the aircraft begins to enter ground effect the pilot in a conventional aircraft will tend to pull further. Thus in landing a conventional aircraft without any trim adjustment the pilot holds back pressure on the stick. If now a corrective change is required in pitch attitude the pilot accomplishes it either by further back pressure or slight release of the back pressure. For the rate command/attitude hold type system, however, no back pressure is held. Consequently if the attitude is to be reduced the pilot must move the control forward from its neutral position. This feature of rate command/attitude hold systems has sometimes been considered as undesirable.

In a conventional aircraft the landing maneuvers are conducted with speed close to that for minimum thrust required (i.e., near the bottom

of the "bucket"). The aircraft attitude dynamics for this flight condition are such that the aircraft attitude to elevator gain at zero frequency and on the $1/T_{\theta_2}$ to short period shelf are essentially identical. This corresponds to $\omega_p^2 T_{\theta_1} T_{\theta_2} \doteq 1$ in Fig. 14. Thus conventional aircraft rate command tendency associated with short period aircraft dynamics in up and away flight is replaced, in the landing condition, by aircraft dynamics which are much closer to attitude command in character. One could, in fact, make the point that a conventional aircraft is inherently task tailored to provide rate command properties in up and away normal flight and attitude command properties in landing. The rate command/attitude hold superaugmented aircraft version, however, remains rate command/attitude hold unless $G_i(s)$ is modified. The pilot command washout or attitude command system given above is one way to accomplish this. The aircraft dynamics then approximate those of a conventional aircraft in the landing condition, have a positive stick force/speed gradient, etc. Consequently, the effective vehicle dynamics will not suffer from the possibly objectional rate command/attitude hold features cited above, although there is a potential problem in tailoring the stick forces and total stick movement to be compatible with maximum control power with this kind of system. The attitude command/attitude hold system also relieves the pilot of the task of closing the attitude loop to equalize the subsequent path loop closure.

At the present time the available flying qualities data for superaugmented aircraft tend to be for the pure rate command/attitude hold type. The extended bandwidth and washed-out pilot command systems are beginning to receive some experimental attention and both appear to offer some potential advantages.

5. First-Order Effects of Nonlinearities

### a. Key Nonlinearities and Associated Phenomena

The primary nonlinearities of concern for superaugmented aircraft designs are those introduced through actuator rate and position limiting. These nonlinearities reduce the effective gain through the

combined action of pilot commands, turbulence, vibrations, and other unwanted inputs, noise, etc.

Data on these noise sources at a sufficient level of completeness are very sparse. The noise sources needed include sensor, structural, atmospheric, pilot remnant spectra, etc. Both periodic and random components will be present in general.

b. Nature of the First-Order Treatments for Nonlinear Effects

Detailed describing function analysis of FCS with effector position and rate limits is well developed, but somewhat involved (e.g., Ref. 9). The problem can be significantly simplified by approximating rate-limiting as an effective time delay. As indicated in the sketch
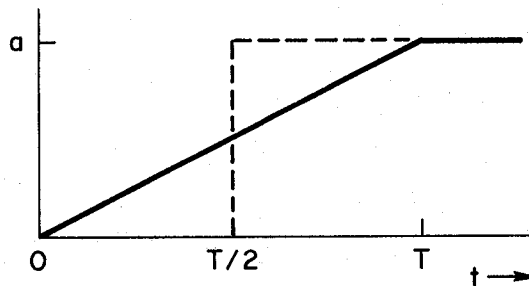
a rate limit of a/T produces, as a first approximation, an incremental effective time delay of $\Delta\tau \doteq T/2$. This would be added to the several other components of effective high frequency lag to form an effective τ for a given actuator input amplitude, a.

High frequency limits are imposed, as noted previously in Fig. 3, by the $q_{c_{max}}$ limit. Low frequency limits are set by the divergence or phugoid criteria noted in Figs. 8 and 9. These limits are approached as the effective gain (K_q) is reduced on the average under the action of noise and command inputs. For harmonics/random processes as the command/noise inputs a describing function approach is useful. Three well-known describing function types are relevant for the position limiting problem:

- single sinusoidal input

- gaussian random input

- dual sinusoidal input

For all three types of describing functions limiting may be treated as an input-amplitude dependent gain change. It is perfectly reasonable to qualitatively consider the stability of flight control systems in terms of shifts in these "gains" as input amplitude is changed. Since limiting characteristics have the effect of reducing gain, it would be suspected that the effective system dynamics would regress toward those of the open-loop, and that the "on the average" dynamics would be those of the reduced gain system. Actually, of course, the system dynamics are those of the linear closed-loop system when the surface(s) are not saturated, and those of the open-loop system when saturation is present. The relative time spans of these two phases is reflected in the describing function gain variation. The describing function approach does assume a degree of stationarity over time which may not be assured for conditionally stable systems such as a superaugmented RSS aircraft where the instability can be a rapid divergence.

The effects noted above are the essence of the control power problems unique to RSS aircraft with advanced FCS. This will be illustrated using a superaugmented aircraft which is a 40 percent $\bar{c}$ unstable vehicle, with high frequency actuator and other lags yielding an effective time delay of $\tau = 0.08$ sec. The system survey of Fig. 16 shows that the additional FCS lags primarily affect the complex pitch mode $[\zeta', \omega_n']$. (Although it does not represent a particular problem, it should be noted that in this case the phugoid and divergence loci couple at lower gains.)

To focus on the two critical loci -- the divergence $\left(1/T_{sp_2}'\right)$ and the superaugmented pitch mode -- the Bode root locus of Fig. 16 is expanded vertically in Fig. 17. Time-to-double amplitude is noted along the divergence σ-locus and, on the right side, damping ratio is indicated along the pitch mode complex Bode-locus. On the left side three describing function scales for position limiting are shown. These were crossplotted from Fig. 18.
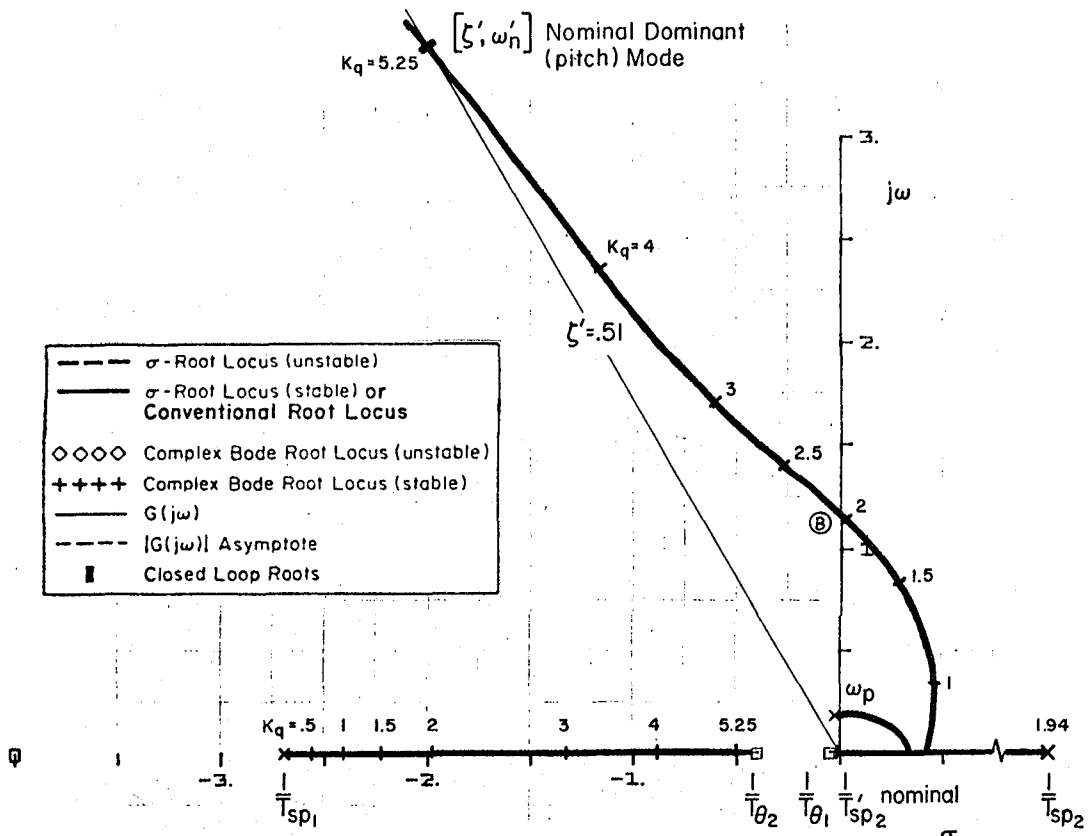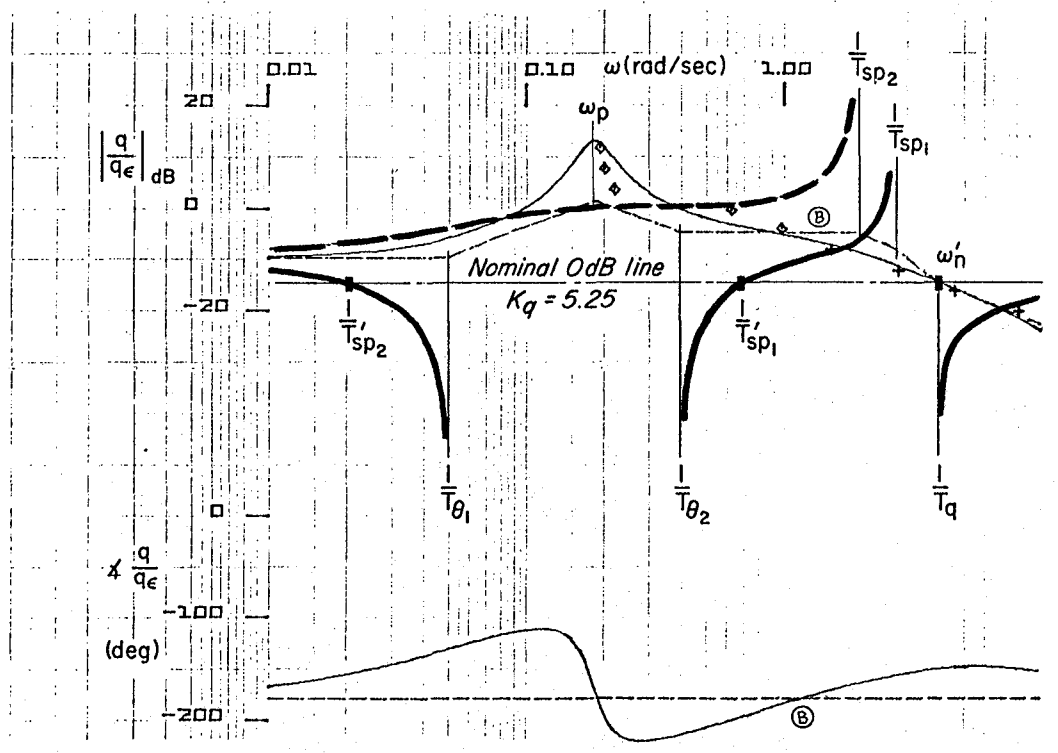
Figure 16. Closure of the Superaugmentation Pitch Rate Loop,
40 Percent $\bar{c}$ Unstable Fighter in Approach Including
High Frequency Lags
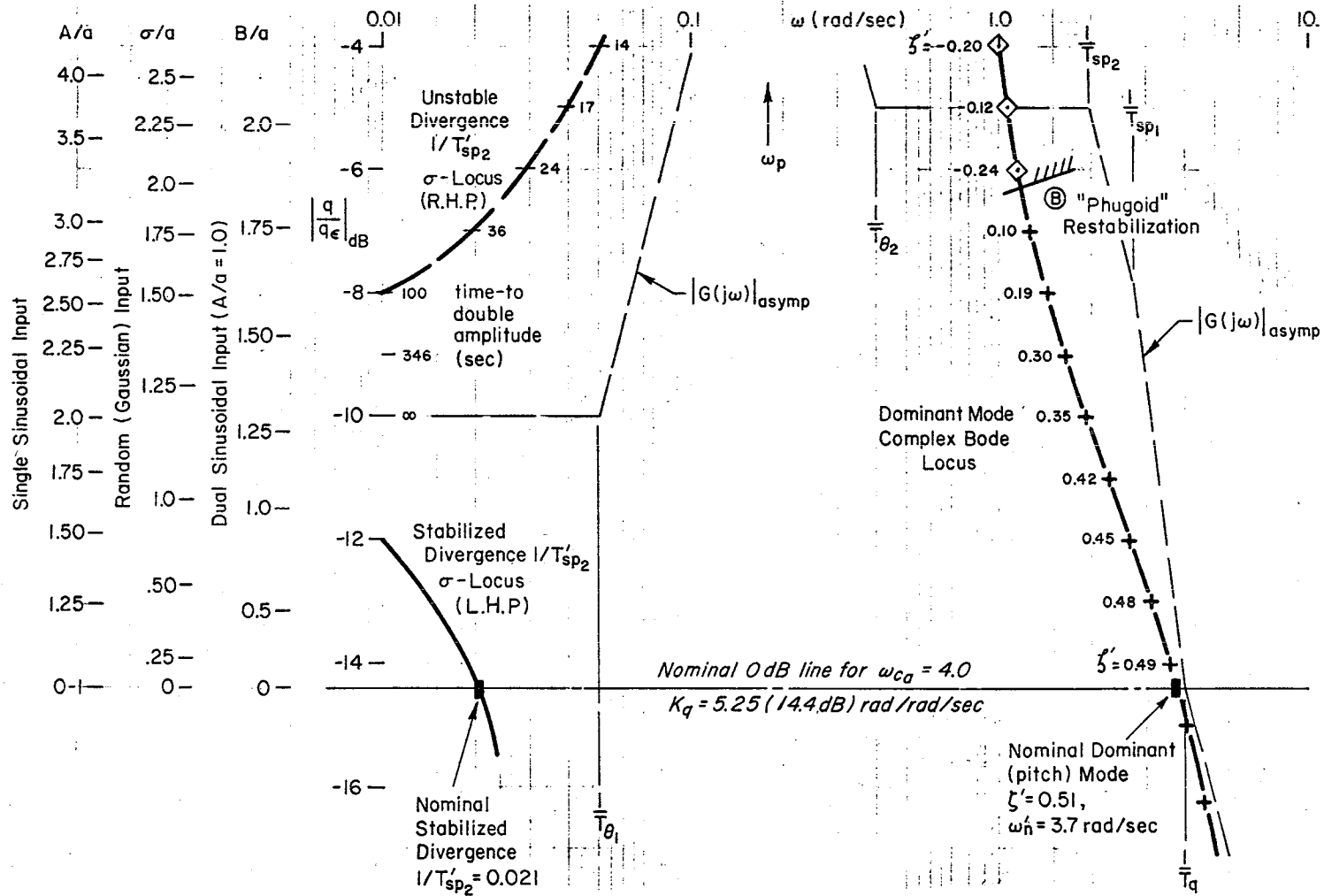
Figure 17. Effect of Control Position Limiting on Superaugmented Dynamics (SM = 40 Percent c̄ Unstable Fighter, Approach)
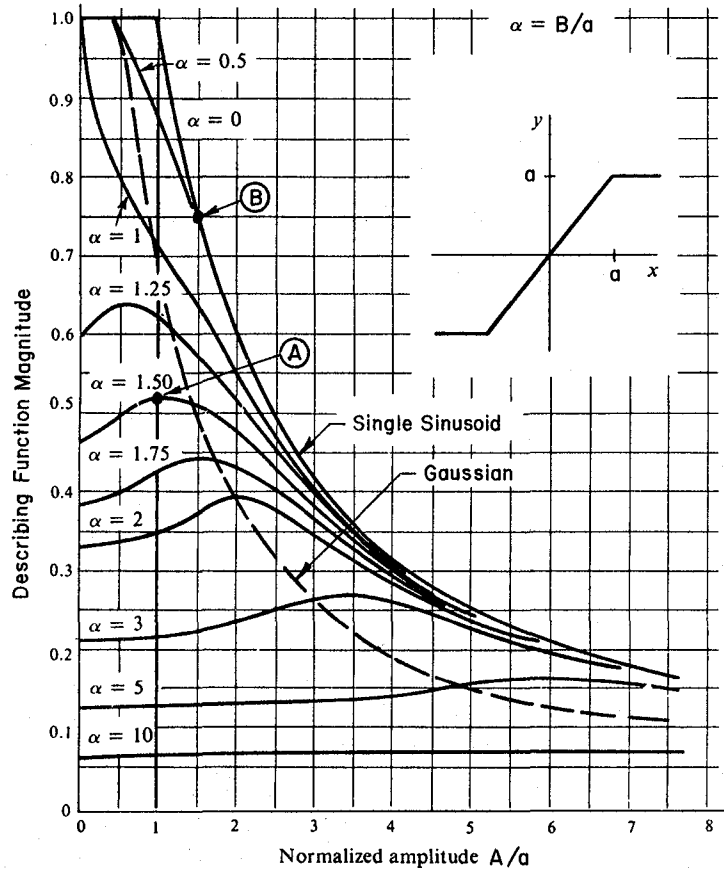
Figure 18. Summary of Three Describing Function Types

The single sinusoidal input scale on the far left side of Fig. 17 was obtained from the solid upper boundary curve ($\alpha = 0$) in Fig. 18. This scale shows the level of the effective "degraded" open-loop zero dB line ($|G| = |K_q q/q_\epsilon| = 1 = 0$ dB) for given input/limit (A/a) ratios. As the input amplitude A is increased, the 0 dB line "rises" reflecting the saturation-induced gain reduction and the corresponding "average" closed-loop roots are found at the intersection with the Bode loci. For instance, if the pilot input was a sine wave with amplitude twice the limit (A/a = 2), the stabilized $1/T'_{sp_2}$ would be driven to the origin and the pitch mode parameters would be reduced from [$\zeta' = 0.51$, $\omega'_n = 3.7$ rad/sec] to [$\zeta' = 0.35$, $\omega'_n = 1.9$ rad/sec].

For a single sine wave input there is, of course, no gain degradation until the limit is actually exceeded (hence, 0 < A/a < 1 corresponds to the nominal 0 dB line in Fig. 17.) However, for random inputs (gaussian random input describing functions are discussed in Ref. 10) there will always be some probability of limiting for any input RMS level as reflected in the random input scale in Fig. 17.

The third class of inputs — dual sinusoidal — is useful in treating some particular phenomena for advanced aircraft. Consider an aircraft with a continuing structural oscillation, well above the pitch mode frequency, driven by turbulence. Figure 19 shows that if a lower frequency sinusoidal input from the pilot is introduced, the superposition of the two inputs may limit even when they are not individually limited. The dual sinusoidal input describing function is appropriate for this case. The corresponding third scale in Fig. 17 is obtained from Fig. 18. To make a specific example, it is assumed in Fig. 17 that the pilot input just limits (A/a = 1). The effect of various amplitudes, B, of structural vibration is obtained from the $\alpha = B/a$ curves in Fig. 18. Even if the structural oscillation amplitude is half the limit ($\alpha = 0.5$) there is a 13 percent effective gain reduction. An interesting comparison is a 50 percent limit exceedence of the structural oscillation, point A in Fig. 18, compared to a 50 percent pilot input exceedence in the <u>single input</u> case, point B in Fig. 17. It may be
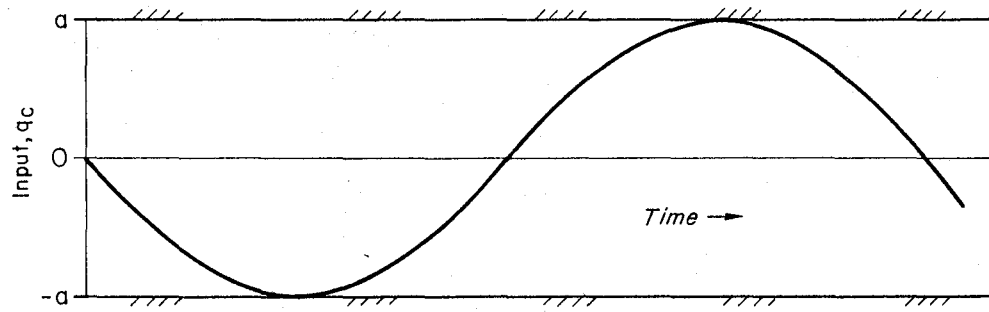
a) Pilots Input
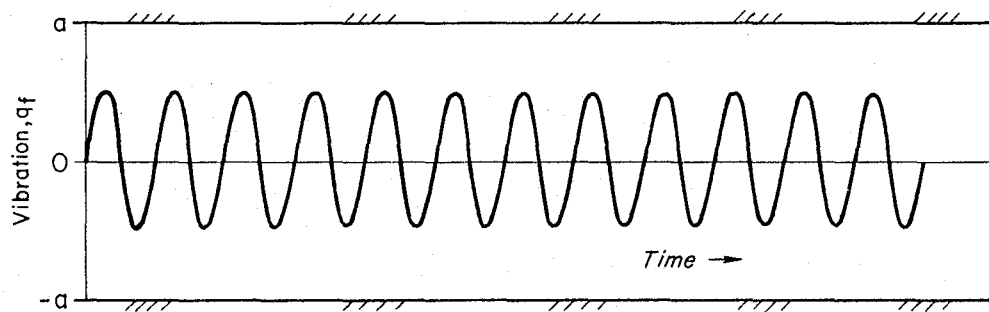
b) Structural Vibration
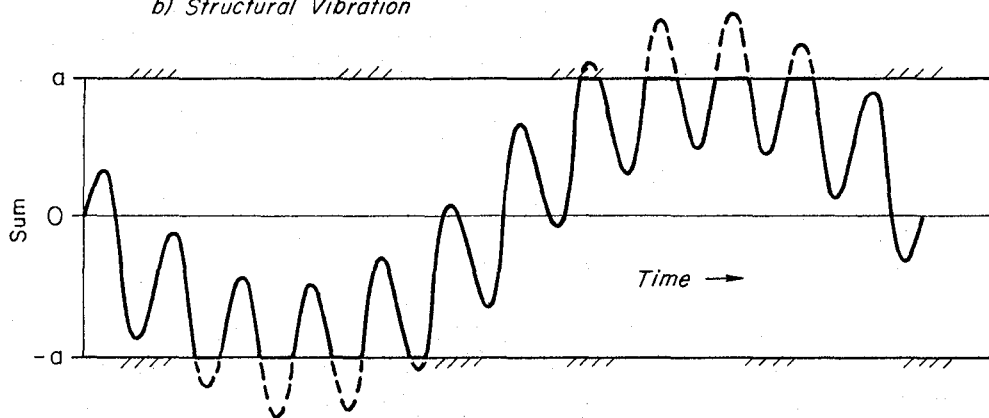
Figure 19. Dual Sinusoidal Input to a Limiter

seen that the dual input case is almost twice as severe. The corres-
ponding dynamic effect in Fig. 17 shows destabilization of $1/T'_{sp_2}$ and
significant reduction in pitch mode frequency and damping.

A final source of degradation of the dynamic response is to further
separate the $1/T'_{sp_1}-1/T_{\theta_2}$ dipole. This introduces a "new" mode which is
almost completely suppressed in a nominal superaugmented design where
good dipole cancellation occurs.

This example provides some broader insights into the nature of con-
trol power problems for superaugmented aircraft. It appears from
Fig. 17 that quite considerable saturation effects might be required to
produce a divergence, $1/T'_{sp_2}$, with a time-to-double which posed a
safety-of-flight problem. On the other hand, realistic saturation
levels may significantly degrade the pitch mode characteristics and
create basic flying qualities problems. Advanced designs, particularly
with radical structural innovations, may have many structural and vibra-
tory modes to nibble away at FCS gain margins. Thus it may emerge that
the greatest problem with highly unstable aircraft designs is not the
potential for catastrophic divergence, but a troublesome sensitivity of
flying qualities to control saturation. The likely impact would be an
increase in the engineering, simulation, and flight test manhours
required for a new design. The environmental disturbance and task-
centered commands will also need to be known with greater precision.

There are some particular problems for flight test in that the
atmospheric conditions needed to reliably test subtle disturbance/input
interactions (as in the example above) can not readily be "ordered."
This may mean that a good deal of traditional stability and control
flight testing may have to be augmented with analytical probabilistic
verification procedures analogous to those used for structural certifi-
cation.

SECTION III

FLYING QUALITIES OF SUPERAUGMENTED AIRCRAFT

A. OVERVIEW OF FLYING QUALITIY POSSIBILITIES

The pilot, as an aircraft controller, is concerned with three different types of interactions with the aircraft. In the first the aircraft is unattended while the pilot, benign as a controller, may monitor the aircraft's motions but is concentrating on some other task such as navigation or communications. In the second type of interaction the pilot may occasionally manipulate the controls as, for example, in setting up a new trim condition. In this type of operation the pilots inputs may well be programmed and the typical response of the pilot-vehicle system may tend to be dominated by the indicial response properties of the aircraft/flight control system. This intermittent and trim control type of flight is akin to that for unattended operation in that for both the aircraft/flight control system transient dynamics in response to initial conditions, aperiodic disturbances, and discrete pilot inputs are the important system entities. In other words, the pilot is not continuously in the loop, and his control actions may force, but do not essentially modify, the effective vehicle dynamics. The third type of pilot-vehicle interaction is one where the pilot is in full-attention manual regulatory or command control of the aircraft. In this case the pilot-vehicle system is essentially closed-loop in that the aircraft motions and pilot-vehicle system dynamics are significantly modified by the pilot's actions.

Those aircraft control functions which demand the greatest pilot attention and skill will require paramount consideration in flying qualities assessments. Probably the most demanding high workload pilot/ aircraft closed-loop control operation is precision path control, which incorporates both flight path changes and flight path maintenance or regulation. Because superaugmented aircraft have attitude-hold features, flight path changes can be made with only intermittent pilot control. On the other hand, in the most demanding high workload situation, where precision path control also involves adjustments and regulation against unfavorable environmental conditions, closed-loop control

operations are important. Thus the pilot-vehicle system path response characteristics in both intermittent and continuous closed-loop piloted operations may be relevant in flying qualities assessments. Both types of control operations will be considered below.

Because of the three different types of control operations (unattended, intermittent, and continuous closed-loop) the flying qualities will in general depend upon effective aircraft (aircraft plus flight control system) responses to pilot command and external disturbance inputs. Similarly the multi-degree-of-freedom character of the aircraft implies that more than one aircraft output variable can be important, either as an object of pilot control or in the system response to disturbances. Figure 20 summarizes these four combinations of responses to commands or disturbances. The figure depicts a generalized longitudinal stability augmentation system. Although the system is shown as a single loop entity the structure will apply just as well to multipoint flight control systems if the airframe dynamics are considered to be effective dynamics modified by controls other than to the elevator.
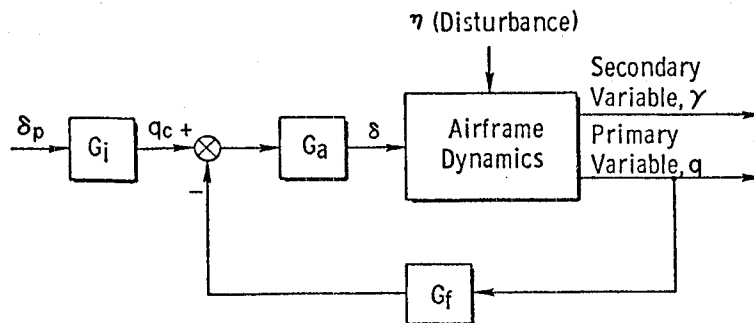
a) ● Primary response/command

$$\frac{q}{\delta_p} = \frac{G_i}{G_f}\left\{\frac{G_a G_f \left[G_\delta^q\right]}{1 + G_a G_f \left[G_\delta^q\right]}\right\} \longrightarrow \frac{G_i}{G_f}$$

b) ● Primary response/disturbance

$$\frac{q}{\eta} = \frac{\left[G_\eta^q\right]}{1 + G_a G_f \left[G_\delta^q\right]} \longrightarrow \frac{\left[G_\eta^q\right]}{G_a G_f \left[G_\delta^q\right]}$$

c) ● Secondary response/command

$$\frac{\gamma}{\delta_p} = \frac{q}{F_s}\left[\frac{G_\delta^\gamma}{G_\delta^q}\right]$$

d) ● Secondary response/disturbance

$$\frac{\gamma}{\eta} = \frac{G_\eta^\gamma + G_a G_f \left[G_{\delta\eta}^{q\gamma}\right]}{1 + G_a G_f \left[G_\delta^q\right]} \longrightarrow \left[\frac{G_{\delta\eta}^{q\gamma}}{G_\delta^q}\right]$$

Figure 20. Effective Aircraft Dynamics Pilot-Command and
Disturbance Input to Aircraft Response Relationships

The primary output variable is the pitching velocity, q, and the secondary variable is flight path angle, γ. The G_i, G_a, and G_f blocks comprise the pitch controller and correspond to the command input elements, the forward loop equalization and actuation system elements, and the sensor y array, mixing, equalization, and observer elements, respectively. The effective aircraft characteristics are given by the transfer functions in boldface enclosed in brackets, such as $[\mathbf{G_\delta^q}]$, which is the effective pitching velocity-to-pitch-controller transfer function. All of the response/command or /disturbance closed-loop transfer functions are also shown in their limiting cases for high open-loop gain, i.e., $G_a G_f [\mathbf{G_\delta^q}] > 1$. Over the closed-loop aircraft/flight control system bandwidth, ω_b, for which this inequality applies, the response properties are much simplified. Among the points illustrated by this figure are,

- Several response/command and response/disturbance system characteristics must be considered by the pilot to completely define the system's flying qualities.

- The primary response/command relationship approximates G_i/G_f over the bandwidth ω_b where feedback is active. Thus this response can be made essentially independent of the basic vehicle dynamics over this control bandwidth.

- The primary response to disturbance can be made almost arbitrarily small by increasing the overall loop gain $G_a G_f [\mathbf{G_\delta^q}]$.

- Three of the four types of responses depend greatly on the properties of the aircraft transfer function numerators.

The secondary response (c and d of Fig. 20) are defined by variables which are not fed back to a control point. The secondary response γ to a pilot command input δ_p can be tailored somewhat by the pitch rate augmentation. This can be of some importance in assuring motion harmony between key primary and secondary variables, such as θ and γ or θ and a_z. The other components in the secondary response relationships are ratios of aircraft numerators, i.e., $[\mathbf{G_\delta^\gamma}]/[\mathbf{G_\delta^q}] = [\mathbf{N_\delta^\gamma}]/[\mathbf{N_\delta^q}]$, because the denominators of these aircraft transfer functions will cancel. The

numerator, $[N_{\delta_\eta}^{q\gamma}]$ of the aircraft transfer function $[G_{\delta_\eta}^{q\gamma}]$, involved in the secondary response to disturbances is a so-called coupling numerator. Intrinsically it depends on system architecture in modifying a secondary response/disturbance, e.g., this numerator would be different if an a_z feedback were used instead of q. The bracketed ratio of airplane numerators shown by c and d of Fig. 20 are indicative of the aircraft's secondary responses to commands and disturbances with pitching velocity constrained.

Control of pitch attitude is a nearly ubiquitous longitudinal control task either as an end in itself or as an inner loop for path control. Consequently the most important primary response/command relationship in determining closed-loop system flying qualities will be for θ/δ_p. In terms of the block diagram of Fig. 20 this will be given in general by

$$\frac{\theta}{\delta_p}(s) = \frac{G_i(s)}{s} \cdot \frac{q}{q_c}(s) \qquad (24)$$

When the dominant mode superaugmented form is present this will take the form

$$\frac{\theta}{\delta_p}(s) \doteq \frac{G_i(s)}{s} \cdot \left\{ \frac{K(s + 1/T_q)e^{-\tau s}}{s^2 + 2\zeta'\omega_n's + \omega_n'^2} \right\} \qquad (25)$$

The terms in braces are the contribution of the closed-loop aircraft flight control system to the superaugmented vehicle response. The actual flying qualities can, of course, be adjusted by the forms selected for $G_i(s)$, which appears outside the closed aircraft plus flight control system loop [as noted in Fig. 20 the primary response/command dynamics are governed by the combination $G_i(s)/G_f(s)$].

B. MANUAL PRECISION PATH CONTROL

We are interested here in exposing any essential differences in flying qualities between conventional and superaugmented aircraft. To examine what these may be we will consider a hypothetical but realistic

pair of aircraft. Because short-term precision path control is essentially two degrees-of-freedom since speed is nearly constant, the conventional aircraft will be modeled using the conventional short period approximation. The value of $1/T_{\theta_2} = 0.5$ rad/sec, and the dominant mode dynamics $[\zeta_{sp}, \omega_{sp}] = [\zeta', \omega_n'] = [0.74, 1.68]$ are set to be the same for both aircraft. For the superaugmented aircraft $1/T_q = 1.5$ rad/sec. The open-loop effective aircraft characteristics therefore differ <u>only</u> in the separation between $1/T_{\theta_2}$ and $1/T_q$.

In the following we shall consider two aspects of path control, corresponding to intermittent and full attention closed-loop pilot activity, respectively.

In intermittent control the pilot is presumed to apply a deft, accurately-programmed, discrete input to the aircraft and then await, with confidence from past experience, for an appropriate aircraft response. With rate command/attitude hold systems this form of pilot action is not uncommon. In essence the pilot lets the airplane under control do the basic responding and stabilization. If the commanded attitude change is not precisely what was originally desired, an additional discrete correction is made. With these types of inputs, the effective system dynamics will be predominantly those of the effective aircraft-alone and the appropriate aircraft transfer functions are those relating flight path to pilot input. They will be given approximately by:

Rate Command/Attitude Hold Superaugmented Aircraft

$$\frac{\gamma}{\delta_p} = \underbrace{\frac{K(s + 1/T_q)e^{-\tau s}}{s^2 + 2\zeta'\omega_n's + \omega_n'^2}}_{\text{Attitude}} \left\{ \underbrace{\frac{1/T_{\theta_2}}{s(s + 1/T_{\theta_2})}}_{\text{Path/Attitude}} \right\}$$

Conventional Aircraft

$$\frac{\gamma}{\delta_p} = \underbrace{\frac{K(s + 1/T_{\theta_2})e^{-\tau s}}{s^2 + 2\zeta'\omega_n's + \omega_n'^2}}_{} \left\{ \underbrace{\frac{1/T_{\theta_2}}{s(s + 1/T_{\theta_2})}}_{} \right\}$$

Although it is not essential to do so, $1/T_q$ will normally be adjusted for closed-loop aircraft flight control system maximum stability and gain margins. Accordingly it will often be considerably larger than $1/T_{\theta_2}$ (as already noted $1/T_q \doteq 3 \times 1/T_{\theta_2}$ for the Shuttle whereas the two are essentially equal for the X-29A). As noted in Ref. 11, when $1/T_q$ is substantially larger than $1/T_{\theta_2}$, the rate command/attitude hold aircraft path response to a step function pilot command will have a lag with a time constant T_{θ_2} appearing as a component in the indicial response. In the conventional aircraft, on the other hand, the attitude lead _is_ $1/T_{\theta_2}$ and thus cancels the path lag at $1/T_{\theta_2}$ in the path/attitude response. This additional lag in the rate command/attitude hold system path response can be alleviated by one of the bandwidth extension techniques mentioned earlier. It does not occur, for example, in the "pseudo conventional" aircraft. A separation between $1/T_q$ and $1/T_{\theta_2}$ clearly has an effect upon the path response to discrete inputs, at least to the extent that the pilot can perceive quantities which are proportionally related to flight path. Under VMC conditions in approach and landing to a runway such quantities can be deduced by the pilot, and consequently any additional lags and path response introduced in this manner may have flying qualities relevance.

In attitude control, on the other hand, the natural values of $1/T_{\theta_2}$ may not be the most desirable and a well selected $1/T_q$ could be superior. This is one feature of the closed-loop piloting characteristics considered next.

A block diagram that indicates the pilot's activities in closed-loop precision path control is shown in Fig. 21. On the right the augmented aircraft has path deviation and pitch attitude as the output variables stemming from aircraft dynamics which are forced by external atmospheric disturbances and the pilot control output, δ. The augmented aircraft itself is a closed-loop system comprising the airplane-alone and augmentation system. Thus, the sensors, computation, and actuation elements involved in the feedback control augmentation system, as well as the aircraft alone, are encompassed by the "Augmented Aircraft Pitch Dynamics" block. (An underlying assumption in this diagram is that

EFFECTIVE AIRCRAFT DYNAMICS

(Aircraft + Augmentation System)
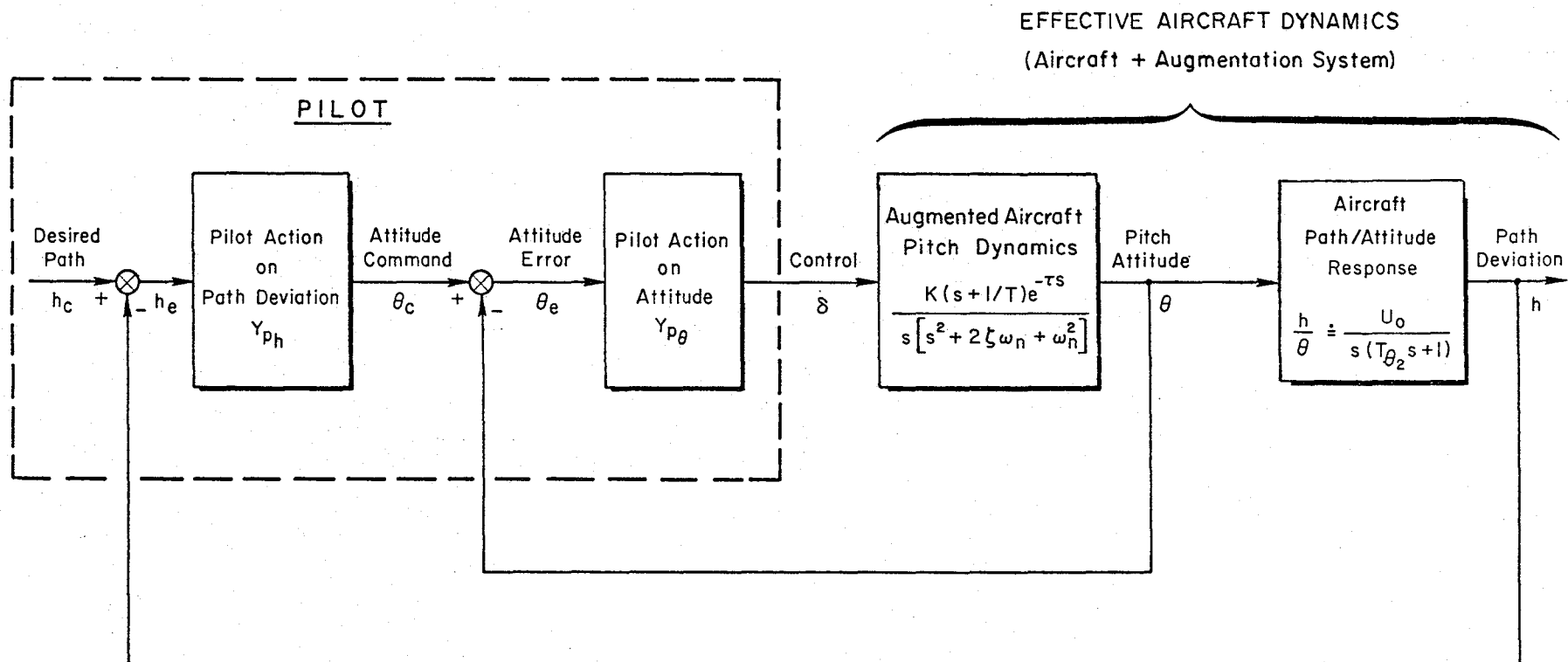
Figure 21. Closed-Loop Precision Path Control with Attitude Control Inner Loop

other aircraft control effectors, such as throttle or flap, are not being continuously modulated by pilot control action; trim management using these aircraft effectors, however, is not excluded.)

Even though trimmed precisely, the augmented aircraft will not by itself maintain exactly the prescribed path and attitude in the presence of disturbances. Consequently, the pilot must exert control not only to establish the desired path but also to correct any deviations from the desired attitude and path. This is accomplished by the pilot acting as a closed-loop controller, which means simply that the pilot's control output is dependent on (i.e., a function of) path deviation and attitude. Thus, a component of the pilot's control output is correlated with an attitude error, and another component is correlated with the difference between the desired and actual path. This relationship is depicted in the Fig. 21 block diagram as a "series" pilot closure, i.e., the pilot's action on path deviation acts in series with, and provides an internal "attitude command" for, the pilot's action on attitude error. These pilot activities are represented in Fig. 21 by the symbolic transfer characteristics Y_{ph} and $Y_{p\theta}$. Several research studies using elaborate and detailed measurements of just this situation (e.g., Refs. 12 and 13) indicate that this series structure and general pilot behavior control model is appropriate for path control situations. In essence, the pilot's higher-frequency control actions are devoted primarily to attitude, so that the "inner" attitude loop is tightly closed, and the attitude is well regulated. This tight inner loop makes possible the effective closure of the "outer" path deviation loop without excessive pilot equalization or compensation. Without good control of attitude the pilot would have to be way ahead of any path changing trends, requiring very difficult anticipation and high workload. (Examples include altitude control using only airspeed and altimeter or control during approach using only airspeed and the raw ILS glidepath data.) If the attitude loop is difficult for the pilot to interact with and close (i.e., if the augmented aircraft pitch attitude dynamics are deficient in that they require excessive pilot compensation and attentional workload), attitude control will suffer directly and path control indirectly.

The inner loop closure for the conventional and superaugmented aircraft are compared in Fig. 22. In both cases an effective pilot time delay of 0.45 sec to cover neuromuscular system lags and other latencies has been used, and pilot leads have been estimated (consistent with the crossover model, Ref. 14) to provide a K/s-like region at crossover. For nominal full-attention pilot gains there are no significant differences between the superaugmented and conventional pilot-vehicle closed-loop system attitude control properties. However, the superaugmented open-loop characteristic has an intrinsic advantage over the conventional characteristic in that it represents a broad region of "K/s" which will allow the pilot to change his gain (e.g., as an increase for very tight control, or a decrease as in intermittent, non full-attention, control) over a large range without requiring changes in equalization. By comparison, the conventional airplane pitch attitude loop closure is characterized by a broad "shelf" between $1/T_{\theta_2}$ and ω_{sp} which presents a rapid drop off in closed-loop system bandwidth with pilot gain reduction. For increases in pilot gain above the values shown in Fig. 22 the characteristics for both aircraft remain K/s-like. In other words, the shelf property for the conventional aircraft, will be manifest in a greater variation in the characteristics of the closed-loop response over a range of gains. For the superaugmented aircraft the variation in pilot gain will primarily effect only the rise time of the attitude to attitude command response. Representative θ'/θ_c responses are compared in Fig. 23.

The primary question concerning the open-loop dynamics of rate command/attitude hold superaugmented aircraft is the effect of the separation of the attitude lead from the path lag $\left(1/T_q \gg 1/T_{\theta_2} \right)$. This question may be approached theoretically by considering the most elementary realistic task, e.g., regulation of flight path angle or sink rate in approach. For this situation the open-loop transfer function for the outer loop closure may be represented by

$$\frac{\dot{h}}{\theta_c} = \frac{\dot{h}}{\theta} \cdot \frac{\theta'}{\theta_c}$$

$$= \frac{U_o}{\left(s + 1/T_{\theta_2} \right)} \frac{\theta'}{\theta_c} \qquad (26)$$

a) Conventional (short-period)   b) Superaugmented (G_i = constant)
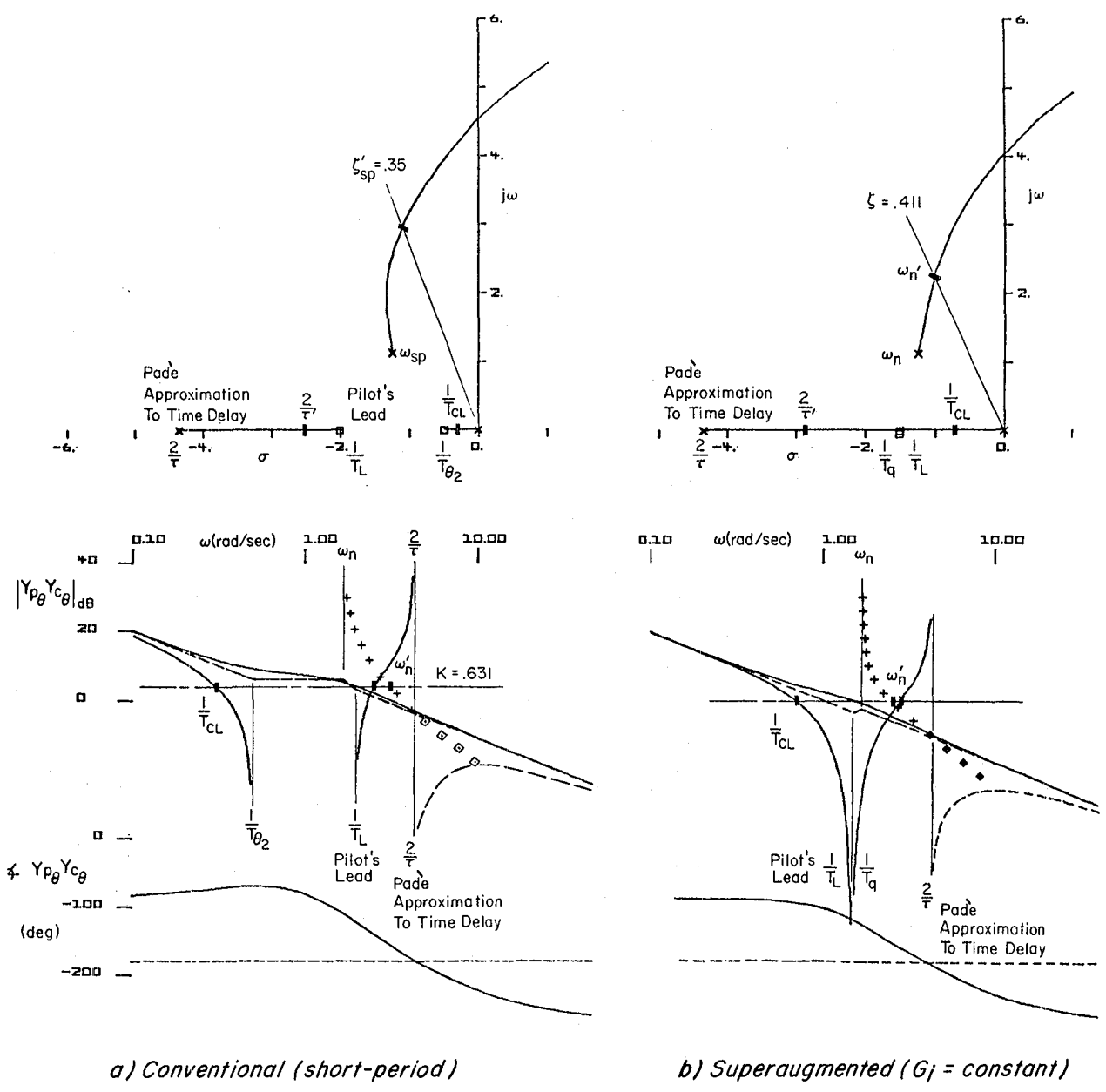
Figure 22. Pilot's Closure of Inner Attitude Loop

0.10   1.00   ω(rad/sec) 10.00   0.10   1.00   ω(rad/sec) 10.00

20   20

$\left|\frac{\theta'}{\theta_c}\right|_{dB}$

$\frac{1}{T_{CL}}$ $\frac{2}{\tau'}$ ω_n' ω_n' $\frac{2}{\tau'}$

0   0

−20   −20

$\frac{1}{T_{\theta_2}}$ $\frac{1}{T_L}$ $\frac{2}{\tau}$ $\frac{1}{T_q}$ $\frac{1}{T_L}$

$\frac{2}{\tau}$

0   0

$\angle\frac{\theta}{\theta_c}$

−100   −100

(deg)

−200   −200

UNIT STEP θ_c

1.0   1.0

θ θ

.5   .5

0   0

0   1   2   3   4   5   6   0   1   2   3   4   5   6
time (sec)   time (sec)

a) Conventional (short period)   *b) Superaugmented (G_i = constant)*
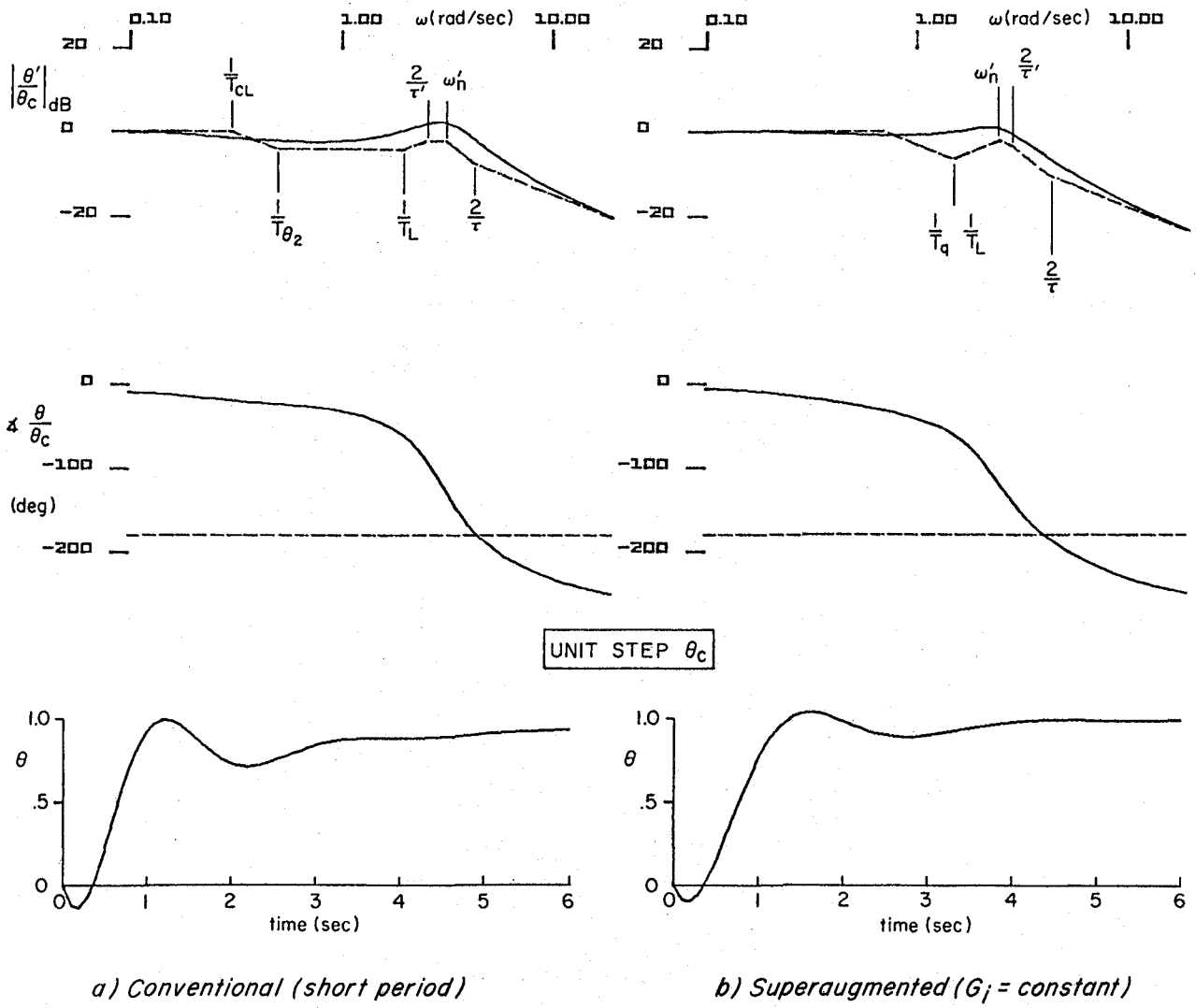
Figure 23. Closed-Loop Attitude Response

For a very high gain attitude closure by the pilot, for either conventional or superaugmented aircraft

$$\frac{\theta'}{\theta_c} \rightarrow 1$$

(The prime indicates closure of the pilot's attitude loop.) Thus, the outer loop closure will be the same for either aircraft and the dominant parameter will be the path/attitude lag time constant T_{θ_2} (determined by basic airframe characteristics).

The fundamental question is whether for realistic finite gain inner loop closures any significant differences will exist in the outer loop closure. The finite gain θ'/θ_c transfer function will be of the form

$$\frac{\theta'}{\theta_c} = \frac{K(s + 1/T_L)(s + 1/T)}{(s + 1/T_{CL})[s^2 + 2\zeta'\omega_n's + \omega_n^2]}$$

where $\hspace{8cm}$ (27)

$$1/T = \begin{cases} 1/T_{\theta_2} & \text{conventional} \\ \\ 1/T_q & \text{superaugmented} \end{cases}$$

A comparison of the conventional and superaugmented outer loop closures is shown in Fig. 24. The open-loop $\dot{h}/\theta_c(j\omega)$ amplitude ratio and phase characteristics are quite similar for the two cases. However, some subtle differences are suggested in the asymptotic "backbone" of the amplitude ratio curves and in the Bode loci. In particular, for the superaugmented case, the separation of $1/T_{\theta_2}$ and $1/T_q$ is seen in the amplitude asymptotes. The primary closed-loop manifestation of this separation is that in the superaugmented case, the low frequency path mode is complex. The corresponding locus in the conventional case is a real axis locus between the pilot's inner (attitude) closed-loop real pole $(-1/T_{CL}')$ and the lead $1/T_L$. However, these are second-order effects and there is no first-order effect on the outer loop closure in

a) Conventional (short-period)   b) Superaugmented (G_j = constant)
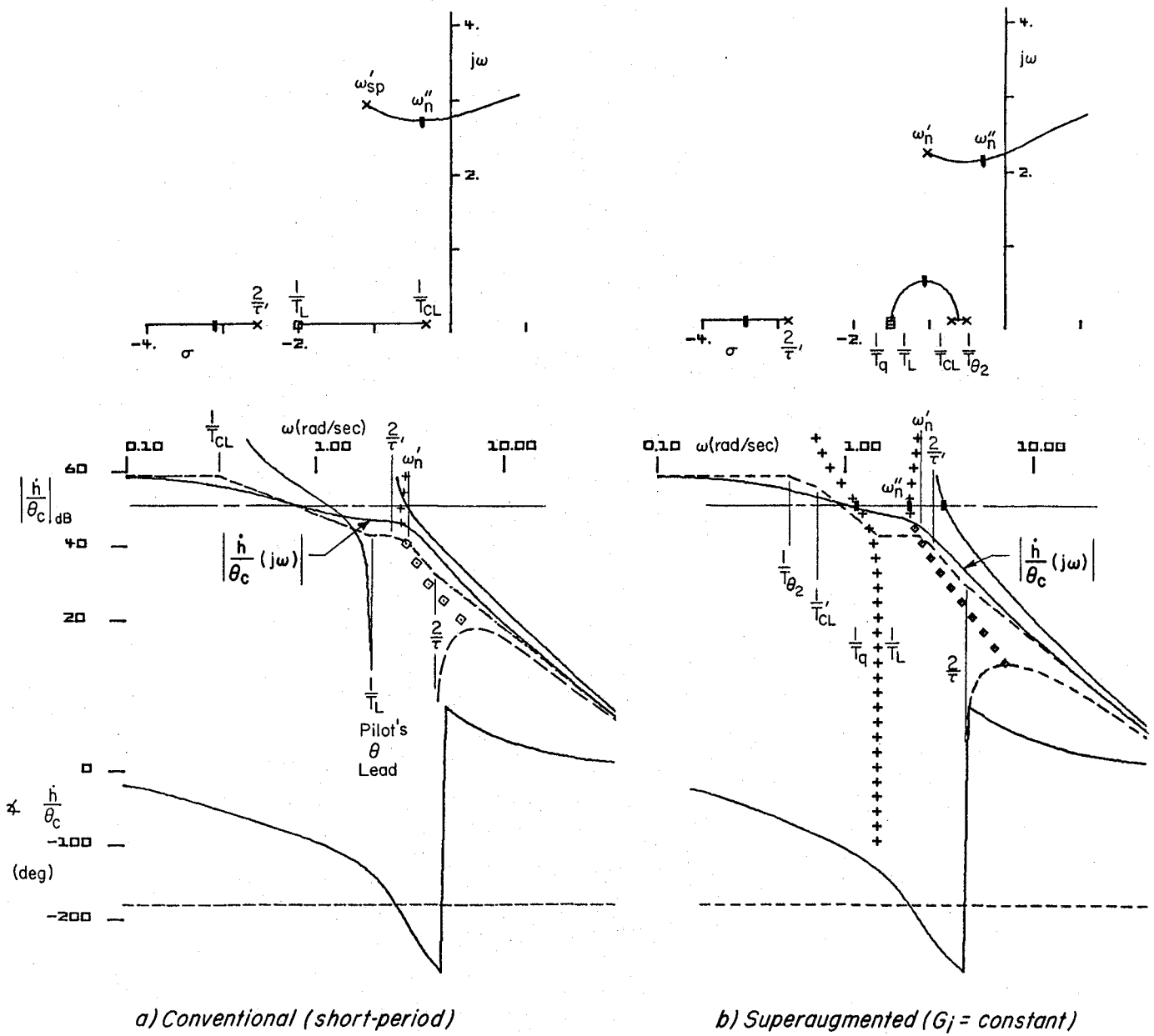
Figure 24. Path Loop Closure with Inner Attitude Loop

terms of gain or phase margin, or other measures of path loop bandwidth. There may be subtle effects on flying qualities due to the detailed differences in these closures, however, it is not at all clear that either path control situation is superior to the other. More specifically the relative α/δ_p and γ/δ_p bandwidth deficiencies of the superaugmented aircraft <u>do not</u> directly translate into closed-loop path control deficiencies. This is simply a manifestation of the fact that it is unreasonable to consider closure of the outer loop without an inner attitude loop (at least intermittant) to provide proper equalization. This is true for both superaugmented and conventional aircraft. However, pilot preferences for the attitude control advantages might be expected in the superaugmented case.

A summary that may be useful in considering differences between conventional and superaugmented aircraft -- specifically regarding the "$1/T_{\theta_2} \neq 1/T_q$" issue -- is as follows.

> During periods of tight closed-loop tracking, path control distinctions between rate command/attitude hold superaugmented and conventional aircraft will be minor; however, pilots might prefer the superaugmented pitch response because of its more "K/s-like" characteristics. During periods of precognitive (open-loop) control, pilots with conventional aircraft experience will notice the greater lag in the h/δ_p response for the superaugmented aircraft. This may result in relatively poor pilot ratings initially; but, with continued exposure to superaugmented aircraft, ratings may improve as confidence is gained that closed-loop control is not seriously affected.

An experiment to test this concept has not been conducted, however, some circumstantial support is available from the data in Ref. 15. This paper reports on a Space Shuttle simulation conducted on the NASA-Ames VMS simulator. The existing Shuttle pitch FCS (the protypical superaugmented aircraft) was compared to alternative FCS designs which had more conventional characteristics. Evaluations and pilot ratings were obtained from two groups of pilots:

1) test pilots with conventional aircraft experience

2) Shuttle pilots

Considerable variation in pilot opinion was observed. The study conclusions from Ref. 15 were

Final Flare and Landing

A control system that had good flight path control response [i.e., conventional $\dot{h}/\delta_e$] was preferred by pilots with conventional aircraft background.

The current Shuttle control system which has good attitude control was preferred by the Shuttle pilots who had extensive training with this system.

Steep Glideslope

No clearcut advantage was seen with either system. There was a general preference for the current system because of the attitude dropback characteristics.

These conclusions are consistent with the above analysis.

SECTION IV

PILOT DYNAMIC BEHAVIOR IN ATTITUDE CONTROL OF SUPERAUGMENTED AIRCRAFT WITH HIGH FREQUENCY TIME LAGS AND TIME DELAYS

As noted in connection with Table 5 superaugmented aircraft may potentially have a larger number of high frequency phase lag elements than a conventional aircraft. Both will share actuator and certain manual control lags. To these the superaugmented or heavily augmented fly-by-wire aircraft may add additional stick filtering, some bending mode filters (needed to permit the large effective aircraft/FCS bandwidth), computational delays, etc. The flying qualities community, in an attempt to extend to augmented aircraft the data and criteria from experience and experiments with conventional aircraft has relied extensively on so-called equivalent systems. These are approximate representations of the effective aircraft dynamics which are valid over a restricted frequency range. In the equivalent system the lower frequency effects of high frequency lags and leads are subsumed in a single effective time delay, represented as a pure delay term $e^{-\tau_{eff}s}$. This representation is adequate for the phase and the amplitude ratio over a bandwidth less than $1/\tau_{eff}$ rad/sec. For some heavily augmented aircraft $1/\tau_{eff}$ is very close to or even within the pilot's nominal range of control interest. As is well known, if the τ_{eff} stems from a pure time lag, $(\tau_{eff} s + 1)^{-1}$, the pilot in these circumstances will adopt a lead which nearly cancels the lag, thereby offsetting its effects. The same type of adjustment on the part of the pilot cannot be accomplished if τ_{eff} actually derives from a pure time delay. It therefore becomes a matter of extreme importance for superaugmented and other heavily augmented advanced flight control systems to be able to distinguish between the effects of pure time delay and time lag components in the effective delay used in equivalent system representations.

As a first step in attempting to better understand pilot dynamics in the presence of lags and pure delays, a short experiment was conducted on a fixed-base simulator. The task given was attitude control corresponding to the usual inner loop in precision path control. The pilot's dynamic characteristics adopted for the several tasks were determined by describing function measurements, and pilot workload was assessed using pilot ratings. The description below starts with an initial article on the theoretical distinctions between time lags and pure time delays. The implications of these distinctions on pilot dynamic behavior are also drawn. The second article describes the experimental design. It is followed by a concluding article giving the results, analysis, and conclusions. As suspected at the outset there are major differences between a time lag of τ_{eff} seconds and a time delay of the same amount.

A. THEORETICAL DISTINCTION BETWEEN TIME LAGS AND PURE TIME DELAY AND THEIR DIFFERENT IMPLICATIONS ON PILOT BEHAVIOR

Consider the pilot to be performing a simple closed-loop compensatory tracking task as represented in Fig. 25.
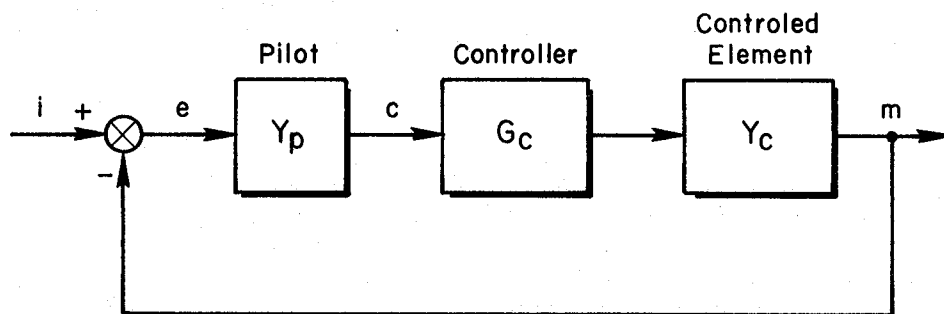
Figure 25. Block Diagram Representation of a Closed-Loop Compensatory Tracking Task

$$G_c = \frac{1}{(Ts + 1)} \text{ or } e^{-Ds}$$

$$Y_c = \frac{1}{s}$$

With this set of effective controlled elements the pilot dynamics in the frequency region about pilot-vehicle system crossover will be given by,

$$Y_p = Ke^{-\tau s} \text{ or } Ke^{-\tau s} (T_L s + 1)$$

For the first condition let G_c be a first-order lag, $1/(Ts + 1)$. Per the loop closure adjustment rules of Ref. 14, if the controller lag is near the desired crossover frequency (control bandwidth), the pilot will adopt a lead (T_L) to cancel the controller lag (T). He then can achieve a higher control bandwidth with minimum oscillatory characteristics. The open-loop transfer function becomes

$$Y_p G_c Y_c = Ke^{-\tau s} (T_L s + 1) \times \frac{1}{(Ts + 1)} \times \frac{1}{s}$$

$$= \frac{Ke^{-\tau s}}{s}$$

This is sketched in Bode amplitude asymptote and phase form in Fig. 26a. The solid lines represent the amplitude and phase without the pilot lead. For the zero dB gain line crossover (ω_{c_1}) shown, the closed-loop system without lead would be highly oscillatory because ω_{c_1} is very close to the 180 deg phase crossover, ω_{180}. The dashed lines in Fig. 26a are the amplitude and phase when the pilot adapts T_L to exactly cancel T. For this case the same gain crossover, ω_{c_1}, now enjoys a 10 dB gain margin from ω_{180} and a well damped control response would be obtained.

Let us now assume the controller consists of a pure time delay of D seconds ($G_c = e^{-Ds}$). Without a lead in the pilot model the open-loop transfer function is

$$Y_p G_c Y_c = Ke^{-\tau s} \times e^{-Ds} \times \frac{1}{s} = \frac{Ke^{-(\tau + D)s}}{s}$$

The Bode amplitude asymptote and phase for this case is sketched by the solid lines in Fig. 26b. The time delay has been chosen to produce very similar phase plots in Fig. 26a and b. Therefore the Fig. 26b system
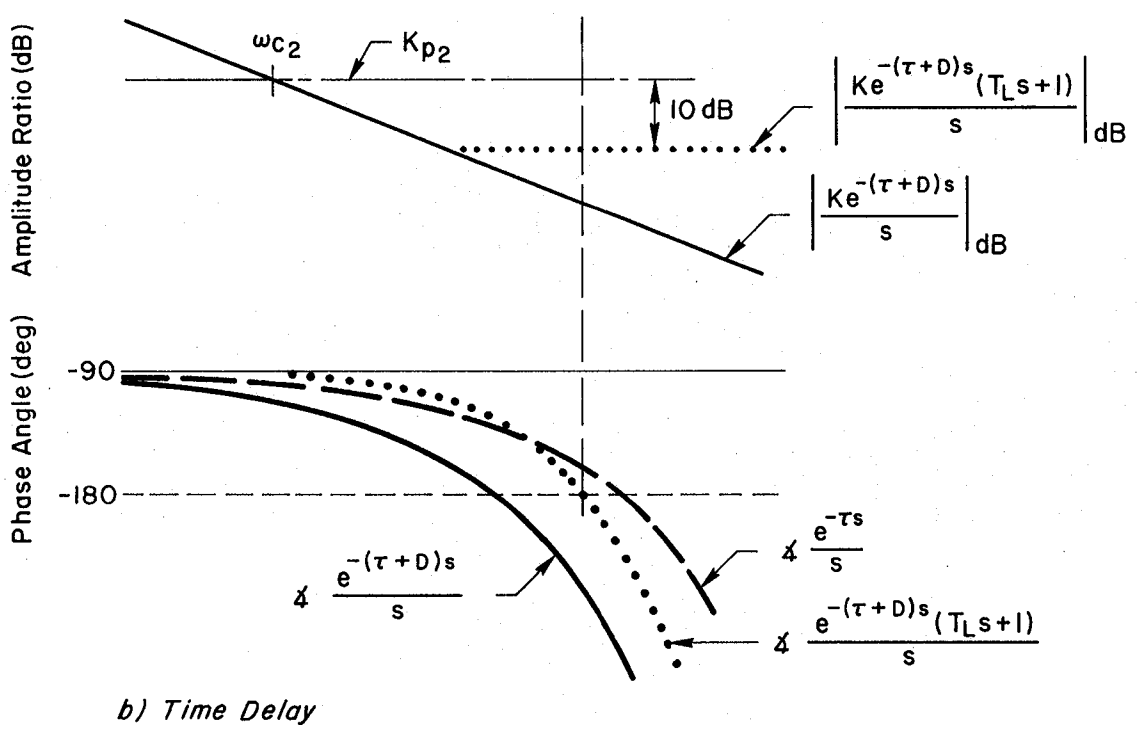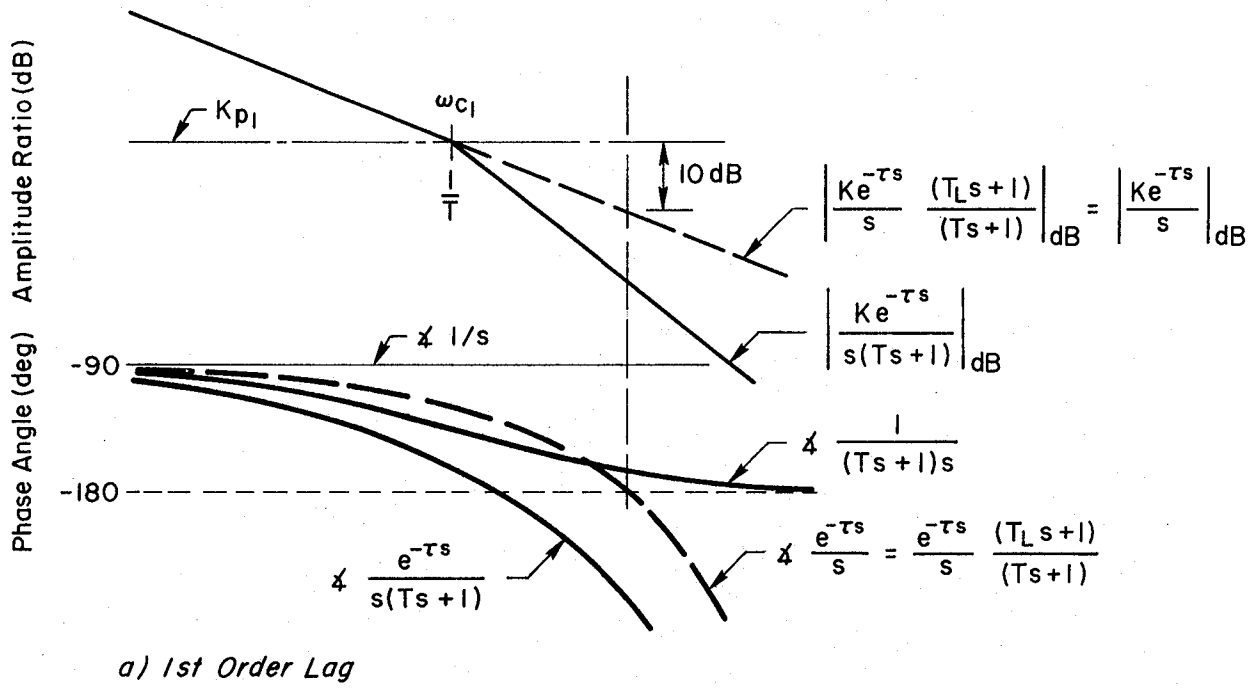
Figure 26. Bode Sketches Showing Crossover
Regression Due to Pure Time Delay

would also be highly oscillatory if the same gain line of Fig. 26a were employed because the gain crossover would occur very close to the 180 deg phase crossover. If the pilot now adapts the _same_ lead (T_L) to offset the controller induced lag, the open-loop transfer function becomes

$$Y_p G_c Y_c = \frac{Ke^{-(\tau + D)s}}{s} \times (T_L s + 1)$$

and the amplitude and phase are indicated by the dotted lines in Fig. 26b. The amplitude ratio high frequency asymptote is now flat and the pilot gain, K_{p_1}, used in the lag example would produce instability. The pilot must therefore reduce his gain to maintain stable control. For the same 10 dB gain margin the crossover would occur at ω_{c_2}.

It is postulated that this crossover regression will occur because of the conflict imposed by the time delay producing phase lag without accompanying high frequency amplitude attenuation. When the time delay becomes significant the pilot will first try lead and then reduce his gain (regress). This will result in degraded tracking performance and rating.

From the theory presented here we can make three predictions about the differences to be expected between a time lag of T seconds as contrasted with a pure delay of D = T seconds.

- The open-loop system characteristics in the crossover region for the time lag case will appear with an amplitude ratio slope of approximately -20 dB per decade. The pilot will develop a lead which offsets the controller-controlled element lag.

- A similar lead will be placed by the pilot for the pure delay case. The amplitude ratio slope about crossover will therefore be shallower than -20 dB per decade.

- The crossover frequency for the time lag case will be larger than for the corresponding delay.

- Pilot rating for the time delay will be poorer than for the time lag.

The following experiment was devised to test these theoretically derived conclusions. The experimental conditions were also selected to determine if the form of superaugmented airframe dynamics might also influence pilot behavior in an unusual way, perhaps as a departure from the classical crossover model law.

B. EXPERIMENTAL DESIGN

The purposes of this experiment were twofold: to examine effects on pilot dynamics of pure time delay versus high frequency lag for super-augmented vehicle dynamic models, and to provide a basis for possible future simulation and flight experiments (e.g., with the DFRF digital FBW F-8 aircraft).

The experimental setup is shown in Fig. 27. The piloting task is a single (pitch) axis regulation task in which attitude error created by a sum of sine waves forcing function is to be nulled. The pilot is to exert control as aggressively as possible consistent with his own criteria of stability and performance. The closed-loop task is reflected by the heavily-lined feedback system. The lighter lines depict the measurements of performance (θ, θ_e) and pilot manipulator activity (δ),
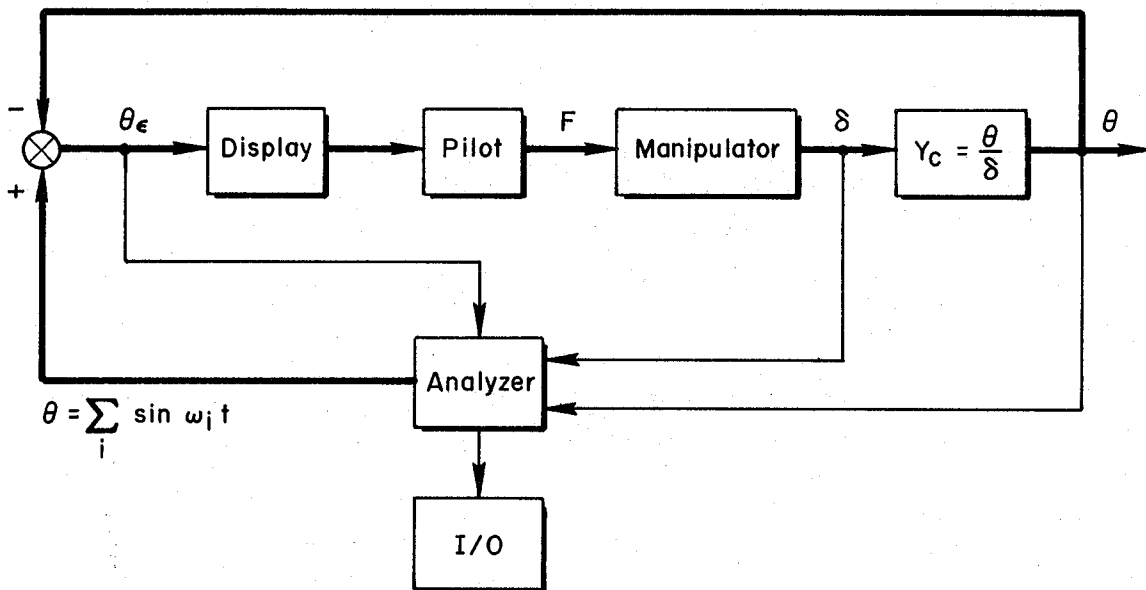
Figure 27. Experimental Setup

which are sent to a describing function analyzer. The anlyzer computes amplitude and phase components of pilot-vehicle describing function measurements at each of the input frequencies as well as basic statistical (mean, rms, etc.) measurements. It also supplies the forcing function. The pilot produces his adjusted dynamics, a verbal commentary, and Cooper-Harper ratings of workload.

The control task is shown in more detail in Fig. 28. The vehicle block approximated airframe short-period pitch attitude dynamics, θ/δ, with parameters adjustable to provide different effective airframe dynamic configurations. The electrical output of the pilot's manipulator served as an input to selectable controller dynamics of either pure gain, pure time delay, or first-order lag. The controller gain was adjustable to the pilots' preference for each effective airframe configuration.

The display consisted of an oscilloscope CRT with an aircraft marker fixed at the center of the CRT. Signal gain was adjusted so that the CRT grid marks approximated a head-up display (HUD) pitch attitude ladder with 2 deg increments. The tracking line represented the horizon bar with displacement from the aircraft marker "wings" proportional to pitch error $(\theta_c-\theta)$. The display gain was 5 deg/cm.

The manipulator was a side-stick type but was mounted in front of the pilot in about the same location as a conventional center stick. It had a simple spring restraint with a detent at neutral. Breakout torque was approximately 6 in.-lb. The mechanical torque/displacement characteristics were fixed but the electrical gain was adjustable (K_q = 0.8, 1.2, 1.6 deg/sec/deg).

Torque/displacement/command characteristics are summarized in Fig. 29 in a form to facilitate comparison with the lateral side-stick characteristics investigated in the NT-33 in-flight simulator (Ref. 16) and the Shuttle Orbiter manipulator (Ref. 17). The lower plot of initial response command gain vs. displacement/torque ratio shows the experiment stick had a greater X/T ratio than the largest available on the NT-33 but close to those of the Shuttle Orbiter manipulator roll and
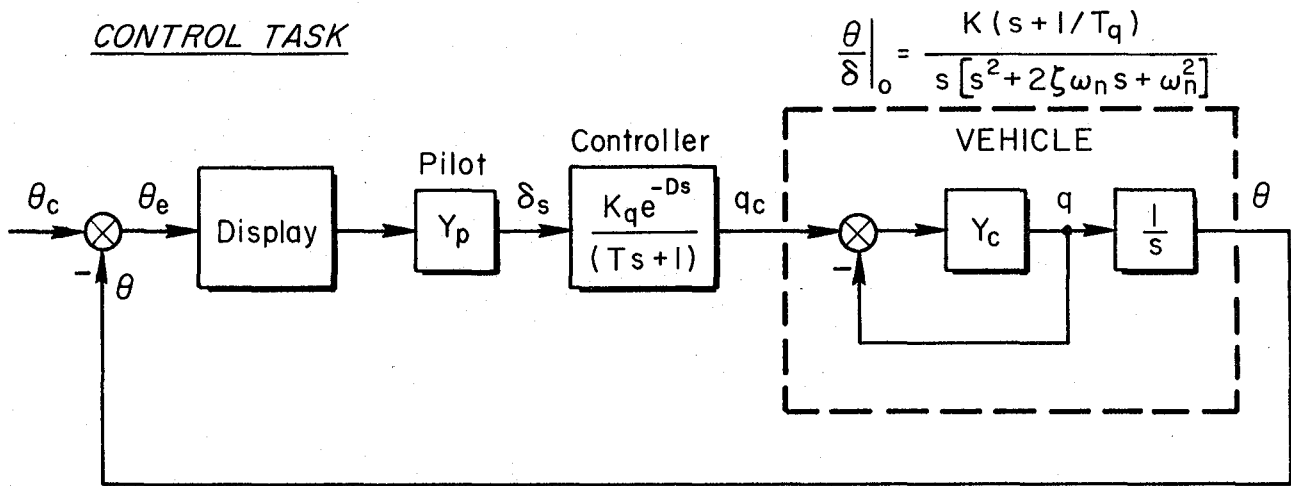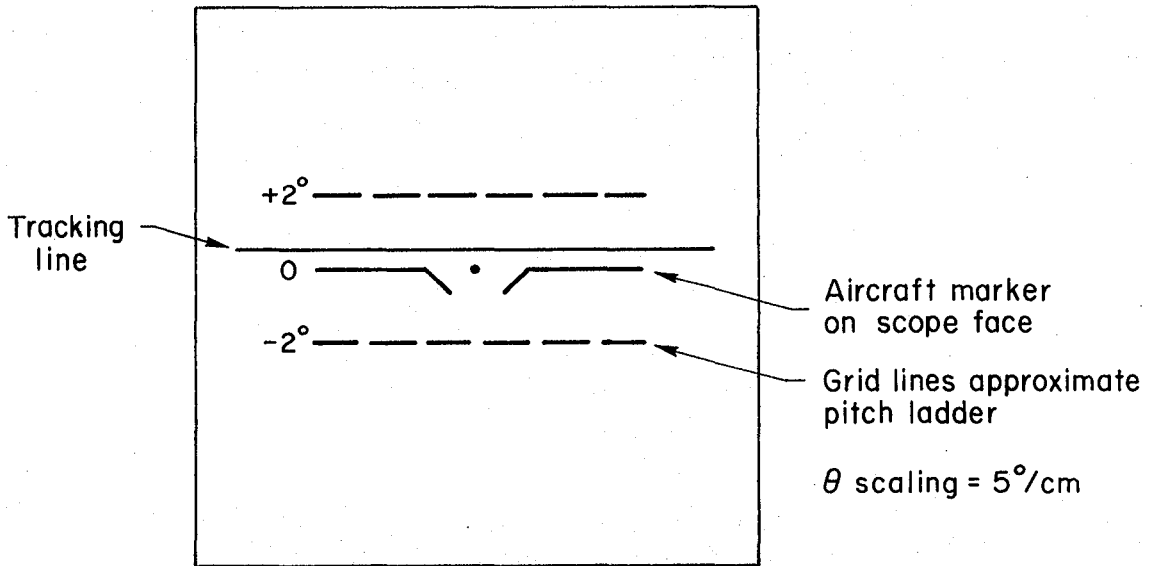
Figure 28. Experimental Design
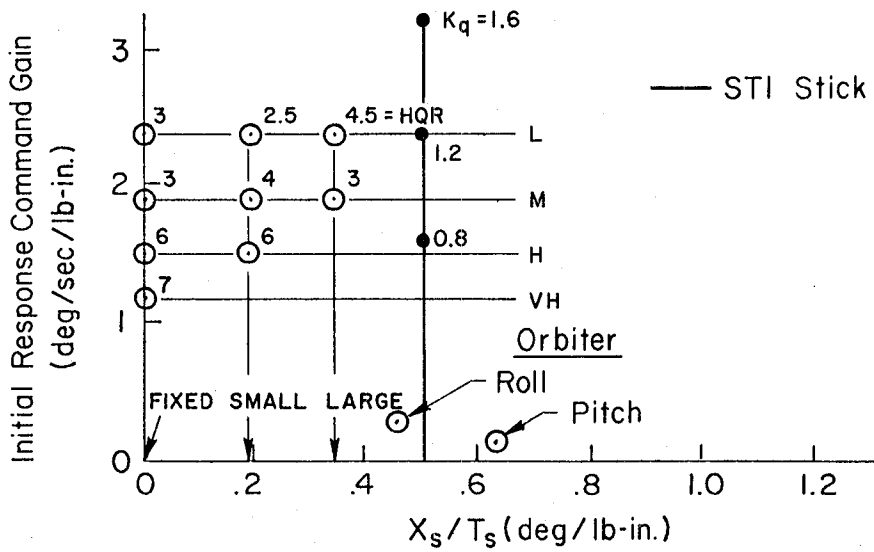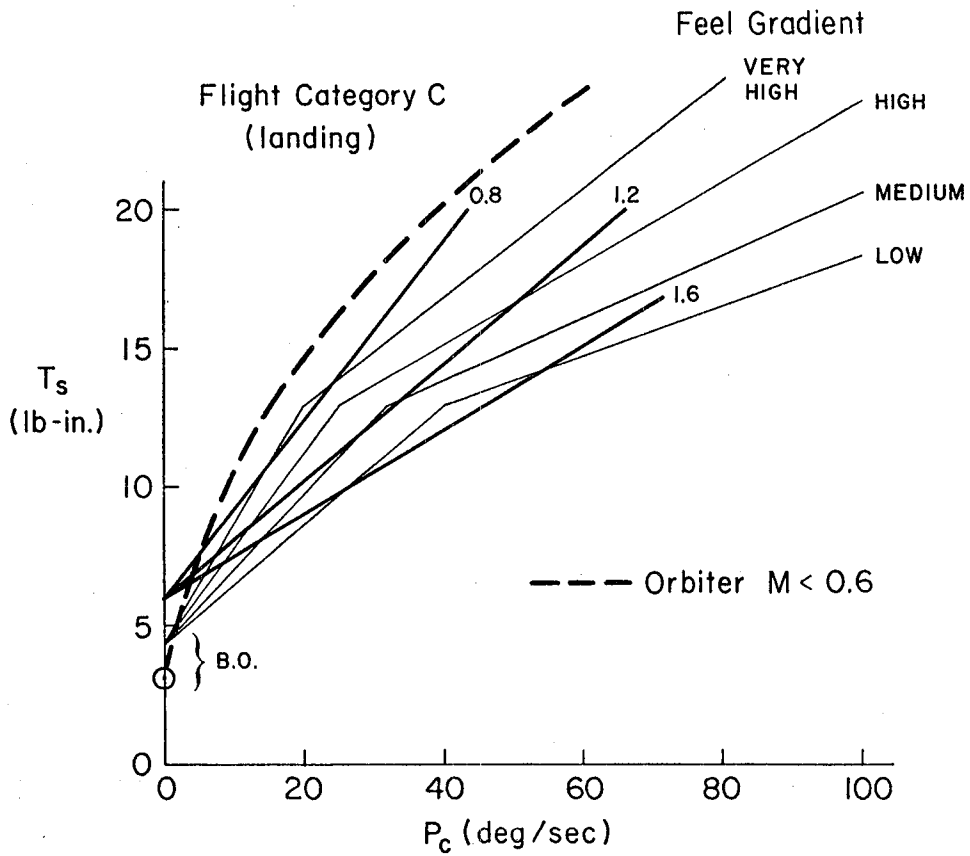
Figure 29. Manipulator Characteristics

pitch controller. Two of the input response command gains (solid circles) matched those of the NT-33 while one gain (1.6) was considerably higher than used in the NT-33. Note a high command gain results in lower feel gradient torques, and vice versa. The numbers next to the open circles are pilot ratings given to the manipulator/command configurations in the NT-33 simulation. Recall that the command gains in this experiment were selected by the pilot subject to provide the best control with specific effective vehicle dynamics. When expressed in units of (deg/sec)/in.-lb all of the gains are considerably higher than employed in the Shuttle Orbiter.

It should also be noted that the manipulator torque/displacement value shown reflects measurements for deflection away from neutral. The pivot and spring had significant friction so that torque in the return direction was somewhat lower.

The input forcing function consisted of nine sine waves. The amplitudes and frequencies shown in Fig. 30 were selected to produce a gradual decrease in forcing function amplitude in the region of anticipated crossover rather than a step change. This has been found in previous experiments to produce less scatter in the describing function measurements, and to provide data throughout the crossover region while still maintaining a definite input bandwidth below the crossover frequency.

The vehicle dynamics employed two basic $\frac{\theta}{\delta}\Big|_o$ forms as shown in Fig. 31. One was the "ideal" first-order K/s used by other experimenters (e.g., Ref. 18), the other was a third-order model whose parameters could be adjusted to approximate a superaugmented (or other) vehicle. The total effective controlled element was then the product of this "vehicle" and the appropriate controller form.

The resulting controlled element matrix is presented in Fig. 32. Four base (no time lag or delay) configurations were employed: the "ideal" K/s; two superaugmentation types with one having $1/T_q$ and ω_n values close to those of the Shuttle Orbiter in landing and the other
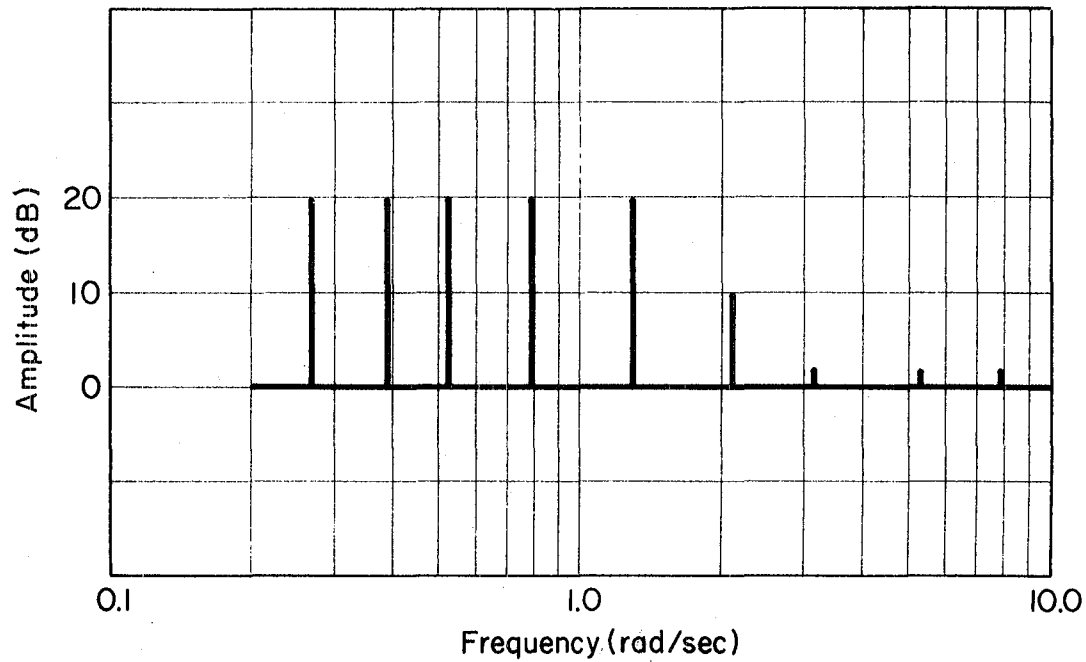
Figure 30. Forcing Function Spectra

$$\left.\frac{\theta}{\delta}\right|_o = \frac{K}{s}$$

$$\left.\frac{\theta}{\delta}\right|_o = \frac{K(s+1/T_q)}{s\left[s^2+2\zeta\omega_n s+\omega_n^2\right]} \text{(BASIC SUPERAUGMENTED } Y_c)$$

$$\frac{\theta}{\delta} = \left.\frac{\theta}{\delta}\right|_o \left(\frac{e^{-Ds}}{Ts+1}\right)$$

Figure 31. Effective Vehicle Dynamics

having double these values; and lastly, pseudo conventional pitch dynamics in which the numerator lead $(1/T_{\theta_2})$ is considerably lower than the short period (ω_{sp}).

The symbols and flags shown in the cells of Fig. 32 are used to identify the data points in the plots to follow. The circles identify the base configurations. The number of flags relate to the configuration number. The configurations were run in a random sequence. The test format for each configuration was as follows:

-- provide about 30 sec of K/s tracking

-- switch in the test configuration and obtain a minimum of 48 sec stationary tracking

-- repeat runs until three valid data runs were obtained

-- obtain pilot commentary and rating

Because this experiment was exploratory, only one experienced pilot was used. This subject is highly qualified in assessing aircraft handling qualities.

NO.	BASE CONFIGURATION	T = D = 0	T = 0.1 (SEC)	T = 0.25 (SEC)	D = 0.1 (SEC)	D = 0.25 (SEC)
0	$\dfrac{1.2}{(0)}$	⊙		✚	△	⊡
1	$\dfrac{1.6(2)}{(0)[0.707;\ 2.83]}$	⊙		✚	△	⊡
2	$\dfrac{1.2(4)}{(0)[0.707;\ 5.66]}$	⊙	✚		△	⊡
3	$\dfrac{0.8(0.75)}{(0)[0.707;\ 2.83]}$	⊙				

configuration notation: $(a) \equiv (s + a)$, $[\zeta,\ \omega_n] \equiv [s^2 + 2\zeta\omega_n s + \omega_n^2]$

Figure 32. Experimental Matrix

C. EXPERIMENTAL RESULTS, ANALYSIS, AND CONCLUSIONS

In this article pilot and pilot-vehicle describing function measurements extracted from the test data will be shown first. It will be seen that these validate the Fig. 26 regression theory sketches. These will be followed by key vehicle parameters plotted against pilot Cooper-Harper ratings for the various vehicle/controller configurations. The object here is to identify which parameters have the most influence on pilot rating and hence pilot perception of performance and/or effort.

Figure 33 presents pilot-vehicle (Y_pY_c) and pilot (Y_p) amplitude and phase data points for the K/s base configuration (0) with no controller lag or delay. The upper plot (Y_p/Y_c) shows a long region of 20 dB/dec slope as would be expected. The closed-loop crossover (ω_c) is about 2.5 rad/sec. The lower plot (Y_p) shows a quite flat amplitude which indicates a pure gain closure ($\overset{\bullet}{K_p} = 5$ dB). The phase angle, $\sphericalangle Y_p$, indicates an effective pilot latency in this task of 0.23 seconds. The pilot rating for this case was PR = 2.

Figure 34 is for the K/s base configuration but with the first-order lag of T = 0.25 sec. In the upper plot an amplitude ratio slope of -20 dB/sec (K/s) again nicely fits the Y_pY_c data. The crossover frequency is about 2.8 rad/sec. The dashed line reflects the controlled element alone (G_cY_c) high frequency asymptote. Pilot generated lead accounts for this high frequency asymptote difference and the lower plot shows the lead break ($1/T_L$) to be very close to 4 rad/sec. Thus the pilot lead is essentially on top of the controller lag. The rating for this configuration was PR = 3 which indicates a slight degradation due to the requirement to generate lead. Note, however, that the pilot also employed a higher gain (approximately 8 dB) and the crossover frequency is slightly higher than for the previous configuration.

Figure 35 again is the K/s base configuration but with the 0.25 sec pure time delay. The upper amplitude plot shows the frequency range between 0.5 and 2.0 rad/sec to have a -20 dB/dec slope and the dashed line continues this slope (representative of the controlled element dynamics alone). The data points at frequencies of 2.5 rad/sec and
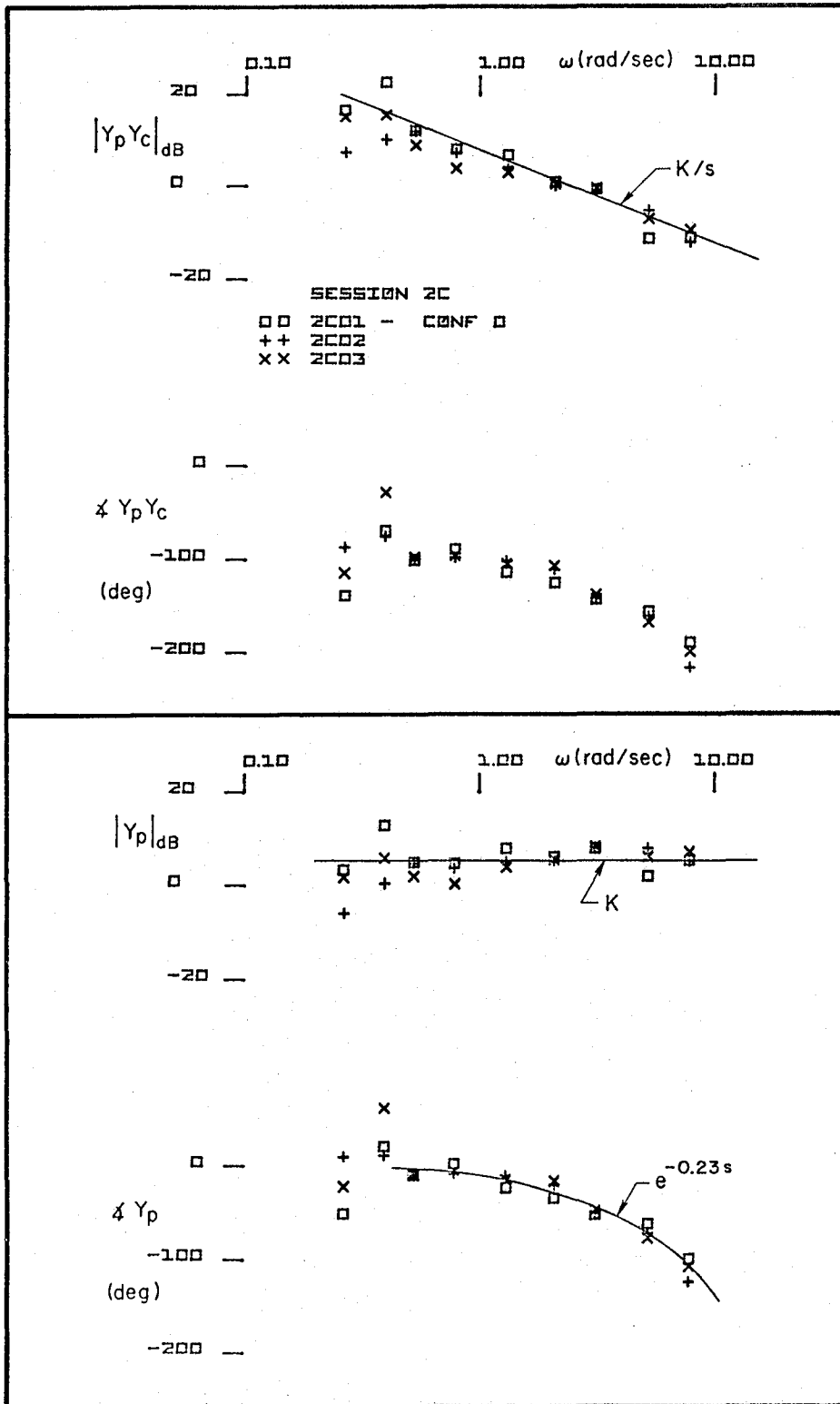
Figure 33.   Describing Function Measurements;
$Y_c = K/s$, $T = 0$, $D = 0$
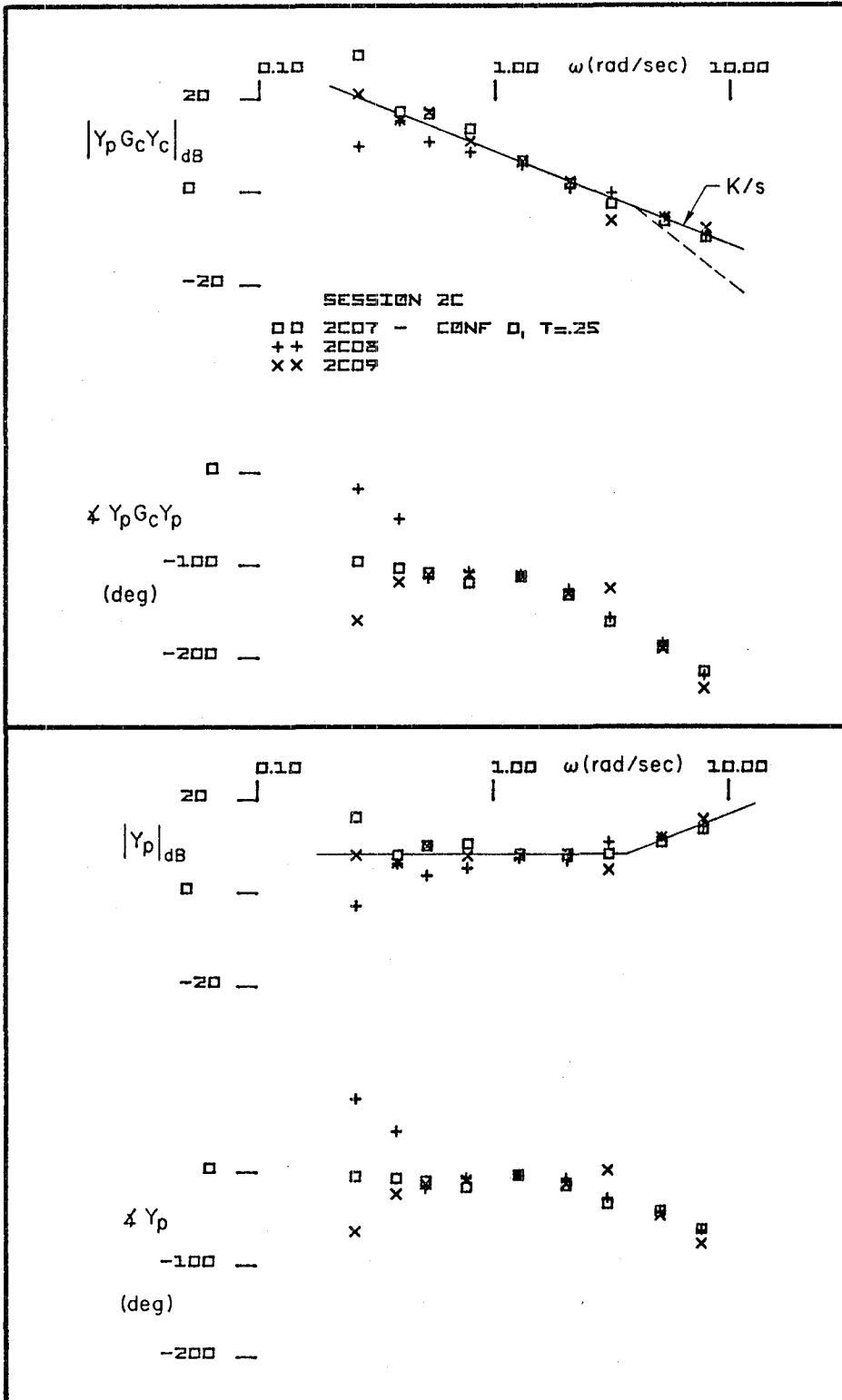
Figure 34. Describing Function Measurements;
$Y_c = K/s$, $T = 0.25$ sec, $D = 0$
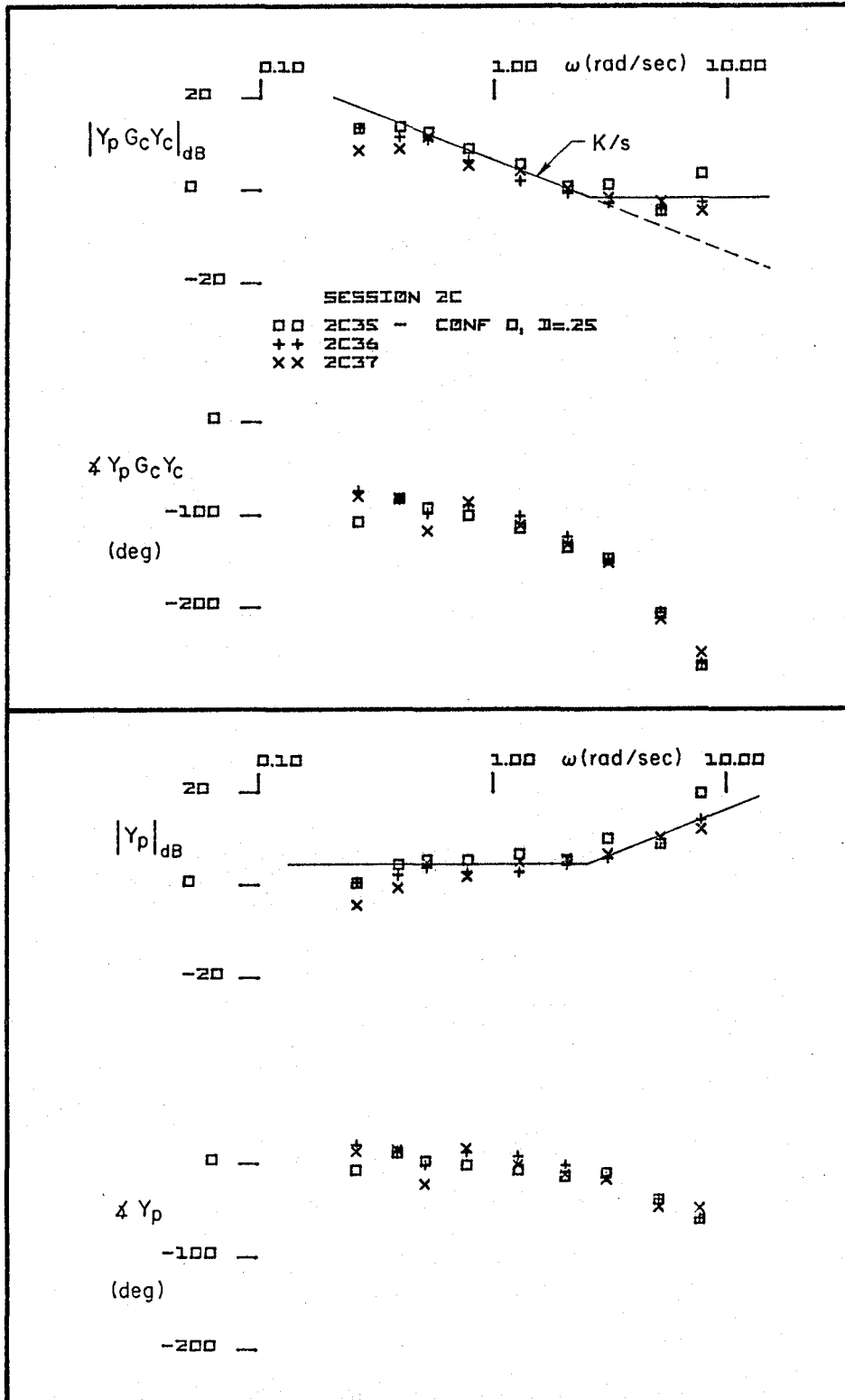
Figure 35. Describing Function Measurements;
$Y_c = K/s$, $T = 0$, $D = 0.25$ sec

above show a definite flattening in amplitude ratio slope. This is caused by the pilot introducing lead with a break frequency $(1/T_L)$ of about 2.5 rad/sec (lower plot). The pilot gain is about 5 dB. Interestingly, in this case the gain selected is about the same as that for the initial configuration without lag or time delay. Thus the crossover (upper plot) of Fig. 35 is but slightly reduced from that of Fig. 33. The pilot commented that for this configuration he was forced to alter his control technique from a continuous to a pulse type activity. The pilot rating for the 0.25 sec delay configuration was PR = 4.

Figure 36 is Configuration 2 (high frequency superaugmentation case) with the 0.25 sec delay. The upper plot shows the amplitude asymptote for the effective vehicle (dashed line) which the data points fit quite nicely between 0.4 and 1.3 rad/sec. Above that frequency the data points again are fitted by a straight line with the lead break corresponding to the pilot lead break identified from the lower figure. In this case the pilot lead occurs at about 1.6 rad/sec and his gain is about -1 dB. This produces a gain crossover in the upper plot at about 1.2 rad/sec. The crossover for the configuration without time delay (not shown here) was about 2.6 rad/sec. Therefore the regression with 0.25 sec time delay has been substantial and the pilot rating degraded to PR = 6.

Based on the above examples, it is apparent that the pilot does attempt to offset phase lag due to time delay by adopting a lead. As predicted by the theory, this lead does cause a flattening of the system amplitude response in the frequency region immediately above his control crossover frequency. This in turn requires a decrease in pilot gain and/or a change in control technique to maintain stable control and results in a decrease or regression in effective control bandwidth.

Analysis of the data from all runs showed that the key parameters which correlate well with pilot rating are crossover frequency (ω_c), pilot gain (K_p), pilot lead (T_L), and time delay (D), plus vehicle base configuration (K/s vs. the superaugmented cases). The first-order lags employed produced comparatively small change in ratings. Since ω_c and K_p are directly related, the key factors come down to ω_c, T_L, D, and
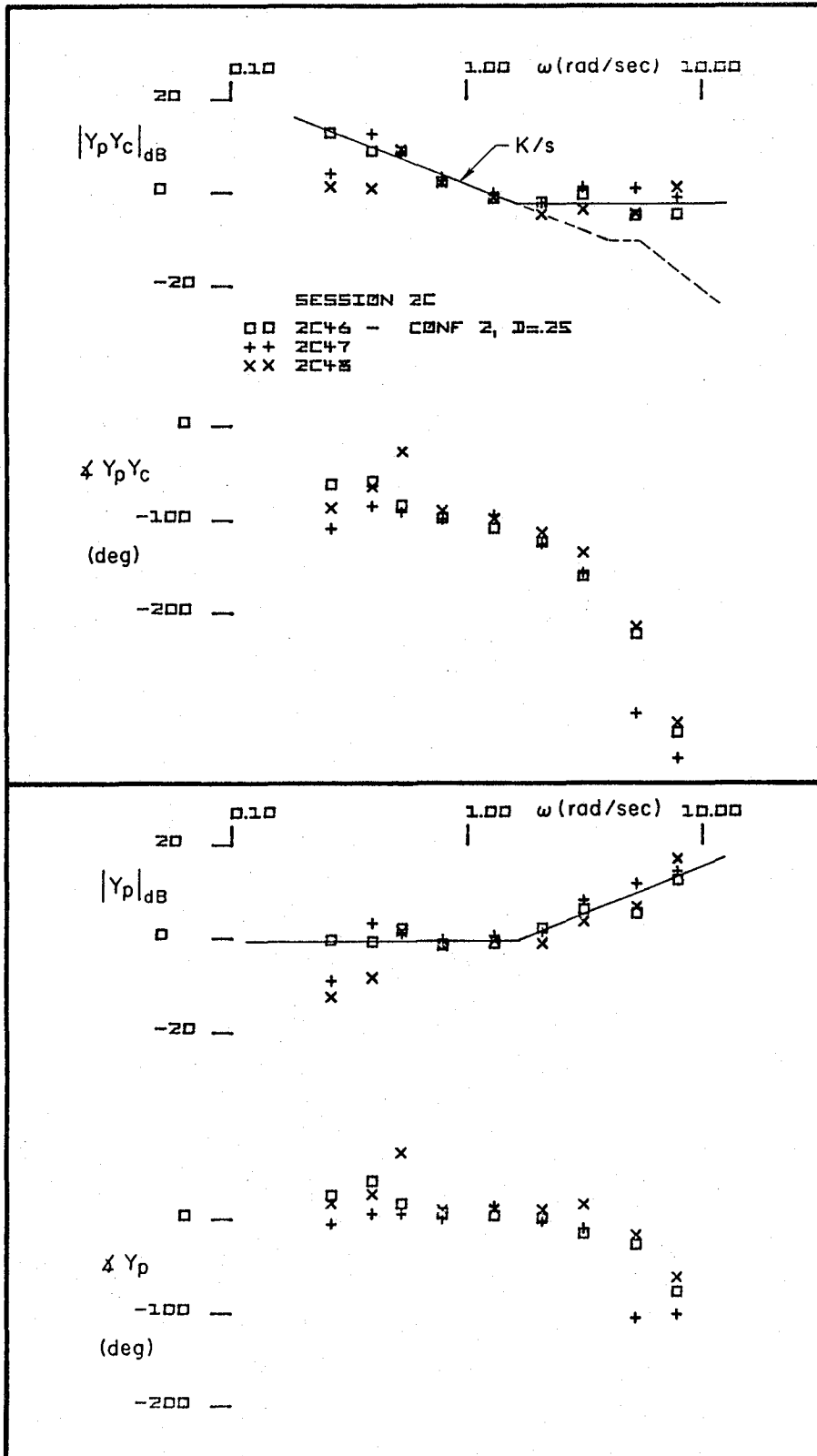
Figure 36. Describing Function Measurements;
$Y_c = \dfrac{1.2(4)}{(0)[0.707;5.66]}$, T = 0, D = 0.25 sec

vehicle base configuration. However, all of the above will be discussed and demonstrated in the following.

The observed relationship between crossover and pilot rating is summarized in Fig. 37. The solid line is a regression fit having a correlation coefficient (r) of 0.82. The dashed lines represent ±1 rating point from the straight line fit. All but three data points fall within the "rating band." The primary trends shown in Fig. 37 are

--- an increase in PR (degradation) with decrease in ω_c

--- time delay (Δ and $\square$ symbols) is more objectionable than time lag $\diamondsuit$

--- deleterious effects of time delay are more pronounced with higher order controlled element (first- or third-order)

Figure 38 presents a similar straight line regression fit to a crossplot of pilot gain (K_p) and pilot rating (PR). In this case the correlation coefficient is 0.9 and all data lie within a band of ±1 rating point. As noted before there should be almost a direct relationship between pilot gain and crossover frequency. The small difference between the results of Figs. 37 and 38 can be attributed to improved accuracy in fitting a line through Y_p data points at several frequencies versus identifying a single frequency crossover on the $Y_p Y_c$ plot. Note in Fig. 38 that all configurations with time delay, except K/s, result in pilot gain reduction of 6 dB or greater. Comparisons of Figs. 37 and 38 show a direct correlation between K_p and ω_c reductions for these cases.

Figure 39 is a plot of PR versus pilot lead time constant (T_L). This has been fitted with a straight line at a correlation coefficient of 0.83. Again, all but one data point fall within ±1 PR. This degradation in pilot rating with lead generation is consistent with previous experimental results (e.g., Ref. 14).

Plots of PR versus time delay are presented in Fig. 40. Straight line fits are shown for each configuration. Interestingly the data show a degradation in PR between base configurations (no delay) on the same order as that due to the delay with a given configuration.
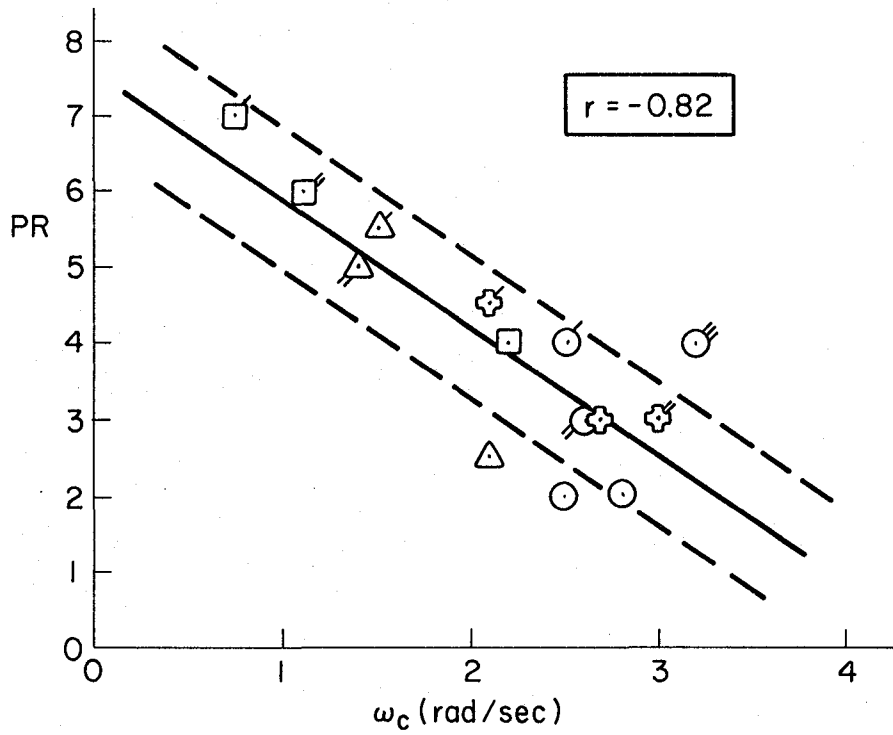
Figure 37. Pilot Rating as Function of Crossover Frequency
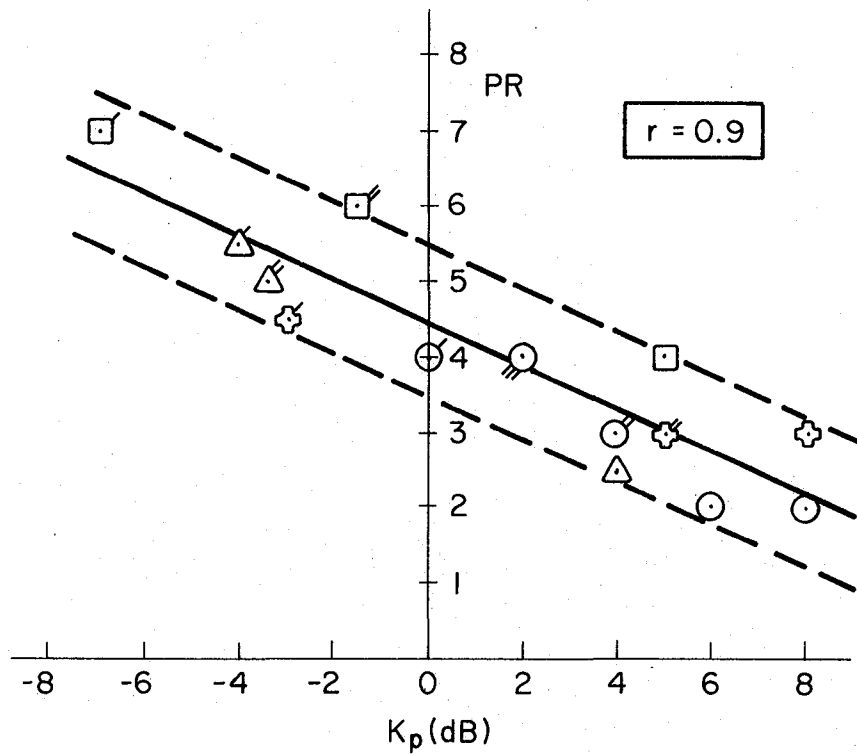
Figure 38. Pilot Rating as Function of Pilot
Mid-Frequency Gain
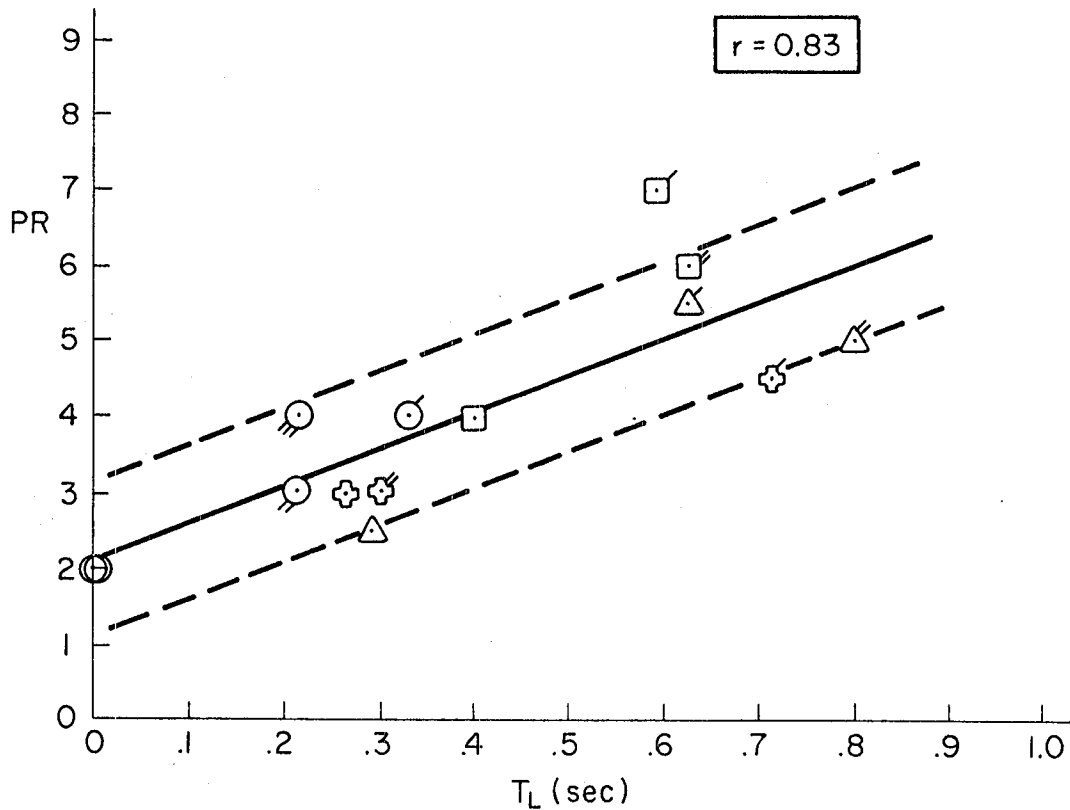
Figure 39. Pilot Rating as Function of Pilot Lead

Figure 41 is a similar set of plots for PR versus lag time constant. These data show that first-order lag up to 0.25 sec has less influence on pilot rating than changing from the first- to third-order configurations employed in this experiment.

Figure 42 presents plots of time delay and lag versus pilot inverse lead ($1/T_L$) with ratings shown next to each data point. Data points for each base configuration are connected and tend to indicate that there is a limit on the lead the pilot will adopt when faced with time delay in the system -- at least for the higher order controlled elements. [Note that for configuration 0 with no time delay the pilot did not generate lead and therefore $1/T_L$ lies at infinity.]
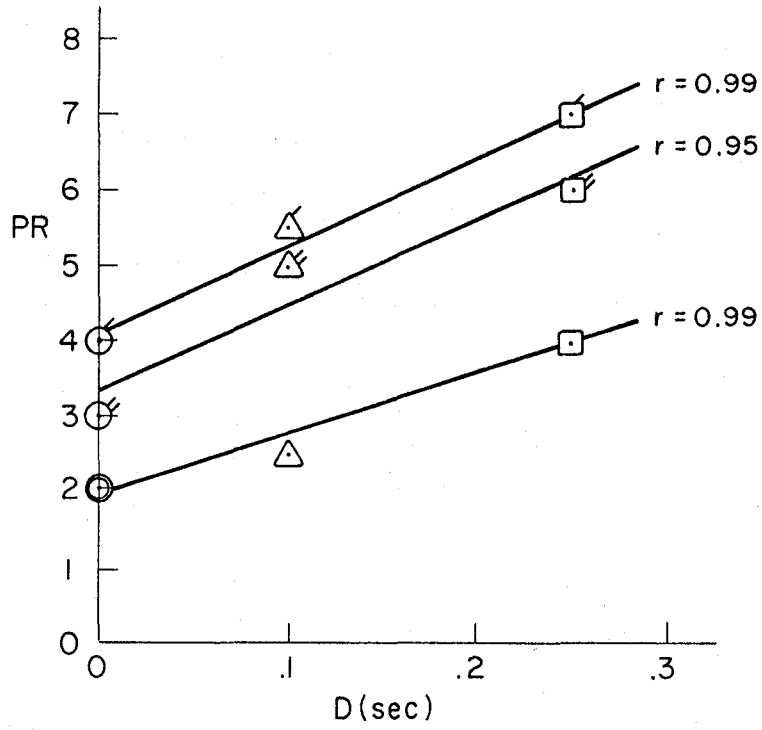
Figure 40. Pilot Rating as a Function
of Time Delay
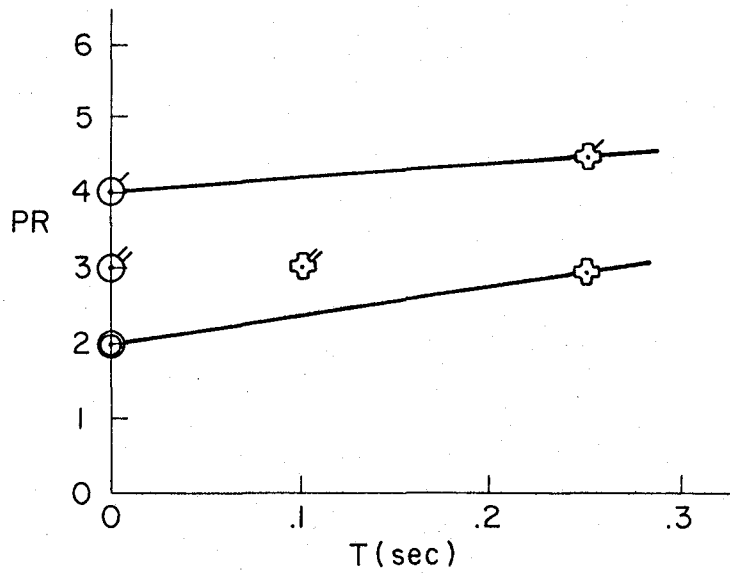
Figure 41. Pilot Rating as Function of
Lag Time Constant
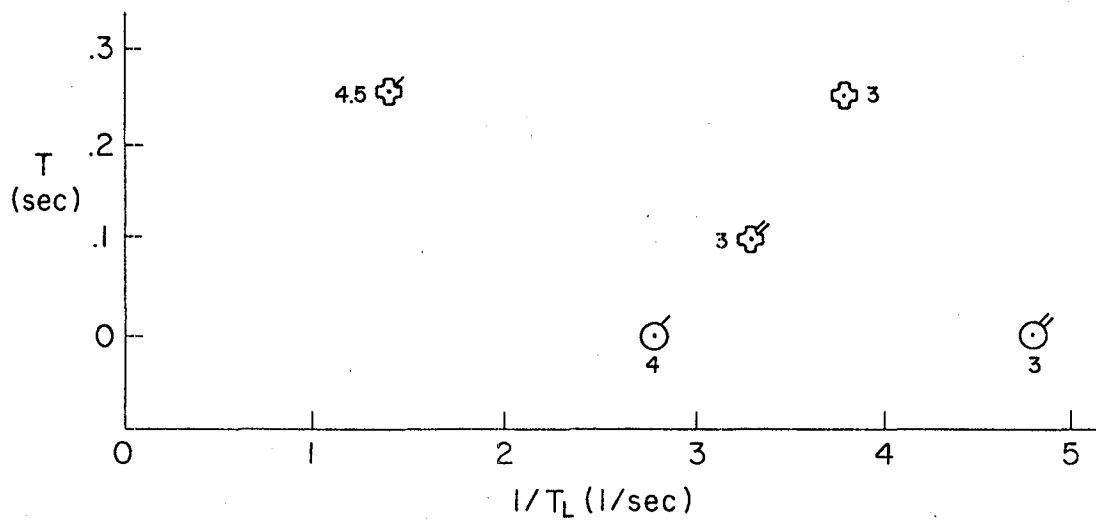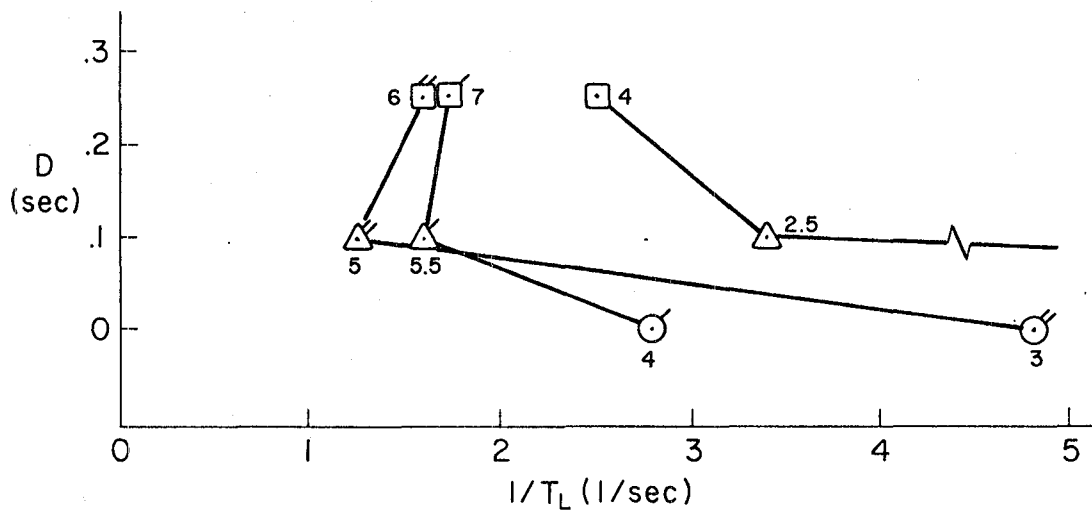
Figure 42. Pilot Lead Break as Function
of Delay or Lag

D. CONCLUSIONS

For the simple pitch tracking task investigated, the experimental data demonstrate that all of the predictions of the regression theory are valid. For controlled elements which contain pure time delay the pilot will generate lead in an attempt to offset the effective phase lag due to the time delay. This causes a flattening of the Bode amplitude ratio at or above the "normal" crossover frequency range and the pilot is then forced to decrease his gain (with a corresponding regression in crossover frequency) to maintain stable control. It further appears the lead the pilot will adopt may be limited to about 0.6-0.7 second.

In terms of pilot dynamics, the data show direct correlations between decreasing crossover (ω_c or K_p) and degraded pilot rating, and between increasing pilot generated lead time constant and degraded pilot rating. When these same degradations are treated as functions of the effective vehicle dynamics, the primary connection is, as would be expected, between increasing delay time constant and degraded pilot rating. However, the latter appears to be no stronger than the difference in rating induced by changing from a first- to third-order (super-augmented) controlled element having break points in the immediate vicinity of the measured crossover frequency.

It is not clear why the pilot subject selected such a large gain differential (factor of 2 which equates to 6 dB) between Configurations 1 and 3.

SECTION V

CONCLUSIONS AND RECOMMENDATIONS

In this study the properties of highly unstable aircraft and of typical control systems used to remedy their dynamic deficiencies have been explored generically. The following topics have been considered in-depth:

1) The dynamics of the aircraft-alone, as they are affected by degree of instability. This examination included the unusual properties of the aircraft-alone dynamics and contrasted them with those of conventionally stable aircraft.

2) Basic flight control system architectures suitable to reduce or completely alleviate the unstable aircraft characteristics.

3) The primary dynamic characteristics and regulatory properties of typical superaugmented aircraft control systems. This portion of the study considered

 — the governing factors in the linear system

 — the dominant mode characteristics, and

 — the fundamental stability margin properties.

 It included the development of the Total Available Gain Range (TAGR) factor as a basic measure which relates degree of instability, control system limitations, and key control system adjustments.

4) The overwhelming importance of control power as the predominant nonlinear characteristics was treated using sinusoidal, dual input, and random input describing function techniques.

5) The potentially critical dependence of superaugmented aircraft flying quality control characteristics on system excitation from vibratory flexible mode, internal noise, and external disturbance sources was emphasized.

6) Flying qualities features for superaugmented air-
craft are considered for rate command/attitude
hold, extended bandwidth, and attitude command
configurations.

7) An experiment to determine pilot dynamic behavior
in the attitude control of superaugmented air-
craft was conducted. Besides superaugmented
dynamic forms these experiments examined the dif-
ferences between high frequency time lags and
pure time delays as approximations to the very
high frequency controlled element characteris-
tics. The theoretical distinctions between time
lags and pure time delays, i.e., reduced ampli-
tude ratio slope and crossover frequency, and
poorer pilot ratings for the pure delay as con-
trasted with time lag, are developed from pilot-
vehicle system theory and validated by the exper-
imental data. Pilot rating decrements for the
time delay are also determined from the empirical
data.

From the results of the study we can conclude that the current high
priority problems with superaugmented aircraft flight control system and
flying qualities characteristics are:

* The increased sensitivity of the control system
design to flexible vehicle, actuator, and other
high frequency controller dynamics as stability-
limiting features in the closed-loop flight
control/aircraft system.

* Increased sensitivity (when compared with conven-
tional aircraft) of the aircraft control power
and control system design to flexible vehicle,
pilot remnant and vibration feedthrough, sensor
noise, and environmental and mission-task-
dependent disturbances and commands. All of
these may seem to have marked effects on the
erosion of the conditional stability margins and
on the flying qualities. A potentially unusual
feature of superaugmented aircraft is a more than
ordinary dependence of the effective vehicle
dynamics as seen by the pilot on turbulence and
other environmental excitation. These excitatory
inputs can, in principle, not only excite but
also modify the average effective aircraft dynam-
ics.

- The aircraft control power/rate requirements to accomplish regulation and command functions do not follow directly from those of conventional aircraft because of the conditional stability character of the closed-loop system, its high gain (or bandwidth), and its sensitivity to unwanted excitation.

- While the type of effective vehicle dynamics which can be provided in a superaugmented control system, at least in the linear range of operation, are exceptionally broad in possibilities, the effective aircraft characteristics for superaugmented aircraft have yet to be thoroughly examined.

From this list of problems it is clear that high priority future research efforts should be directed toward: control power/rate determination factors; flying qualities characteristics/requirements; and definition/measurement of controller noise sources (flexible modes, sensor noise, pilot remnant, vibration feedthrough, etc.) that may affect the average operation of the aircraft flight control system combination.

REFERENCES

1. McRuer, Duane, Irving Ashkenas, and Dunstan Graham, Aircraft Dynamics and Automatic Control, Princeton University Press, Princeton, NJ, 1973.

2. Myers, Thomas T., Donald E. Johnston, and Duane McRuer, Space Shuttle Flying Qualities and Flight Control System Assessment Study, NASA CR-170406, Dec. 1983.

3. McRuer, Duane, "Progress and Pitfalls in Advanced Flight Control Systems," AGARD CP-321, presented at the 35th AGARD Guidance & Control Panel Symposium, Lisbon, Portugal, Fall 1982.

4. Ashkenas, I. L., and T. S. Durand, "Simulator and Analytical Studies of Fundamental Longitudinal Control Problems in Carrier Approach," AIAA Simulation for Aerospace Flight Conference, A Volume of Technical Papers, presented 26-28 Aug. 1963, Columbus, OH, AIAA, New York, 1963, pp. 16-34.

5. Mooij, H. A., W. P. de Boer, and M. F. C. van Gool, Determination of Low-Speed Longitudinal Maneuvering Criteria for Transport Aircraft with Advanced Flight Control Systems, National Aerospace Lab., NLR TR 79127 U, Dec. 1979.

6. Franklin, J. A., R. C. Innis, G. H. Hardy, and J. D. Stephenson, Design Criteria for Flightpath and Airspeed Control for the Approach and Landing of STOL Aircraft, NASA TP 1911, Mar. 1982.

7. Mooij, H. A., and M. F. C. van Gool, The Need for Stick Force Stability for Attitude Stabilized Aircraft, NLR TR 77027U (Part II), 1976.

8. Mooij, H. A., and M. F. C. van Gool, "Flight Test of Stick Force Stability in Attitude-Stabilized Aircraft," J. Aircraft, Vol. 15, No. 9, Sept. 1978.

9. Hofmann, L. G., K. V. Shah, and D. Graham, Analysis of Limited Authority Manual Control Systems, AFFDL-TR-71-6, July 1971.

10. Graham, D., and D. T. McRuer, Analysis of Nonlinear Control Systems, John Wiley and Sons, Inc. (ed.), 1961.

11. Weingarten, Norman C., and Charles R. Chalk, Application of Calspan Pitch Rate Control System to the Space Shuttle for Approach and Landing, NASA CR-170402, May 1983.

12. Krendel, E. S., and G. H. Barnes, Interim Report on Human Frequency Response Studies, WADC-TR-54-370, June 1954.

13. Seckel, E., I. A. M. Hall, D. T. McRuer, and D. H. Weir, _Human Pilot Dynamic Response in Flight and Simulator_, WADC-TR-57-520, Oct. 1957.

14. McRuer, D. T., and E. S. Krendel, "Mathematical Models of Human Pilot Behavior," AGARDograph No. 188, Jan. 1974.

15. Powers, Bruce G., "Shuttle Low Speed Control System Tests," presented to the Control and Guidance Advisory Subcommittee, 29 Nov. 1983.

16. Hall, G. Warren, and Rogers E. Smith, _Flight Investigation of Fighter Side-Stick Force-Deflection Characteristics_, AFFDL-TR-75-39, May 1975.

17. Myers, T. T., D. E. Johnston, and D. T. McRuer, _Space Shuttle Flying Qualities and Flight Control System Assessment Study, Phase II_, NASA CR-170406, Dec. 1983.

18. Hess, Ronald A., "The Effects of Time Delays on Systems Subject to Manual Control," _AIAA Guidance & Control Conference Proceedings_, San Diego, CA, 9-11 Aug. 1982, pp. 165-172.

16. Abstract

"Superaugmented" aircraft are an important subclass of actively controlled, highly augmented aircraft which: are statically unstable without augmentation, have a degree of pitch attitude stability with respect to inertial space which is provided by the flight control system, and have pitch attitude command response characteristics which are largely independent of the aerodynamic stability derivatives except for pitch control effectiveness.

The report addresses aircraft-alone dynamics and superaugmented control system fundamental regulatory properties including stability and regulatory responses of the basic closed-loop system; fundamental high and low frequency margins and governing factors; and sensitivity to aircraft and controller parameters. Alternative FCS mechanizations, and mechanizational side effects are also discussed. An overview of flying qualities considerations encompasses general pilot operations as a controller in unattended, intermittent and trim, and full-attention regulatory or command control; effective vehicle primary and secondary response properties to pilot inputs and disturbances; pilot control architectural possibilities; and comparison of superaugmented and conventional aircraft path responses for different forms of pilot control.

Results of a simple experimental investigation into pilot dynamic behavior in attitude control of superaugmented aircraft configurations with high frequency time lags and time delays are presented.

17. Key Words (Suggested by Author(s)) Flying qualities Flight control Superaugmented aircraft Relaxed static stability	18. Distribution Statement Unclassified-Unlimited STAR category 08

19. Security Classif. (of this report) Unclassified	20. Security Classif. (of this page) Unclassified	21. No. of Pages 115	22. Price* A06

End of Document